INDC(CCP)- 430

IAEA
International Atomic Energy Agency

INDC International Nuclear Data Committee

Translations of Selected Papers published in

Jadernye Konstanty (Nuclear Constants) 1, 2000

Translated by the IAEA

December 2001

IAEA Nuclear Data Section, Vienna International Centre, A-1400 Vienna, Austria

Selected INDC documents may be downloaded in electronic form from
http://www-nds.iaea.org/reports-new/indc-reports/
or sent as an e-mail attachment.
Requests for hardcopy or e-mail transmittal should be directed to *services@iaeand.iaea.org*
or to:
Nuclear Data Section
International Atomic Energy Agency
Vienna International Centre
PO Box 100
A-1400 Vienna
Austria

Printed by the IAEA in Austria

December 2001

CONTENTS

NEUTRON CONSTANTS AND PARAMETERS

01-10118 (119) [1]
Translated from Russian

UDC 621.039.51

STUDY OF NEUTRON CROSS-SECTIONS AND THE $\alpha=\sigma_\gamma/\sigma_f$ VALUE FOR U-235 IN THE 1 meV-2 eV ENERGY RANGE

Yu.V. Grigoriev, V.V. Sinitsa
Russian Federation National Research Centre - Institute for Physics and Power Engineering, Obninsk, Russia

S.B. Borzakov, G.L. Ilchev, H. Faikov-Stanczyk[*]*, Ts.Ts. Panteleev*
Joint Institute for Nuclear Research (JINR), Dubna, Russia

N.B. Yaneva
Institute for Nuclear Research and Nuclear Energy, Sofia, Bulgaria

STUDY OF NEUTRON CROSS-SECTIONS AND THE $\alpha=\sigma_\gamma/\sigma_f$ VALUE FOR U-235 IN THE 1 meV-2 eV ENERGY RANGE. The time-of-flight and amplitude spectra of low-energy capture gamma rays and prompt fission gamma rays were measured on the 34 m and 27 m time-of-flight bases of the IBR-2 at the Neutron Physics Laboratory of the JINR using HPGe and Ge(Li) detectors. The sample-radiator was a thin metal disk of ^{235}U (90%) and ^{238}U (10%), 0.25 mm thick and 48 mm in diameter. The alpha value was obtained from the amplitude spectra for 27 energy groups in the 1 meV-2 eV energy range, as the ratio of the measured gamma-rays yields per capture to fission events; this was normalized to the standard alpha value for the thermal neutron energy.

The radiative capture and fission cross-sections for ^{235}U have been measured and remeasured by many authors, starting in the 1940s [1-3], since this isotope is the main fuel material in the nuclear power sector. However, the accuracy of the nuclear physics values obtained is still far from the level required. We have previously studied neutron cross-sections, the alpha value, resonance shielding effects and the Doppler effect in ^{235}U cross-sections in the 1 eV-20 keV energy range using fission chambers and radiation-multiplicity spectrometry [4-6]. We have now developed an apparatus for the time-of-flight measuring the γ-ray and amplitude spectra from absorption of neutrons by the nuclei of fissile materials. This means that spectroscopic methods can be used to determine σ_c, σ_f and $\alpha = \sigma_\gamma/\sigma_f$ over a wide energy range, including at thermal neutron energies. The time-of-flight measurements are now being carried out of γ-ray and amplitude spectra using neutron beams from the IBR-2 with a view to obtaining more accurate values for the energy dependence of the cross-sections and the alpha value.

---

[*] Permanent address: Lódz University, Lódz, Poland.

Experimental technique

Measurements were carried out on the 34 m and 27 m time bases of the IBR-2 using an HPGe detector with a volume of 80 cm^3 and a Ge(Li) detector with a volume of 55 cm^3. A mirror neutron guide was installed on the 34 m time base of beam 6, enabling research to be carried out in the 3-70 meV range and providing a $3 \cdot 10^6$ $n/cm^2 \cdot s$ thermal neutron flux with a minimum background of around 1% fast and delayed neutrons from the burst and satellites. The HPGe detector was installed at a distance of 15 cm from the ^{235}U (90%) and ^{238}U (10%) metallic sample-radiator which had an overall thickness of 0.25 mm and weighed 8 g. The germanium detector was shielded from γ-rays and neutrons in all sides with 10 cm of lead and boron carbide blocks with paraffin wax. The detector scanned the entire sample at an angle of 90^o. A Ge(Li) detector was used on the 27 m time-of-flight base of beam 1. It was not shielded, since the neutron beam had good collimation at a distance of 15 m from the reactor and a trap at 30 m. The neutron flux on the sample was approximately 10^6 $n/cm^2 \cdot s$. There was no mirror neutron guide on this channel, enabling measurements to be performed over the 3 meV–2 eV energy range. A metallic disk of uranium 48 mm in diameter was used as the sample-radiator for the measurements in beam 6. A PC based measurement module was used for data acquisition over a continuous period of 24 hours; the data was then sorted into amplitude and time spectra in different energy groups. The time-of-flight and amplitude instrumental spectra are shown in Figs 1 and 2. Filters made of Cd (2 mm), In (1 mm) and Be (20 mm) were used to measure the delayed and scattered neutron and gamma-ray background components. They were installed in the beam at a distance of 15 m from the reactor. The background levels at the thermal spectrum maximum at an energy of 0.06 eV do not exceed 1%. They are around 90% at 0.005 eV. Since the reactor power is stable, the duration of the measurement was used to monitor the beam. The energy resolution of the HPGe detector was 3 keV, and for the Ge(Li) detector it did not exceed 5 keV. These detector characteristics were sufficient to distinguish the characteristic radiative capture and fission line.

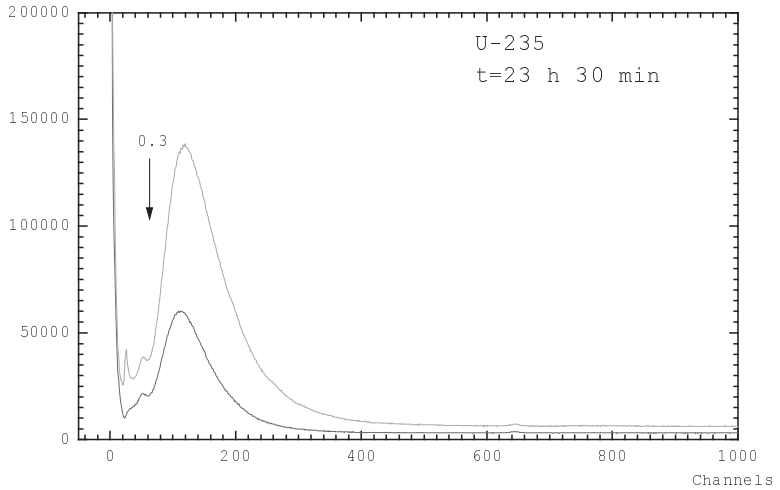

Fig. 1. Time-of-flight spectra for absorption of neutrons by ^{235}U nuclei, with an open beam and an In sample-filter in the beam. Time channel - 32 μs.

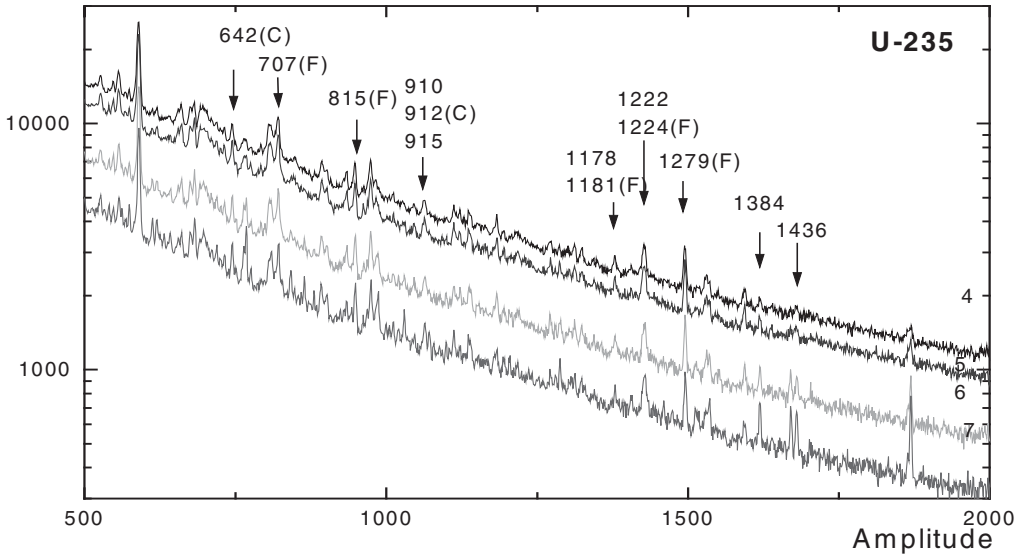

Fig. 2. Gamma-ray amplitude spectra for absorption of neutrons by ^{235}U nuclei with an open beam. Amplitude channel - 1 keV.

Processing and results of measurements

After sorting the amplitude spectra by energy group and calculating the background components, the areas were determined under the peaks for the 642 keV radiative capture gamma lines (c), the (910+912+915) keV triplet, the 707 and 815 keV "fission" gamma lines (f), the (1178+1181) and (1222+1224) keV doublets, and 1279 keV. The areas under the peaks were calculated by two methods: using the "Activ" program in which the peaks were approximated with Gaussian functions, and using the "Graphica" program where the total counts were determined at set intervals under the peaks. It is assumed that the areas under the γ-lines are proportional to capture and fission cross-sections ($A_{xi} = K_{xi}\ \sigma_x\ \varphi_j$, where A_{xi} is the area of the i-th γ-line of the reaction ($x = c, f$), K_{xi} is the proportionality coefficient; σ_x is the partial cross-section; and φ_j is the neutron flow). If we assume that the cross-section σ_x within the boundaries of the energy group j is a constant, the cross-section may be expressed in the following form:

$$\sum_{i=1}^{n} A_{xi} = \sigma_x \varphi_j \sum_{i=1}^{n} K_{xi}; \quad \sigma_x = \frac{\sum_{i=1}^{n} A_{xi}}{\varphi_j \sum_{i=1}^{n} K_{xi}} \tag{1}$$

Clearly, the alpha value in the energy group j will be expressed as follows:

$$\alpha = \sigma_c / \sigma_f = \frac{\sum_{i=1}^{n} A_{ci}}{\sum_{i=1}^{n} K_{ci}} \Bigg/ \frac{\sum_{i=1}^{l} A_{fi}}{\sum_{i=1}^{l} K_{fi}} = \frac{\sum_{i=1}^{n} A_{ci}}{\sum_{i=1}^{l} A_{fi}} \cdot \frac{\sum_{i=1}^{l} K_{fi}}{\sum_{i=1}^{n} K_{ci}} \tag{2}$$

As we can see from formulae (1) and (2), to determine the cross-sections and the alpha value, we must know the spectrum of the neutron beam φ and the proportionality coefficients. The proportionality coefficients can be determined from the well-known values of the alpha value in the lower resonance region and at thermal neutron energy. The spectrum of the neutron beam was measured using an SNM-13 boron counter, which was permanently placed in the beam near the sample-radiator. Moreover, in the amplitude spectra, the gamma lines with $E_\gamma = 478$ keV were calculated; it was therefore possible to determine the shape of neutron spectrum averaged with respect to the energy dependence of the (n,γ) reaction in ^{10}B ($\varepsilon \sim 1/\sqrt{E}$). For the purposes of comparison with the experiment, analogous values of σ_c, σ_f and α were calculated using the GRUKON program [7] and evaluated data from the BROND-2, ENDF/B-VI, JENDL-3, and JEF-2 libraries. The data calculated using ENDF/B-VI [8] at the thermal point were used as reference values. Table 1 and Fig. 3 give experimental and calculated values for α. In addition, Fig. 3 gives the experimental values from Ref. [9], which employs a similar methodology.

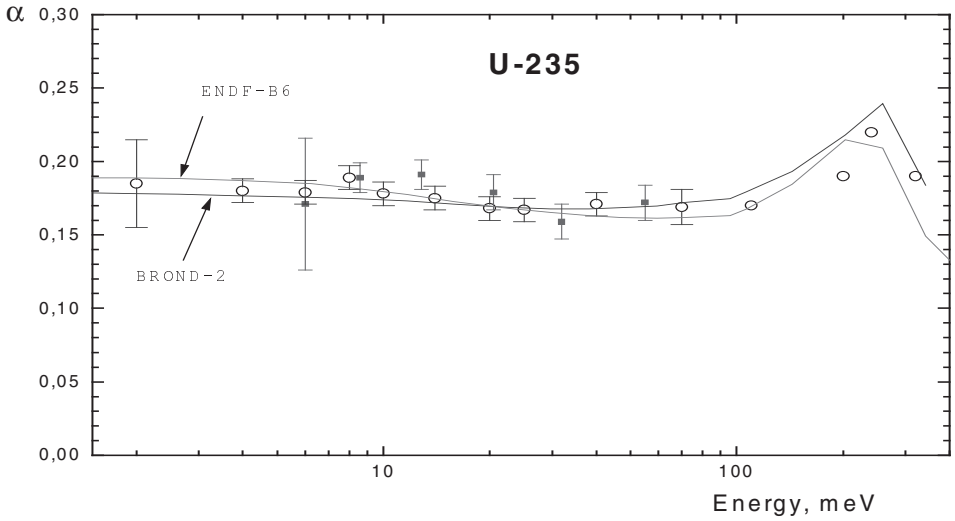

Fig. 3. Experimental and calculated values for $\alpha = \sigma_c/\sigma_f$ for ^{235}U. ■ - Ref. [9], ○ - this paper.

Table 1

Experimental and calculated alpha values for ^{235}U

E_n (meV)	BROND-2	ENDF/B6	α (this work)
6.0	0.176	0.185	0.171±0.045
8.6	0.175	0.182	0.189±0.010
12.8	0.173	0.178	0.191±0.010
20.5	0.169	0.168	0.179±0.012
32.0	0.168	0.163	0.159±0.012
55.0	0.170	0.161	0.172±0.012

As can be seen from Fig. 3 and the Table 1, our data and the data from Ref. [9] agree with the calculated values. It should be noted that the data on alpha in the various libraries differ by 1-6%.

Conclusion

In view of the importance of such constants for reactor calculations, work should continue in this area, and other methodologies should be applied such as radiation-multiplicity spectrometry, for example. Clearly, the results of this study could be used to refine the parameters for negative resonances. This is being planned for the future.

References

[1] D. Harvey, D. Sanders, Review of data on effective cross-sections and neutron yields for ^{233}U, ^{235}U and ^{239}Pu, Achievements in the field of nuclear energy, Moscow, I.L. (1958).

[2] S.I. Sukhoruchkin, Resonance parameters of fission nuclei, Atomnaya Ehnergiya, v. 31, No. 6 (1971) p. 595.

[3] R. Gwin, E.G. Silver, R.W. Ingle, H. Weaver, Measurement of the Neutron Capture and Fission Sections of ^{239}Pu and ^{235}U, 0.02 eV to 200 keV the Neutron Capture Cross Sections of ^{197}Au, to 50 keV, and Neutron Fission Cross Sections of ^{233}U, 5 to 200 keV, Nuclear Science and Engineering, v. 59 (1976) p. 79.

[4] Yu.V. Grigoriev, V.V. Sinitsa, N.A. Gundorin, Study of the resonance structure and temperature dependence of neutron cross-sections for plutonium-239, Voprosy Atomnoj Nauki i Tekhniki, Ser.: Yadernye Konstanty, No. 1-2, (1997) p. 3.

[5] Yu.V. Grigoriev, V.Ya. Kitaev, K.V. Moiseev, Ts.Ts. Panteleev, H. Faikov-Stanczyk, Study of the resonance shielding effect in the alpha value for plutonium-239 in the 4.65-2150 eV energy range, Voprosy Atomnoj Nauki i Tekhniki, Ser.: Yadernye Konstanty, No. 2 (1998) p. 23.

[6] Yu.V. Grigoriev, V.Ya. Kitaev, K.V. Moiseev, H. Faikov-Stanczyk, Ts.Ts. Panteleev, The investigation of a resonance self-shielding effect in the α-value of ^{235}U, ^{239}Pu in the 4.65-2150 eV energy range. ISINN-7, Dubna (1999) p. 233.

[7] V.V. Sinitsa, Program for calculating group constants using an evaluated data library, Voprosy Atomnoj Nauki i Tekhniki, Ser.: Yadernye Konstanty, No. 5 (59) (1984) p. 34.

[8] P.F. Rose, C.L. Dunford, Ed., ENDF-102, Data Formats and Procedures for the Evaluated Nuclear Data File, ENDF, report BNL, Upton, New York, 11973, USA (1988).

[9] H. Weigmann, J.A. Wartena, C. Burknolz, On alpha of ^{235}U for sub-thermal neutron energies, Proc. of Inter. Conf. “Nucl. Data for Science and Technology”, 13-17 May 1991, Jülich, Germany, p. 38.

01-10118 (115) [2]
Translated from Russian

UDC 539.171.017

GAMMA-RAY PRODUCTION CROSS-SECTION AND SPECTRUM MEASUREMENT RESULTS FOR INELASTIC INTERACTION OF 14 MeV NEUTRONS WITH NUCLEI OF Na, S, Cl, Ti, V, Cr, Ni, Zn, Ge, Nb, Cd, In, Sn, Bi, ^{235}U and ^{238}U*

Yu.Ya. Nefedov, V.I. Nagornyj, V.I. Semenov, A.K. Zhitnik, R.A. Orlov, A.E. Shmarov
Russian Federal Nuclear Centre
All-Russia Scientific Research Institute for Experimental Physics, Sarov, Russia

GAMMA-RAY PRODUCTION CROSS-SECTION AND SPECTRUM MEASUREMENT RESULTS FOR INELASTIC INTERACTION OF 14 MeV NEUTRONS WITH NUCLEI OF Na, S, Cl, Ti, V, Cr, Ni, Zn, Ge, Nb, Cd, In, Sn, Bi, ^{235}U and ^{238}U*. The measurements were carried out in the 0.5-14 MeV gamma-ray energy region by the time-of-flight method. An NaI(Tl) scintillation spectrometer was used. Total and differential gamma-ray production cross-sections were obtained for 16 nuclei. The experimental errors measured 9% for the total cross-sections and varied from 6% to 50-70% for the differential cross-sections.

1. Measurements

The problem of obtaining reference data on gamma-ray production cross-sections and spectra has still not been fully resolved. This is attributable to a number of objective experimental difficulties which from the outset have been inherent both in the measurement technique itself and in the procedure used to obtain physical gamma-ray spectra from the distributions obtained in experiments.

For this reason, any new experimental information always arouses considerable interest, particularly among the specialists whose task it is to evaluate elementary gamma-ray production cross-sections and build up a bank of reference data. Where thermonuclear applications are concerned, there is special interest in measurements of the gamma-ray cross-sections and spectra produced by the interaction of 14 MeV neutrons with the nuclei of elements used in construction materials.

This paper presents the results of new measurements of the gamma-ray cross-sections and spectra produced by inelastic interaction of neutrons with an effective energy of

* Work carried out with financial support from the International Science and Technology Center, project No. 731-97.

14.3 MeV with nuclei of Na, S, Cl, Ti, V, Cr, Ni, Zn, Ge, Nb, Cd, In, Sn, Bi, ^{235}U and ^{238}U. The measurement method is based on the use of a single-crystal scintillation spectrometer containing a large NaI(Tl) crystal, ∅ 150 x 100 mm, and the time-of-flight technique [1, 2]. The measurement procedure and the geometry, as well as the approach used to evaluate the results, are described in detail in [3].

Disc-shaped samples of natural isotopic content, 150 mm diameter and varying in thickness between 1.14 and 30 mm, were arranged at a distance of 200 mm from the centre of a titanium-tritium target. The sample mass ranged from 294.7 g for ^{235}U to 1183.6 g for vanadium. The Cl measurements involved the use of LiCl salt. Gamma-ray production for Li was assumed to be negligible. NaCl salt was used for the Na measurements. The gamma-ray production cross-sections for Cl were subtracted from the results obtained for NaCl in order to obtain the gamma-ray production cross-sections for Na.

For the measurements involving LiCl, NaCl, S, Cr, Ge, ^{235}U and ^{238}U, the samples were placed in plastic containers weighing, respectively, 47.0, 47.0, 39.0, 39.5, 29.4, 39.0 and 39.0 g.

2. Results

Table 1 shows the results for total and differential cross-sections in 15 different energy groups.

The errors given have a 95% confidence level. The error magnitude of the differential cross-sections depends on the energy range. The main source of error in the data in the 0.5-1.0 MeV range is uncertainty in corrections for multiple neutron and gamma-ray scattering in the sample, owing to the considerable uncertainties in current gamma-ray production constants. In future, a useful way to improve the accuracy of the results in this energy range would be to carry out additional measurements using thin samples, which are much less affected by multiple neutron and gamma-ray scattering.

In the high-energy part of the spectra the major source of data error is statistical error in the experimental amplitude distributions. Achieving greater accuracy in this energy range is solely a matter of increasing the statistical accuracy of the source data; this can be achieved by carrying out additional measurements on samples having a greater mass.

In the central part of the spectra, the error in the differential cross-sections shown drops virtually to the error attributable to the method. Accordingly, no improvements will be possible in this area unless new and more accurate measurement methods are developed.

Table 1

Differential and total gamma-ray production cross-sections, mb

E_γ.MeV	Na	S	Cl	Ti	V	Cr	Ni	Zn	Ge	Nb	Cd	In	Sn	Bi	^{235}U	^{238}U
0.50 - 0.75	82±35	36±17	92±20	98±57	190±30	264±64	192±38	495±47	791±73	486±84	1466±213	660±62	608±63	1562±147	3968±380	3094±356
0.75 - 1.00	47±20	33±7	94±12	520±48	205±22	437±42	252±27	767±73	764±71	548±58	960±91	732±69	642±63	856±86	2708±257	1901±216
1.00 - 1.50	245±46	156±21	186±18	995±91	280±28	1249±114	1027±94	1451±137	731±69	667±64	900±86	1782±167	1672±153	903±91	2960±296	2195±236
1.50 - 2.00	222±53	225±23	263±26	250±24	485±45	318±30	247±25	443±45	701±68	415±40	513±49	467±46	458±44	579±59	1496±147	1360±145
2.00 - 2.50	129±60	479±44	376±36	265±25	141±14	191±19	170±17	224±23	251±25	392±37	366±37	353±35	338±34	271±28	879±90	824±91
2.50 - 3.00	74±29	130±13	166±17	180±18	107±12	129±14	163±16	160±18	237±24	163±17	225±26	224±24	200±21	418±45	449±71	398±45
3.00 - 4.00	121±51	125±14	311±30	230±23	270±27	261±26	215±22	232±24	256±25	171±20	196±22	187±21	173±20	271±32	377±70	296±40
4.00 - 5.00	86±25	126±15	109±13	172±19	152±17	168±18	147±17	156±20	194±22	70±10	81±16	85±16	75±12	241±30	89±46	83±18
5.00 - 6.00	64±17	66±8	54±9	118±16	103±13	149±18	108±14	99±16	124±18	34±10	35±14	35±12	33±16	56±23	2^{+3}_{-2}	16±12
6.00 - 7.00	46±16	43±8	51±9	84±11	76±11	104±16	80±11	56±13	91±15	18±14	19±19	17±10	24±20	10^{+19}_{-10}		4^{+5}_{-4}
7.00 - 8.00	42±12	23±6	19±6	50±8	34±7	70±13	49±10	23±9	56±12	5^{+8}_{-5}	4^{+9}_{-4}	7^{+13}_{-7}	3^{+9}_{-3}	3^{+7}_{-3}		
8.00 - 9.00	20±8	6±5	8±5	21±7	26±6	44±10	22±10	13±10	31±10	4^{+7}_{-4}	3^{+6}_{-3}	2^{+5}_{-2}	2^{+3}_{-2}	2^{+15}_{-2}		
9.00 - 10.0	11±7	1^{+3}_{-1}	2^{+4}_{-2}	9±5	15±5	23±9	4^{+6}_{-4}	2^{+3}_{-2}	32±11	1^{+3}_{-1}	1^{+3}_{-1}	1^{+2}_{-1}	1^{+6}_{-1}			
10.0 - 12.0			1±1	6^{+9}_{-6}	7±7	6^{+7}_{-6}	1^{+3}_{-1}	1^{+5}_{-1}	9±7			1^{+2}_{-1}				
12.0 - 14.0																
Total	1189±107	1449±130	1732±156	2998±270	2091±188	3413±307	2677±240	4122±371	4268±384	2974±268	4769±429	4553±410	4229±381	5172±465	12928±1164	10171±915

References

[1] Yu.Ya. Nefedov, et al., Gamma-ray production cross-sections for interactions of 13.8 MeV neutrons with Cu, W and ^{235}U, in Proc. Int. Conf. on Nucl. Data for Science and Technology, Gatlinburg, Tennessee, USA, Vol. 2, (1994) 950.

[2] Yu.Ya. Nefedov, et al., Gamma-ray production cross-sections for interactions of 13.8 MeV neutrons with nuclei of Cu, W and ^{235}U, in Voprosy Atomnoj Nauki i Tekhniki, Ser. Yadernye Konstanty No. 2, (1996) 47.

[3] Yu.Ya. Nefedov, et al., Measurement results for gamma-ray production cross-sections and spectra in inelastic interaction of 14 MeV neutrons with nuclei of C, O, Mg, Al, Fe, Cu, Zr, Mo, W and Pb. Abstracts of Ninth Intl. Conf. on Radiation Shielding, 17-22 October 1999, Tsukuba International Congress Center, Tsukuba, Ibaraki, Japan.

01-10118 (121) [3]
Translated from Russian

UDC 539.17.013

EVALUATED RESONANCE PARAMETERS OF ^{234}U

G.B. Morogovskij, L.A. Bakhanovich
Radiation Physics and Chemistry Problems Institute
Belarus National Academy of Sciences

EVALUATED RESONANCE PARAMETERS OF ^{234}U. Multilevel Breit-Wigner parameters were obtained for the representation of neutron cross-sections in the 10^{-5}–1500 eV energy range from evaluation of ^{234}U experimental cross-sections in the resolved resonance region. The resonance energies and parameters of 25 previously missing resonances were calculated.

The evaluated ^{234}U files that are currently available, Refs 1-3, are based on the resolved resonance region from the same source data; since the ENDF/B-VI, Ref. 1, and JEF, Ref. 2, files coincide in this region, the Ref. 2 evaluation will not be considered further.

The ENDF/B-VI file, Ref. 1, uses the parameters of James et al., Ref. 4, to represent the resolved resonance region; the value Γ_γ = 40 meV is taken for all resonances, while the background resonance parameters are selected in such a way as to obtain thermal cross-sections corresponding to Ref. 5. At the same time, in the unresolved resonance region the value $\langle\Gamma_\gamma\rangle$ = 25 meV is used.

The JENDL-3.2 file, Ref. 3, takes the same base parameters from Ref. 4 as Ref. 1; however, for all but the first two resonances the value of Γ_γ is not taken to be 40 meV, as in Ref. 4, but 26 meV, which is close to the value Γ_γ = 25 meV from Ref. 6, and so the neutron widths were modified. The value $\langle\Gamma_\gamma\rangle$ = 26 meV is also used in the unresolved resonance region. The parameters of the first two resonances were selected in such a way as to obtain thermal cross-section and resonance integral values that coincided with the values from Ref. 7.

Table 1 shows the average resonance parameters, thermal cross-sections and resonance integrals for these evaluations.

Table 1

Average resonance parameters, thermal cross-sections and resonance integrals of ^{234}U. Comparison of evaluations[1]

Value	ENDF/B-VI	JENDL-3.2	Present paper
$\langle\Gamma_n^0\rangle$, meV	1.0957	1.2393	0.9565
$\langle\Gamma_\gamma\rangle$, meV	40.00	25.97	40.00
$\langle\Gamma_f\rangle$, meV	0.6839	0.6525	0.5881
<D>, eV	12.6627	12.6632	10.4499
S_0	8.7262×10^{-5}	9.8698×10^{-5}	9.2168×10^{-5}
R', fermi	8.930	9.80	8.9358
σ_t, barn	115.799	119.166	110.342
σ_γ, barn	103.034	99.751	99.055
σ_f, barn	0.464	0.0062	0.300
σ_n, barn	12.301	19.409	10.987
g_γ	0.9969	0.9970	0.9998
G_f	0.9953	1.0112	0.9985
I_γ, barn (0,5-1500 eV)	654.98	626.94	627.94
I_f, barn (0,5-1500 eV)	0.5589	0.7563	0.7191

[1] The values in the table were obtained using the PSYCHE and INTER programs, Ref. 14.

If we compare the curve of the $\sigma_t(E)$ and $\sigma_f(E)$ cross-sections obtained using the evaluation parameters in Refs 1 and 3 with the $\sigma_t(E)$ cross-sections measured experimentally by Harvey et al. in Ref. 8 and the $\sigma_f(E)$ cross-sections measured experimentally by James et al. in Refs 4 and 6, we can see that:

1) There is appreciable disparity between the total cross-section values calculated using the parameters in Refs 1 and 3, (taking into account the experimental conditions), and those measured in Ref. 8. This is particularly noticeable in the 25-200 eV energy interval, where the resonances in $\sigma_t(E)$, Ref. 8, are fairly well resolved (see Figs 2 and 3);

2) By using the $\sigma_f(E)$ measurements from Refs 4 and 6 a number of missing resonances can be identified and their parameters obtained. (According to James, Ref. 4, they account for about 20%.) This enables more accurate description of the fission cross-section curve in the resonance energy region, as well as more accurate average resonance parameters.

The following source data were used in the present paper to calculate a system of resonance parameters using multilevel Breit-Wigner formalism in the 10^{-5}-1500 eV energy interval:

1) The evaluated cross-section values in the 10^{-5}-1 eV region, scattering radius, and background resonance parameters from Ref. 9, except for the value of σ, which was taken to be 300 mb in line with Ref. 13 (see below), and, consequently, the values of the background resonance values of Γ_f, which should be non-zero;

2) The experimental measurements of $\sigma_t(E)$ from Refs 8 and 10;

3) The experimental measurements of $\sigma_f(E)$ from Refs 4, 6 and 11;

4) The starting set of resonance parameters from Ref. 4.

Thus, the present paper includes practically all the information related to the resolved resonance region.

Since the ^{234}U fission cross-sections in Refs 4, 6 and 11 were normalized to the $\sigma_f(E)$ ^{235}U of various authors, and at various energy intervals, unified normalization is needed for parameterization taking all these studies into account. To that end, the normalization values of σ_f (E) ^{235}U from the above papers were reduced to the values calculated in the relevant regions from the ^{235}U ENDF/B-VI file. The coefficients thus obtained were used to renormalize the measurements of $\sigma_f(E)$ ^{234}U in Refs 4, 6 and 11.

Since calculations of resonance parameters higher than 1 eV took all the available experimental data into account in Refs 4, 6, 8, 10 and 11, each set of measurements was given a statistical weighting based on a comparative evaluation of the quality of the authors' cross-section values. An example of a similar evaluation for the thermal energy region can be found in Ref. 9. This kind of procedure is especially necessary when calculating the resonance parameters for E_r = 5.16 eV, where 7 sets of data are used in conjunction. (In the resonance region in question, Ref. 10 gives three sets of measurements in samples of various thicknesses.) It should be pointed out that the total cross-section curve and, consequently, the radiative capture cross-section curve for this resonance, have quite a strong influence on the value of I_γ obtained from parameterization.

Average radiative widths merit discussion in their own right, especially since the contribution of the partial width Γ_γ to the total width of practically every resonance is a determining factor. In Refs 4 and 6, James et al. used the values 40 and 25 meV, respectively and this was also reflected in the evaluations in Refs 1 and 3, as noted earlier. Two sets of parameters satisfying the conditions $<\Gamma_\gamma>$ = 25 meV and $<\Gamma_\gamma>$ = 40 meV were obtained from the parameterization process. It became clear that the cross-sections generated from the set of parameters for which $<\Gamma_\gamma>$ = 40 meV enable more accurate reproduction of the energy curve of all the experimentally measured cross-sections taken into account when calculating the parameters. In the nucleus under investigation, the link between the magnitude of Γ_γ and the parameter quality (understood as the degree of coincidence of the experimental cross-sections and the cross-sections generated from the parameters, taking into account the experimental conditions) is particularly evident for the resonance E_r = 5.16 eV which has been measured

repeatedly (see Fig. 1). The value which we obtained for this, $\Gamma_\gamma = 41.97$ meV, is the best one for generating all the measured cross-sections used in our evaluation. The authors of a recent study, Ref. 12, measured a ^{234}U fission cross-section and obtained parameters for 10 low-lying resonances. It is clear from the figures presented in this paper that, as a result of the authors taking the value $\Gamma_\gamma = 25$ meV for all levels, the resonance $E_r = 5.16$ eV, reconstructed from parameters based on experimental conditions, is significantly narrower than the resonance measured experimentally. Our calculations showed that the value $\Gamma_\gamma \approx 51$ meV is required in order to describe the fission cross-section, Ref. 12, in the region of the first resonance. The radiative width of the background resonance, which enables the given thermal cross-section values (see below) to be obtained, was 57.22 meV. All of the above leads us to assert that the value $\langle\Gamma_\gamma\rangle = 40$ meV is more plausible than $\langle\Gamma_\gamma\rangle \approx 25$ meV, at least for the resolved resonance region.

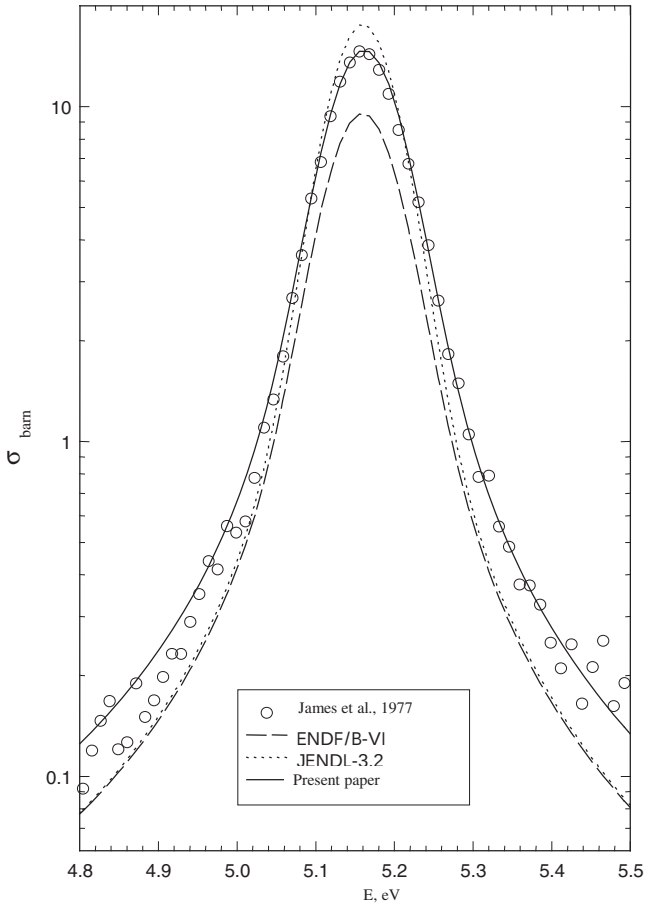

Fig. 1. Comparison of the experimental fission cross-section and the fission cross-section calculated using the various evaluation parameters of James et al., Fig. 4, in the 5.16 eV resonance region.

During parameterization, the resonance energies of a number of resonances from the starting set in Fig. 4 were made more accurate and for most of them new parameter values were obtained. In addition, 25 previously missing resonances were identified, for which resonance energies were determined and parameters were calculated. Taking these resonances into account helped improve agreement between the cross-sections measured experimentally and those calculated using the parameters in our paper, and also allowed us to obtain values of <D> and S_0 fairly close to those evaluated in Ref. 4. The resonance energy and width Γ_γ of the background resonance were assumed to be the same as in Fig. 9; the neutron and fission widths were calculated on the basis that the following conditions should be met:

1) The values obtained for σ_t^{2200} and σ_n^{2200} should be as close as possible to the evaluation in Ref. 9;

2) The magnitude of σ_γ^{2200} should, fairly accurately, coincide with the weighted average value of σ_γ^{2200} obtained in Ref. 9 for the Maxwellian spectrum, taking into account the value of g_γ in the present paper;

3) The magnitude σ_f^{2200} should be close to 0.3 b.

The reasons underlying the last requirement are as follows. In the previous evaluations, Refs 1-3 and 9, the boundary condition σ_f^{2200}<0.65 b was used. Ref. 12 gives a value of $<\sigma_f>$, evaluated by the authors according to their measurements, in the 0.013-0.038 eV range of 140±43 mb. According to the authors of Ref. 13, evaluation of the experiment in Ref. 12 gives σ_f^{2200} = 110±70 mb. At the same time, from their own measurements the authors of Ref. 13 obtained the value σ_f^{2200} = 300±20 mb. Thus, there are at least two different measured values of σ_f^{2200}. The evaluation of σ_f^{2200}, carried out using a statistical method ($\sigma_f^{2200} = \sigma_t^{2200} \frac{<\Gamma_f>}{<\Gamma>}$), for the same 0-300 eV and 0-200 eV energy intervals as in Fig. 13, using our value of σ_t^{2200} and the parameters in Table 2, yields 0.26 and 0.028 b respectively, and this was also the basis for assuming $\sigma_f^{2200} \approx 300$ mb.

The average resonance parameters, thermal cross-sections and resonance integrals, calculated from the parameters given in the present paper, are shown in Table 1. From this Table it is clear that:

1) Use in the JENDL-3.2 evaluation of the value Γ_γ = 26 meV for all resonances and the resulting neutron width modification in Ref. 4, leads to a substantial increase in the value of $<\Gamma_n^0>$ and, consequently of S_0;

2) The values of $<\Gamma_n^0>$ and $<\Gamma_f>$ obtained in the present paper are somewhat lower than in the evaluations in Refs 1 and 3 owing to the presence of the 25 additional resonances that were missing from the previous evaluations;

3) The values <D> = 10.45±0.46 eV and $S_0 = (9.2\pm1.1)\cdot10^{-5}$ of the present paper are in good agreement with the evaluated values of James et al. in Fig. 4: <D> = 10.6±0.5 eV and $S_0 = (8.6\pm1.1)\cdot10^{-5}$.

Table 2

Resonance parameters of ^{234}U

E_r, eV	J	Γ_n, meV	Γ_γ, meV	Γ_f, meV
-2.140	1/2	2.53706	57.22	0.190584
5.162	1/2	3.95620	41.97	0.029728
22.100	1/2	0.01800	41.29	0.125000
23.700	1/2	0.16000	37.58	0.008175
31.110	1/2	3.11640	39.71	0.026764
45.610	1/2	0.45499	36.07	0.091769
48.560	1/2	2.28220	33.63	0.001728
77.380	1/2	5.41940	41.53	0.009325
94.290	1/2	12.09400	34.98	0.081775
106.130	1/2	2.33120	37.56	0.221440
111.060	1/2	7.36840	34.29	0.689150
130.00*	1/2	5.98370	36.25	0.001747
146.250	1/2	7.96100	37.47	0.042453
152.160	1/2	12.02400	34.20	0.026504
176.180	1/2	20.37200	42.95	0.128360
182.490	1/2	6.26150	35.34	0.458060
187.520	1/2	36.12000	43.71	0.016608
191.800	1/2	4.13880	38.19	0.004110
208.400	1/2	8.01210	54.67	0.052559
220.000	1/2	0.34100	36.75	0.089100
226.700	1/2	11.11000	46.57	0.013614
237.800	1/2	10.16400	51.87	0.012541
245.00*	1/2	2.18150	40.18	0.006545
254.300	1/2	12.79800	38.51	0.133730
258.300	1/2	3.61080	45.98	0.410290
267.00*	1/2	5.16530	36.62	0.005197
276.500	1/2	5.77000	44.95	0.103190
285.20*	1/2	0.10164	43.38	0.176830
290.700	1/2	37.20000	39.91	0.177000
307.500	1/2	16.40000	35.48	0.150000
322.600	1/2	57.83000	46.99	0.017602
331.100	1/2	16.88000	42.73	0.013892
342.50*	1/2	3.42670	33.86	0.020400
349.7 00	1/2	35.19500	44.52	0.245650
359.100	1/2	42.45800	54.63	0.012845
363.500	1/2	1.79820	33.67	0.325890
388.100	1/2	0.79000	33.35	2.160000
391.000	1/2	14.86100	39.41	1.006600
412.600	1/2	8.10000	30.86	0.411000
437.000	1/2	5.14000	30.81	0.040800
440.900	1/2	2.44000	51.99	1.430700
455.200	1/2	28.41000	31.91	2.766700
463.800	1/2	32.00100	46.66	0.562010
465.500	1/2	6.15000	39.02	0.187000
488.700	1/2	93.31000	33.40	0.584410

E_r , eV	J	Γ_n , meV	Γ_γ , meV	Γ_f , meV
503.900	1/2	29.39600	35.62	0.124180
511.000	1/2	13.10000	28.92	0.298500
515.800	1/2	15.46000	53.60	8.042500
518.900	1/2	17.57300	45.37	1.238400
526.100	1/2	17.50200	50.20	0.635260
547.400	1/2	68.50000	36.14	0.054988
555.700	1/2	46.30000	41.06	3.220000
560.900	1/2	8.76000	42.62	5.050000
574.400	1/2	26.30000	37.29	1.150000
582.300	1/2	8.83000	46.40	6.970000
585.100	1/2	6.76000	45.59	4.248400
593.900	1/2	2.84000	33.42	0.560400
614.300	1/2	8.17000	48.60	0.529100
625.700	1/2	11.10000	42.11	0.690000
636.900	1/2	1.68000	27.45	1.814100
643.400	1/2	7.02000	39.78	4.970000
658.00*	1/2	23.00000	28.06	0.015556
670.900	1/2	3.46000	36.80	1.500000
685.600	1/2	14.95000	35.68	0.083979
690.000	1/2	10.30000	44.40	6.578000
702.100	1/2	16.14000	37.79	0.371950
709.100	1/2	14.30000	41.20	0.019834
721.50*	1/2	22.91900	39.67	0.047174
726.100	1/2	5.27000	39.17	5.640300
734.600	1/2	5.27000	41.75	0.120360
745.50*	1/2	28.60000	36.93	0.026117
757.100	1/2	90.30000	41.68	0.062824
764.700	1/2	265.00000	31.53	0.043500
766.700	1/2	69.30000	48.08	0.015836
780.000	1/2	3.30000	42.86	0.713180
788.300	1/2	39.00000	49.35	0.260780
800.10*	1/2	3.27000	41.56	0.199410
813.300	1/2	25.80000	41.48	0.520380
814.800	1/2	180.00000	45.03	0.161080
822.500	1/2	7.98000	47.93	0.367000
836.00*	1/2	3.27000	37.15	0.096057
846.100	1/2	3.27000	34.28	0.125400
855.800	1/2	11.70000	32.96	0.484890
858.900	1/2	15.40000	46.01	0.401350
866.00*	1/2	3.27000	37.81	0.073884
876.00*	1/2	3.27000	42.19	0.070708
882.200	1/2	19.40000	35.46	0.208690
889.100	1/2	33.10000	30.24	0.092880
910.00*	1/2	74.60001	34.21	0.024194
920.00*	1/2	6.49000	40.61	0.040397
931.50*	1/2	6.49000	39.42	0.047904
945.00*	1/2	6.49000	48.84	0.161670
957.800	1/2	6.49000	38.85	0.095807
974.000	1/2	159.40000	40.96	0.240830
981.800	1/2	3.97000	35.56	0.624450
995.00*	1/2	6.49000	42.75	0.040397
1011.000	1/2	74.60001	43.62	0.037735
1037.700	1/2	64.30000	45.46	0.114530
1052.400	1/2	10.70000	42.89	0.158300
1067.300	1/2	6.75000	34.81	0.203820
1073.500	1/2	42.50000	34.84	0.048288

E_r, eV	J	Γ_n, meV	Γ_γ, meV	Γ_f, meV
1086.200	1/2	113.80000	34.79	0.023603
1093.100	1/2	1.43000	33.84	4.632400
1108.600	1/2	49.50000	48.21	0.058211
1114.00*	1/2	22.57900	37.25	0.048412
1126.100	1/2	6.00000	46.95	0.190640
1129.600	1/2	8.90000	42.73	0.101330
1134.000	1/2	1.50000	41.86	1.815300
1151.200	1/2	22.60000	36.87	0.092951
1157.500	1/2	7.40000	47.31	0.040185
1167.100	1/2	21.80000	46.30	0.094149
1183.600	1/2	11.10000	36.45	0.054246
1195.600	1/2	8.80000	40.80	0.712800
1216.500	1/2	24.30000	38.57	0.169130
1222.400	1/2	29.60000	49.75	0.518600
1231.400	1/2	138.00000	42.64	0.264970
1248.000	1/2	31.00000	25.44	0.086215
1254.900	1/2	36.40000	28.19	0.186430
1265.00*	1/2	11.10000	41.74	0.111140
1272.900	1/2	40.40000	45.12	0.000000
1279.800	1/2	4.50000	39.57	0.607470
1288.700	1/2	4.40000	46.59	0.210710
1295.300	1/2	11.90000	41.28	0.012066
1318.00*	1/2	4.20000	37.95	0.081171
1325.600	1/2	56.50000	48.30	0.097085
1327.800	1/2	26.80000	31.45	0.325250
1341.500	1/2	65.90000	35.04	0.062795
1345.50*	1/2	4.20000	40.02	0.194810
1354.200	1/2	4.20000	32.17	0.081171
1362.000	1/2	38.10000	45.04	0.019864
1373.000	1/2	38.09800	40.33	0.018058
1378.000	1/2	13.20000	36.48	0.066676
1385.50*	1/2	13.20000	40.61	0.066676
1391.00*	1/2	13.17900	38.21	0.049279
1397.000	1/2	71.40000	35.60	0.056906
1409.500	1/2	126.00000	45.94	0.073041
1411.500	1/2	24.80000	29.43	0.065625
1419.00*	1/2	4.19870	41.58	0.076642
1436.200	1/2	29.70000	37.73	0.062105
1439.300	1/2	110.00000	39.84	0.042571
1462.90*	1/2	82.80000	40.74	0.020592
1470.000	1/2	10.60000	40.15	0.041097
1481.400	1/2	10.60000	37.61	0.110020
1492.200	1/2	41.10000	36.87	0.032509

*- previously missing resonance

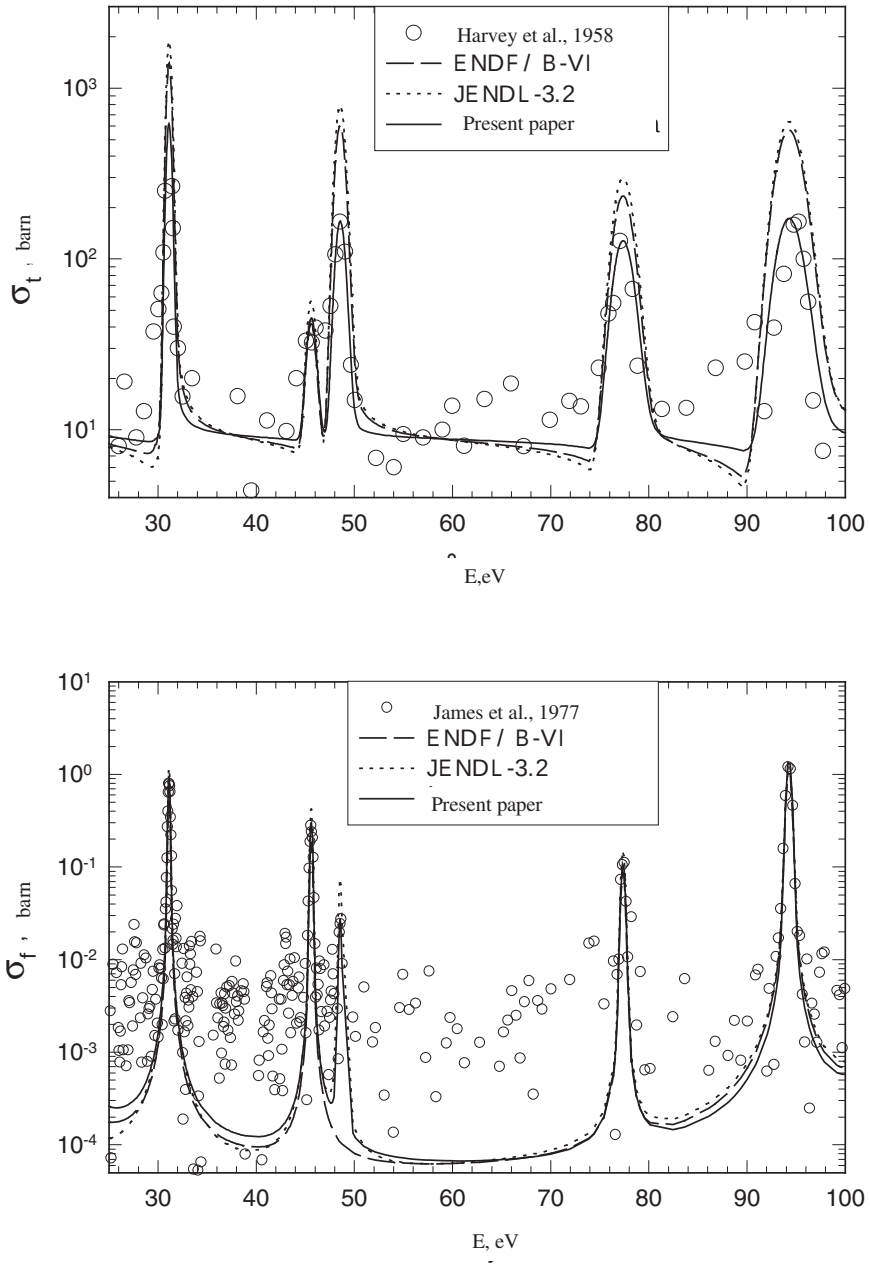

Fig. 2. Comparison of the ^{234}U experimental cross-sections and the ^{234}U cross-sections calculated according to the parameters of various evaluations in the energy interval 25-100 eV.

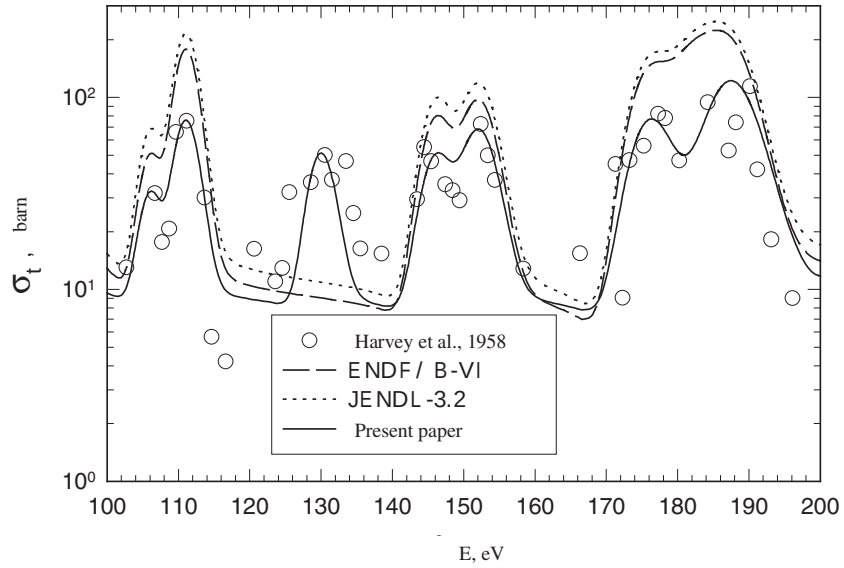

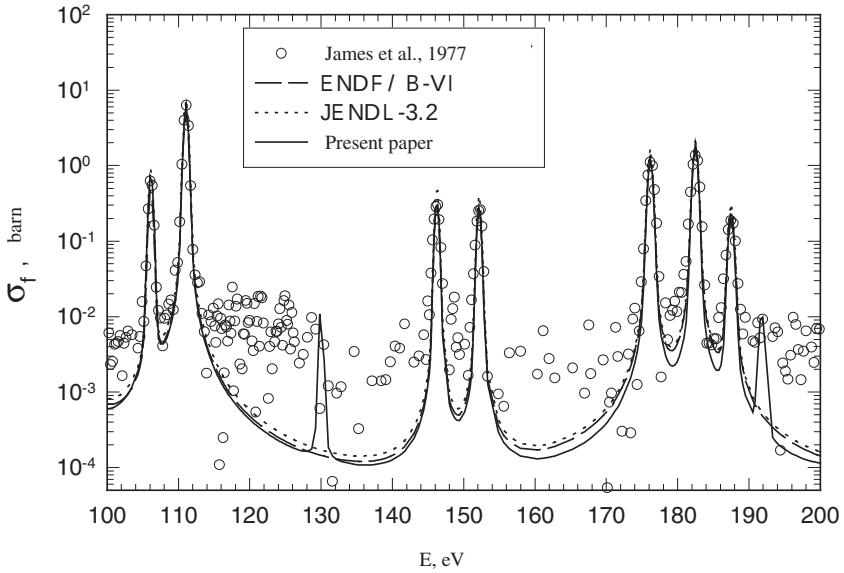

Fig. 3. Comparison of the ^{234}U experimental cross-sections and the ^{234}U cross-sections calculated according to the parameters of various evaluations in the energy interval 100-200 eV.

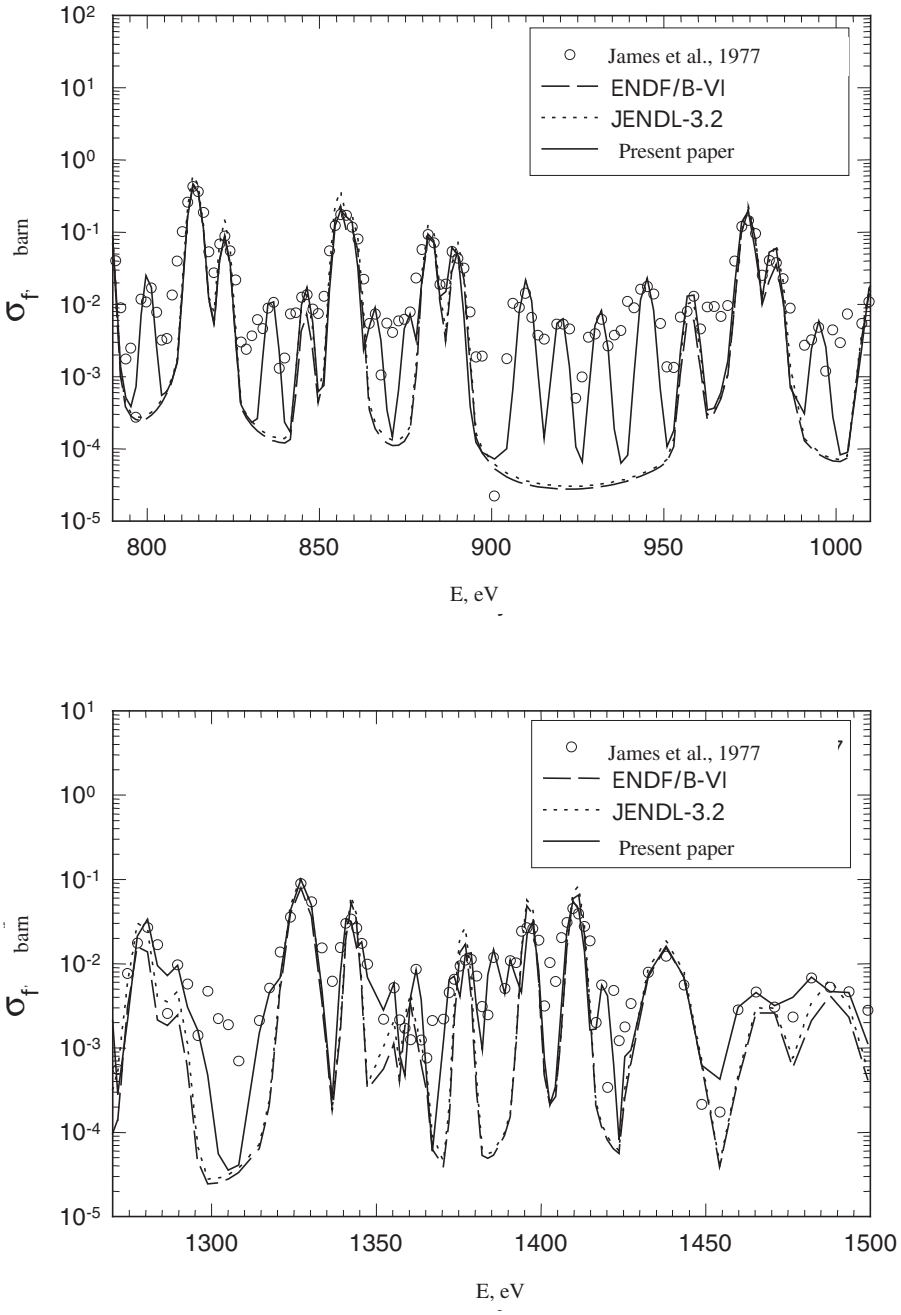

Fig. 4. Comparison of the ^{234}U experimental fission cross-sections and the ^{234}U fission cross-sections calculated according to the parameters of various evaluations in the energy intervals 790-1010 V and 1270-1500 eV.

The cross-sections σ_t (E) and σ_f (E) obtained using the parameters of the present paper (Table 2) better reproduce the energy curve of the experimentally measured cross-sections used for parameterization than the evaluations in [1, 3] and this is shown clearly in Figs 2-4.

In conclusion, it should be pointed out that the resonance parameters of the 25 previously missing resonances were determined mainly on the basis of the σ_f(E) measurements in [4, 6] and so will need to be improved when new total cross-section measurements with good resolution become available.

References

[1] C.L. Dunford, Nuclear Data for Science and Technology, Proc. Int. Conf., Jülich, 1991, 788, Springer-Verlag, 1992, Berlin.
[2] C. Nordbord, M. Salvatores, Nuclear Data for Science and Technology, Proc. Int. Conf., Gatlinburg, Tennessee, USA, 9-13 May 1994, **2**, p. 680.
[3] Japanese Evaluated Data Library, Version 3, JAERI 1319, 1990.
[4] G.D. James, J.W. Dabbs, J.A. Harvey, et al., Phys. Rev. C, 1977, **15**, p. 2083.
[5] S.F. Mughabghab, D.I. Garber, BNL-325, Neutron cross-sections, 1973, **1**.
[6] G.D. James, E.R. Rae, Nucl. Phys. A., 1968, **118**, p. 313.
[7] S.F. Mughabghab, BNL-325, Neutron cross sections, 1984, **1**.
[8] J.A. Harvey, D.J. Huges, Phys. Rev., 1958, **109**, p. 471.
[9] G.B. Morogovskij, Voprosy atomnoj nauki I tekhniki, Ser.: Yadernye konstanty, No. 4 (1991) 52.
[10] G.J. Mc.Callum, J. Nuclear Energy, 1958, **6**, p. 181.
[11] R.H. Odegaarden, R, HW-64866, 1960, **4**.
[12] S. Borzakov, M. Florek, V. Konovalov, et al., Proc. Int. Workshop on Fission and Fission Fragment Spectroscopy, Seyssins, France, AIP Conf. Proc. 447, p. 269, 1998.
[13] C. Wagemans, J. Wagemans, P. Geltenbort, et al., Nucl. Sci. Eng., 1999, **132**, p. 308.
[14] C.L. Dunford, ENDF Utility Codes Release 6.9, IAEA-NDS-29, 1993.

01-10118 (119) [4]
Translated from Russian

UDC 539.17

DETERMINATION OF THE POTENTIAL SCATTERING PARAMETER AND PARAMETERIZATION OF NEUTRON CROSS-SECTIONS IN THE LOW-ENERGY REGION

G.M. Novoselov, L.L. Litvinskij
State Scientific and Engineering Centre for Emergency Response and Control Systems
Ministry for Fuel and Energy, Kiev, Ukraine

DETERMINATION OF THE POTENTIAL SCATTERING PARAMETER AND PARAMETERIZATION OF NEUTRON CROSS-SECTIONS IN THE LOW-ENERGY REGION. Different cross-section parameterization methods in the low-energy region are considered. It is shown that the potential scattering parameter value derived from analysis of experimental cross-section data is dependent essentially on the method used to take account of the nearest resonances. A formula describing this dependence is obtained. The results are verified by numerical model calculations.

Introduction

The potential scattering parameter is one of the characteristics of the nucleus whose determination is given significant attention when analysing experimental data on cross-sections in the resonance region [1]. In the various formalisms this parameter is associated with different values: the optical radius, the potential scattering radius R', the potential scattering parameter R^{∞} (R-matrix approach), the potential scattering phase shift φ (S-matrix approach), etc. However, all these values are interrelated and may be regarded as one and the same parameter.

Most information on the potential scattering parameter is obtained by analysing cross-section data in the resolved resonance region. The problems that occur in this region are usually related to inadequate experimental resolution, possible partial resonance overlap, the Doppler effect, etc.

Nevertheless, however accurate the experimental data and however reliable the knowledge of the other resonance parameters, the reconstruction of the potential scattering parameter can be ambiguous. The cause, as will be shown below, lies in incorrect allowance for the contributions of the nearest resonances.

1. Influence of the number of resonances taken into account on the calculated cross-sections

As an example we shall examine how a difference in the numbers of resonances taken into account affects the neutron cross-section energy dependence. We shall confine ourselves to a very simple case of well isolated resonances of a non-fissionable even-even nucleus,

taking only the s-wave into account. In this case, both S- and R-matrix formalism employ Breit-Wigner formulae to describe the cross-section energy dependence [2-5]. Specifically, the total cross-section and radiative capture cross-section are represented as follows:

$$\sigma_t(E) = \frac{4\pi}{k^2}\left[\sin^2\varphi + \sum_\lambda \frac{\Gamma_{\lambda n}\Gamma_\lambda \cos 2\varphi - 2(E_\lambda - E)\Gamma_{\lambda n}\sin 2\varphi}{4(E_\lambda - E)^2 + \Gamma_\lambda^2}\right], \tag{1a}$$

$$\sigma_\gamma(E) = \frac{4\pi}{k^2}\sum_\lambda \frac{\Gamma_{\lambda n}\Gamma_{\lambda\gamma}}{4(E_\lambda - E)^2 + \Gamma_\lambda^2}, \tag{1b}$$

where k is the wave number, φ is the potential scattering phase shift, E_λ is the energy of the λ-th resonance and $\Gamma_{\lambda n}$, $\Gamma_{\lambda\gamma}$, and Γ_λ are its neutron, radiation and total widths: $\Gamma_\lambda = \Gamma_{\lambda n} + \Gamma_{\lambda\gamma}$.

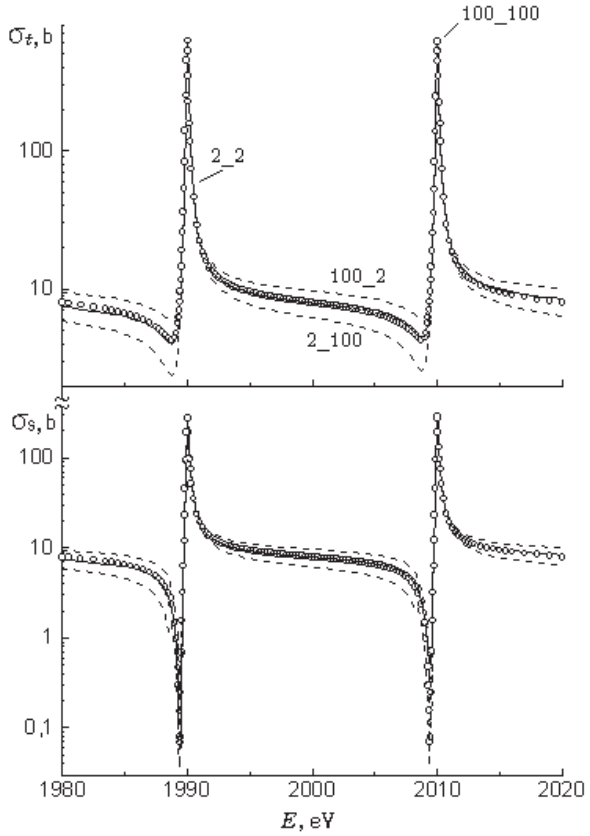

Total neutron cross-sections (top) and scattering cross-sections (bottom) calculated taking into account a different number of resonances to the left and right of E°= 2000 eV: 100_100 - one hundred resonances on each side (o); 100_2 and 2_100 - 100 resonances to the left and 2 to the right and vice versa. The unbroken curves in both figures represent the 2_2 situation where 2 resonances are taken into account on each side.

In the upper figure, points are used to represent the total neutron cross-sections (1a) in the 1980-2020 eV energy range, calculated using a set of equidistant resonances with identical radiation widths ($\overline{\Gamma}_{\lambda\gamma} = \overline{\Gamma}_\gamma$) and reduced neutron widths ($\Gamma^0_{\lambda n} = \overline{\Gamma}^{\,0}_n$) with the following average values:

$$\overline{\Gamma}_n^0 = 0.002 \text{ eV}, \ \overline{\Gamma}_\gamma = 0.1 \text{ eV}, \ \overline{D} = 20 \text{ eV}, \ \varphi = 0.0776. \qquad (2)$$

In these calculations account was taken of 200 resonances arranged symmetrically relative to E^0 = 2000 eV (we designate this case 100_100). The broken curves show the results of two other calculations: for the variant 100_2, which takes into account 100 resonances to the left of E^0 and 2 resonances to the right (upper curve), and for the reverse situation 2_100 (lower curve). Lastly, the unbroken curve (almost coinciding with the points) corresponds to the 2_2 case, taking into account 2 resonances on either side of E^0.

As the figure shows, a difference in the numbers of resonances taken into account on the different sides of the energy level under investigation causes a clear and systematic increase or decrease in the total cross-sections. A similar situation may be observed for the scattering cross-sections $\sigma_s(E) = \sigma_t(E) - \sigma_\gamma(E)$ (lower figure).

Since the resulting deviations are small, the relative changes in the $\sigma_t(E)$ or $\sigma_s(E)$ cross-sections caused by these differences are not significant near the resonances, but they become noticeable between resonances, especially at the interference minima. Therefore, when solving the reverse problem of determining the resonance parameters from experimentally observed cross-sections, one might expect that such differences would have little effect on the parameter values of the resonances themselves but could noticeably influence the value of the phase shift φ to be determined.

It is interesting that, in the radiative capture cross-sections $\sigma_\gamma(E)$, there are practically no differences caused by the different numbers of resonances taken into account.

2. Cross-section parameterization in R-matrix theory

We shall use the R-matrix approximation to evaluate how the numbers of resonances taken into account affect the potential scattering parameter value to be determined. In formal R-matrix theory, cross-sections are expressed as elements of the collision matrix *U,* which in turn is combined with the *R*-matrix [4, 5].

$$U = \Omega P^{1/2} (1-RL^0)(1-RL^{0*})^{-1} P^{-1/2} \Omega, \qquad (3)$$

where *R* is the matrix with the elements

$$R_{ab} = \sum_\lambda \frac{\gamma_{\lambda a}\gamma_{\lambda b}}{E_\lambda - E}; \qquad (4)$$

$\gamma_{\lambda c}$ are the width amplitudes in the channel *c*; Ω, L^0, and *P* are diagonal matrices with the elements $\Omega_c = \exp(-i\varphi_c)$, $L_c^0 = S_c^0 + iP_c$ and $S_c^0 = S_c - B_c$; S_c and P_c are the permeability and shift factors, and B_c is the boundary condition parameter.

In moving from the matrix of channels $(1-RL^{0*})^{-1}$ to the matrix of levels, the elements of matrix (3) for isolated resonances may be represented thus:

$$U_{ab} \approx e^{-i(\varphi_a+\varphi_b)}\left(\delta_{ab} + i\sum_{\lambda}\frac{\Gamma_{\lambda a}^{1/2}\Gamma_{\lambda b}^{1/2}}{E_\lambda - E + \Delta_\lambda - \frac{i}{2}\Gamma_\lambda}\right). \qquad (5)$$

Here

$\Gamma_{\lambda c} = 2P_c\gamma_{\lambda c}^2$ is the partial width of the λ-th resonance in the channel *c*,
$\Gamma_\lambda = \sum_{\tilde{n}}\Gamma_{\lambda\tilde{n}}$ is its total width, and
$\Delta_\lambda = -\sum_c S_c^0\gamma_{\lambda c}^2$ is the energy shift.
For neutral particles $\varphi_c = \phi_c$ is the scattering phase on an impermeable sphere.

The summation in (4) and (5) is carried out for all levels, which is clearly not feasible in practice. More acceptable expressions are obtained if the R-matrix element (4) is broken down into two parts: a resonance part $\tilde{R}_{ab}$ containing the sum for actually observable levels, and a background part R_{ab}^{∞} which takes into account the contributions of all remaining resonances:

$$R_{ab} = \tilde{R}_{ab} + R_{ab}^{\infty}, \qquad (6)$$

$$\tilde{R}_{ab} = \sum_{\lambda}\frac{\gamma_{\lambda a}\gamma_{\lambda b}}{E_\lambda - E}. \qquad (7)$$

Expressions (3) and (5) retain their form pursuant to the formal substitution $R \to \tilde{R}$, $L^0 \to L'$, $S^0 \to S'$, $P \to P'$, $\varphi \to \varphi'$,

where

$$L'_c = \frac{L_c^0}{1 - R_{cc}^{\infty}L_c^0};\ S'_c = \frac{S_c^0 - (S_c^{02} + P_c^2)R_{cc}^{\infty}}{d_c};\ P'_c = \frac{P_c}{d_c};$$

$$d_c = (1 - R_{cc}^{\infty}S_c^0)^2 + (R_{cc}^{\infty}P_c)^2;\ \varphi'_c = \varphi_c - arctg\frac{R_{cc}^{\infty}P_c}{1 - R_{cc}^{\infty}S_c^0}.$$

For l=0 $P_0=\rho$, S_0=0, $\phi_0=\rho$ (here $\rho=ka$; a is the channel radius, it being usual to assume that a=1.35$A^{1/3}$ fm [1]; and A is mass number). Thus, when expression (6) is broken down in the above case of a single neutron channel and a large number of radiation channels, the neutron cross-sections $\sigma_t(E)$ and $\sigma_\gamma(E)$, expressed via the elements of the collision matrix (5), can be represented in the form of expression (1), where

$$\varphi = \rho - arctg(\rho R^{\infty}), \qquad (8a)$$

$$\Gamma_{\lambda n} = \frac{2\rho}{d_0}\gamma_{\lambda n}^2, \qquad \Gamma_{\lambda\gamma} = \frac{2\rho}{d_0}\gamma_{\lambda\gamma}^2, \qquad d_0 = 1+(\rho R^\infty)^2, \tag{8b}$$

and E_λ incorporate the shifts

$$\Delta_\lambda \approx \frac{1}{2}\Gamma_\lambda \rho R^\infty. \tag{8c}$$

In the above expressions, and below, the neutron channel indices in the designation of the element R_{nn}^∞ are omitted.

Owing to their simplicity, formulae of type (1) are used widely for neutron cross-section parameterization in the low-energy region. However, the applicability of these formulae, and of expression (5), is limited by the condition [4]

$$\overline{\Gamma}_n << \overline{D}, \tag{9}$$

where $\overline{\Gamma}_n$ is mean neutron width, and $\overline{D}$ the mean distance between levels. Even if there is only partial resonance overlap, formulae (1) and (5) can not be applied. Thus, even in the 2_100 example looked at above, the scattering cross-section, determined as the difference between cross-sections (1a) and (1b), is negative at the interference minima.

It should be noted that, in contrast to (1a), expression (1b) is obtained from (5) using another approximation - disregarding of the level cross-terms when calculating the elements $|U_{n\gamma}|^2$. However, by using the more detailed Breit-Wigner formulae to calculate the cross-sections, which take into account these terms [6], does not substantially alter the situation: in the 2_100 case, the calculated values for the total cross-section at the interference minima are not equal to the sum of the radiative capture and scattering cross-sections. The reason is that the unitarity of the properties of the collision matrix (5) is not preserved.

A more systematic multi-level R-matrix approach which does preserve unitarity has been proposed by Reich and Moore [7]. In this approach, when selecting the boundary condition B_c=S_c (for l=0 this is equivalent to B=0) in the above example of s-neutron interaction with a non-fissionable even-even nucleus, the diagonal element of the collision matrix (3) may be expressed in the form:

$$U_{nn} = e^{-i2\varphi}\frac{1+iK(E)}{1-iK(E)}, \tag{10a}$$

where

$$K(E) = \frac{1}{2}\sum_\lambda \frac{\Gamma_{\lambda n}}{E_\lambda - E - (i/2)\Gamma_{\lambda\gamma}}, \tag{10b}$$

and the total neutron cross-section and radiative capture cross-section are, respectively,

$$\sigma_t = \frac{4\pi}{k^2}\left(\sin^2\varphi + \frac{(a^2+b^2+b)\cos 2\varphi - a\sin 2\varphi}{(1+b)^2+a^2} \right), \tag{11a}$$

$$\sigma_\gamma = \frac{4\pi}{k^2}\frac{b}{(1+b)^2+a^2}, \tag{11b}$$

where a=Re $K(E)$ and b=Im $K(E)$.

Although in [7] the R-matrix was not broken down into the resonance and background components in expression (6), the approach described there enables this to be done easily. Breaking down expression (6), for the matrix C used in our paper (zero in our example) we must assume $C=P^{1/2}\,R^{\infty}\,P^{1/2}$. R^{∞} being the quadratic diagonal matrix,

$$C_{ij} = P_i R_i^{\infty} \delta_{ij}.$$

Consequently, the diagonal element of the collision matrix takes the form:

$$U_{nn} = e^{-i2\phi}\frac{1+i(K+PR^{\infty})}{1-i(K+PR^{\infty})}, \tag{12}$$

and in the expressions for the cross-sections (11) it must be assumed that a = Re $K + PR^{\infty}$.

It can be shown [8] that, within the limit set by expression (9), the multi-level expressions given above for the cross-sections convert to the corresponding Breit-Wigner expressions. When calculating the cross-sections shown in the figure, multi-level approximation yields virtually the same result as approximation of isolated resonances.

3. Evaluation of resonance contribution

An evaluation of the contribution of different numbers of resonances in expression (4) in the equidistant resonance approximation was carried out in [9]. Here we will examine how such an evaluation may be carried out taking into account both types of fluctuation: both of the width amplitudes and the inter-level distances.

Assuming that the width amplitudes are distributed normally with a zero average (for the widths this corresponds to the Porter-Thomas distribution [10]), averaging (7) with respect to the amplitude distribution yields:

$$\tilde{R} = \overline{\gamma^2}\sum_{\lambda}\frac{1}{E_\lambda - E}, \tag{13}$$

where $\overline{\gamma^2}$ is the average value of the square of the width amplitude.

Let E_0 be the energy of the resonance nearest to the point E. If we assume that it is zero and assign positive numbers in series to the resonances situated to the right of E_0 (with energies of $E_\lambda > E_0$) and negative numbers to the resonances to the left ($E_{-\mu} < E_0$), we get

$$E_\lambda = E_0 + \sum_{i=1}^{\lambda} D_i \,,\; E_{-\mu} = E_0 - \sum_{j=-1}^{-\mu} D_j \,. \tag{14}$$

Let us assume that in the summation in (13) m resonances are taken into account to the left of E_0 and n to the right. Then

$$\tilde{R} = \frac{\overline{\gamma^2}}{\overline{D}} \left(\sum_{\mu=1}^{m} \frac{1}{x - \sum_{j=-1}^{-\mu} d_j} + \frac{1}{x} + \sum_{\lambda=1}^{n} \frac{1}{x + \sum_{i=1}^{\lambda} d_i} \right), \tag{15}$$

where $x = \dfrac{E_0 - E}{\overline{D}}$, $d_i = \dfrac{D_i}{\overline{D}}$.

When averaging (15) with respect to the distributions of the d_i values, it is advisable to switch to new independent variables, namely the summations of the d_i values contained in this expression. According to the central limit theorem, regardless of the specific distribution pattern of the d_i values, the sum of k such terms may be assumed to be normally distributed with a mathematical expectation k and a dispersion $k\eta^2$, where η^2 is the dispersion of d_i. For the Wigner distribution [11]

$$\eta^2 = \frac{4}{\pi} - 1 \approx 0.273. \tag{16}$$

However, here for the sake of simplicity we shall assume that the values $t_k = \sum_{i=1}^{k} d_i$ have a Cauchy distribution:

$$p_k(t) = \frac{I_k}{\pi} \frac{1}{(t-k)^2 + I_k^2} \;;\; I_k^2 = 2k\eta^2 \,. \tag{17}$$

Averaging (15) with respect to the distributions (17) and then to the possible values of x from the (-1/2, 1/2) range yields the following:

$$\tilde{R} = \frac{\overline{\gamma^2}}{2\overline{D}} \left(\sum_{\lambda=1}^{m} \ln \frac{(\lambda - 1/2)^2 + I_\lambda^2}{(\lambda + 1/2)^2 + I_\lambda^2} + \sum_{\lambda=1}^{n} \ln \frac{(\lambda + 1/2)^2 + I_\lambda^2}{(\lambda - 1/2)^2 + I_\lambda^2} \right). \tag{18}$$

Assuming for the sake of specificity that $m<n$,

$$\tilde{R} = \frac{\overline{\gamma^2}}{2\overline{D}} \sum_{\lambda=m+1}^{n} \ln \frac{(\lambda + 1/2)^2 + I_\lambda^2}{(\lambda - 1/2)^2 + I_\lambda^2} \approx \frac{\overline{\gamma^2}}{2\overline{D}} \ln \frac{(n + 1/2)^2 + I_n^2}{(m + 1/2)^2 + I_{m+1}^2} \,. \tag{19}$$

When $m=n\to\infty$, expression (19) yields the known limit value of (4), namely $R=0$ [5]. Therefore, in accordance with (6), the following formula may be used to evaluate R^{∞}

$$R^{\infty}=\frac{\overline{\gamma^2}}{2\overline{D}}\ln\frac{(m+1/2)^2+I_{m+1}^2}{(n+1/2)^2+I_n^2}, \tag{20}$$

where, according to (16), $I_n^2\approx 0.546\,n$.

Since I_n^2 is linearly dependent on n, in most cases the second terms in the numerator and denominator in (20) may be disregarded in favour of the quadratic first terms. Then expression (20) equates to the formula we obtained earlier in our formula for approximation of equidistant resonances [9].

$$R^{\infty}=\frac{\overline{\gamma^2}}{\overline{D}}\ln\frac{2m+1}{2n+1}. \tag{21}$$

4. Numerical verification

The following calculations were performed to verify the formulae obtained. In a process similar to that used to construct the graphs in the upper figure, the total neutron cross-sections $\sigma_t^0\left(E_i\right)$ of an arbitrary nucleus (A=200) were calculated for 160 equidistant values of E_i in the 1980-2020 eV energy range using formulae (1) and (8). Apart from the two resonances shown in the figure, a further 99 resonances on either side of the energy range in question were taken into account. Their energies and the squares of their neutron width amplitudes were obtained using the Monte Carlo method. The general procedure for this is described in detail in [12]. It was assumed that inter-level distances had a Wigner distribution and the reduced neutron widths a Porter-Thomas distribution. The radiation widths were assumed not to fluctuate: $\Gamma_{\lambda\gamma}=\overline{\Gamma}_{\gamma}$. For the mean resonance parameter values, the set in (2) was used, with $R^{\infty}=0$.

The values obtained for $\sigma_t^0\left(E_i\right)$ were assigned 1% error levels; these cross-sections were then treated as if they were experimental. The advantage of such model cross-sections as compared with actual experimental data for any specific nucleus is that we have an a priori accurate knowledge of all the required resonance parameters, thus avoiding further uncertainties.

As before, in each variant of the calculation different numbers of resonances were assigned to the left and right of E^0 (these numbers are given in the first column of the table). Using the least squares method, the value of R^{∞} was varied to fit the calculated cross-sections to the "experimental" cross-sections $\sigma_t^0\left(E_i\right)$. The R^{∞} values obtained in this manner are given in the fourth column of the table. The second and third columns of the table give the values calculated using formulae (20) and (21).

In practice, another parameter is often used instead of R^{∞}, namely the potential scattering radius $R'=a\,(1-R^{\infty})$ [1]. Accordingly, in the fifth column of the table, alongside the values obtained for R^{∞}, the corresponding values for R' are given; the sixth column gives the phase shift values φ (8a). The error levels given in brackets were obtained exclusively using

the least squares method and do not incorporate fluctuation errors due to the limitations on the number of resonances taken into account [5, 13]. As the table shows, on the whole the calculated values of R^{∞} are fully consistent with those determined using (20) or (21).

Potential scattering parameter obtained taking into account different numbers of resonances to the left and right of the energy interval under investigation

Calculation variant	R_{∞}			R', fm	φ
	evaluation using (20)	evaluation using (21)	numerical calculation		
100_100	$0.78 \cdot 10^{-6}$	0.0	$0.76(46) \cdot 10^{-5}$	7.89(1)	0.0776
2_2	0.0010	0.0	-0.0022(15)	7.91(1)	0.0777(1)
1_1	0.0026	0.0	-0.0044(33)	7.93(3)	0.0779(3)
1_5	- 0.0330	- 0.0375	-0.037(2)	8.19(2)	0.0805(2)
5_1	0.0358	0.0375	0.023(1)	7.71(1)	0.0757(1)
1_100	- 0.116	- 0.121	-0.156(4)	9.13(3)	0.0897(3)
100_1	0.118	0.121	0.120(2)	6.95(2)	0.0683(2)
1_2000	- 0.202	- 0.207	-0.228(5)	9.69(4)	0.0953(4)

The calculations also showed that differences in the numbers of resonances taken into account have little effect when determining other resonance parameters. For example, at the 1% accuracy level assigned to the "experimental" cross-sections, for both the 100_1 and 1_100 case, the neutron widths of the two resonances shown in the figure are reproduced with a minimum accuracy of 3%.

5. Discussion and conclusions

The numerical calculations also confirm the other important conclusions which may be drawn from formulae (20) and (21). Thus, the potential scattering parameter may be determined correctly not only within the limit $m=n\to\infty$, but even where there are small but equal numbers of resonances ($m=n$) on either side of the energy under investigation, if the local strength functions are identical. Conversely, if these numbers are not equal, errors inevitably arise.

According to (20) or (21), if the relationship between m and n changes from $m<<n$ to $m>>n$, the parameter R^{∞} may, in principle, change from $-\infty$ to $+\infty$, which corresponds to a change in the phase in (8a) over the whole period from $\rho-\pi/2$ to $\rho+\pi/2$. Naturally, a spread of this kind is unlikely in practice, although sometimes such errors can be significant. Usually, when studying neutron cross-sections in the very low energy region (e.g. thermal), there are a large number of known resonances in the higher energy side but no information is available on resonances on the lower energy side. This situation does not change significantly even when one, two or three negative levels are introduced, with a view to achieving a better description of the cross-sections of a series of nuclei [1].

Finally, we would note that, although in this paper we have used a very simple case of s-neutron interaction with an even-even nucleus as an example, the results obtained are also

valid for the general case of non-zero spin and an arbitrary partial wave, since each system of resonances J^{π} with a specific moment J and parity π may be studied independently. Clearly, these conclusions are also valid for overlapping resonances.

This work was carried out with support from the International Atomic Energy Agency.

References

[1] S.F. Mughabghab, Neutron Cross Sections, Acad. Press Inc. (1987).
[2] R.L. Kapur, R.E. Peierls, Proc. Roy. Soc., 1938, V. A166, p. 277.
[3] D.B. Adler, F.T. Adler, Proceedings Conference on Breeding in Fast Reactors, Argonne, ANL-6792 (1963) p. 695.
[4] A.M. Lane, R.G. Thomas, Rev. Mod. Phys., V. 30, No. 2 (1958) p. 257.
[5] J.E. Lynn, The Theory of Neutron Resonance Reactions, Oxford, Clarendon Press (1968).
[6] P.F. Rose, C.L. Dunford, ENDF-6 Formats Manual, IAEA-NDS-76 (1992).
[7] C.W. Reich, M.S. Moore, Phys. Rev., V. 111 (1958) p. 929.
[8] G.M. Novoselov, V.M. Kolomiets, Voprosy atomnoj nauki i tekhniki, Ser.: Yadernye konstanty, No. 5 (44) (1981) p. 10.
[9] G.M. Novoselov, L.L. Litvinskij, Yadernaya fizika, V. 60, No. 4 (1997) p. 1.
[10] C.E. Porter, R.G. Thomas, Phys. Rev., V. 104 (1956) p. 483.
[11] E.P. Wigner, Proceedings Conference on Applied Mathematics, Toronto, 1959, Univ. Toronto Press (1959) p. 174.
[12] G.M. Novoselov, V.P. Vertebnij, Preprint KIYaI-77-9, Kiev (1977).
[13] G.M. Novoselov, Yadernaya fizika, V. 58, No. 1 (1995) p. 21.

01-10118 (121) [5]
Translated from Russian

UDC 539.173.8

NEUTRON AND γ-EMISSION FROM FISSION FRAGMENTS

O.T. Grudzevich
Institute of Nuclear Power Engineering, Obninsk, Russia

NEUTRON AND γ-EMISSION FROM FISSION FRAGMENTS. The statistical model of nuclear reactions is applied to describe the fission fragment neutron and gamma emission characteristics for spontaneous fission of ^{252}Cf and fission of ^{235}U by thermal neutrons. Averaged excitation energies of fission fragments were obtained from experimental neutron multiplicities. The observable characteristics of an emission are reproduced in a wide range of complementary fragments' total kinetic energies and fragment masses. Observed averaged spins are also reproduced. The fractional independent isomeric yield calculation method, based on the gamma-cascade model, is used to describe experimental data for the ^{235}U(n_{th},f) and ^{238}U(α,f) reactions. The influence on the calculated isomeric yields of two opposing assumptions regarding the nuclear population spin distributions - one based on the rotational degrees of freedom and one on the internal degrees of freedom of completely accelerated fragments - is investigated.

Because of the complexity of the fission of atomic nuclei, owing to the fundamental redistribution of charge and mass and the formation of highly deformed and highly excited fragments, a detailed description of the dynamics and mechanism of this process has not yet been produced. In this context, the use of consistent theoretical models to describe the fission characteristics identified is a step forward towards a unified fission theory. Such models have been used successfully in research into the properties of other reactions.

In this paper we have chosen to study the pre-neutron fission fragment formation processes and de-excitation (discharge) of such fragments through neutron and gamma emission. It seems obvious that fragment discharge must be statistical in nature, since the fission process itself passes through the compound nucleus stage. Consequently, use of the statistical model of nuclear reactions [1-3] seems an entirely logical step, though it is complex from a practical point of view.

The observable characteristics of excited fragment discharge are derived by averaging with respect to many variables - charges, masses, excitation levels, kinetic energies, total angular momenta, etc. Therein lies the complexity of describing these characteristics in terms of a theory, since a large number of parameters are included in the calculations. The situation is made more complex by the fact that the nuclei which comprise the fission products are, as a rule, only formed during this process and their properties are not well known.

In order to apply the statistical model of nuclear reactions successfully to describe the properties of fission fragments, we must answer one basic question: what is the distribution of the excitation energies and the total angular momentum of these fragments? Once this distribution is known, and the difficulties caused by the undeterminacy of the parameters of nuclei with surplus neutrons have been overcome, virtually any of the observable characteristics of fission fragment discharge can be calculated, i.e. neutron and γ-ray spectra and multiplicities, isomeric ratios and even nucleus yields.

By studying the formation process for the isomeric states of fission fragments of atomic nuclei, we can obtain information on the formation mechanism and the total angular momentum values of the fragments. The practical aspect of this research lies in the fact that, at the current stage of development of nuclear power, when we are faced with the task of creating a new generation of reactors with increased reliability, and research is being done into the possibility of reprocessing and destroying radioactive waste from reactors now in operation, we need more detailed and reliable data on the activity levels and composition of spent fuel.

In this paper, a theoretical approach which has been used successfully to calculate isomers in various reactions [4-7] and γ-ray spectra from fragments produced by spontaneous fission of ^{252}Cf [8] is used to calculate the isomer yields for fission fragments from the ^{235}U(n_{th},f) and ^{238}U(α,f) reactions. In order to test the feasibility of using the statistical model of nuclear reactions to calculate the emission properties of fission fragments, experimental data on γ-ray and neutron emission from fission fragments over a wide range of total kinetic energies and masses were analysed, the mean excitation energies of primary fragments were obtained and the energy balance of those energies checked.

1. THEORETICAL MODEL

The statistical model of nuclear reactions in Hauser-Feshbach-Moldauer formalism [1-2] and its generalization for γ-decay of excited nuclei - the cascade-evaporation model [3] - are used successfully for theoretical analysis of γ-ray and particle emission, and of isomeric level yields in various nuclear reactions [4-8]. Use of the statistical model of nuclear reactions and the cascade-evaporation model to describe processes related to emission from fission fragments is hampered by a number of circumstances. The most important ones are as follows:

1. Since the total kinetic energy of a pair of additional fragments varies within the range 140-220 MeV, the excitation energies of the fragments may vary from 0 to 50 MeV. The distribution of excitation energies between additional fragments is not known;

2. A major change in the excitation energies must cause significant changes in the population distributions for the total angular momenta, and the mechanism by which these are generated in fragments is not well known;

3. The reproduction in the calculations of the observable mean fission characteristics requires the inclusion of a large number of nuclei in the calculations. Consequently, special libraries of source data need to be created, different from the data libraries used to calculate other reactions.

The number of γ-rays (multiplicity) $S_\gamma(Z,A,U,\varepsilon_\gamma)d\varepsilon_\gamma$ with energy ε_γ in the energy range from ε_γ to $\varepsilon_\gamma+d\varepsilon_\gamma$ emitted by the nucleus (Z,A) at the excitation energy U is calculated using the cascade-evaporation model. The number of γ-ray, emitted by fragments in the mass number range from A_1 to A_2, per single fission event, can be calculated using the formula

$$S_\gamma(\varepsilon_\gamma)d\varepsilon_\gamma = \sum_i Y_i \cdot \int_0^{U_m} S_\gamma(Z_i, A_i, U, \varepsilon_\gamma) f(U) dU \cdot d\varepsilon_\gamma \,, \qquad (1)$$

where Y_i is the independent yield of the fragment (Z,A) up to emission of neutrons, f(U) is the primary population distribution function for the excitation energy. The summation is performed for all the fragments in the specified mass range. The value obtained from formula (1) we will call the γ-ray spectrum. A similar expression can be used to calculate neutron spectra.

The total number of γ-rays μ and neutrons ν, emitted by fragments with mass A is calculated by integrating the corresponding multiplicities and subsequent summation with weighing of independent yields for all nuclei with the given mass number:

$$\mu,\nu(A) = \sum_Z Y(Z,A) \int_0^{U_m} f(U)dU \int_0^{E_m} S_{\gamma,n}(Z,A,\varepsilon,U)d\varepsilon \,. \qquad (2)$$

The basic equation of the statistical model of nuclear reactions are well known and are implemented in many computer programs as a standard procedure (GNASH [9], STAPRE [10]). Thus it is not necessary to give the basic formulae here. We will merely point out that the results of emission spectrum calculations using the statistical model of nuclear reactions are determined by two model functionals: the level density of excited nuclei in the entrance and exit channels of the reaction and the penetrabilities for particles and γ-quanta. The level density is calculated using the version in [11] of the generalized superfluid nucleus model with parameters from the specially created LDPL-98 library, which contains asymptotic parameters for the level density *a*, shell corrections δW, corrections for even-odd differences δ, energies of quadrupole phonons ϖ_{2+}, and schemes of discrete excitation levels for almost two thousand nuclei. The penetrability coefficients for neutrons are calculated using an optical model of the nucleus with the set of global optical potential parameters in [12].

Source data for calculations

LDPL-98 LIBRARY. Theoretical calculations of fission fragment disintegration taking into account the laws of conservation of total angular momentum and parity are very laborious, since a large amount of source data is needed, primarily on the excitation characteristics: level density and discrete level schemes. The situation is complicated by the fact that the fragments are neutron-excess nuclei for which, as a rule, no experimental information on the neutron resonance density is available.

A lot of work has been done by an international expert group which, under the aegis of the IAEA, has set up a library of source data for theoretical calculations of nuclear reaction cross-sections [13]. Unfortunately, this library is devoted only to nuclei for which information on the neutron resonance density is available, and the recommended data file on discrete levels prepared from the file in [14] contains a number of fundamental and technical errors.

In order to calculate the cross-sections and spectra generated by transformations of nuclei far from the stability line, a new version of the LDPL-98 library of discrete level schemes and level density parameters containing information on two thousand nuclei. When setting up the library, the advantages of the generalized superfluid nucleus model, which takes into account shell, collective and superfluid effects, became fully apparent. In the generalized superfluid nucleus model variant in [11], it is assumed that four values are needed to calculate the level densities: a - the asymptotic level density parameter, δ - the effective correction for even-odd differences, δW - the shell correction and ω_{2+} - the quadrupole phonon energy, which may be assumed to be identical with the energy of the first level where $J^{\pi}=2^{+}$ for even-even slightly deformed nuclei. The latter two values are determined from experimental data not related to the level density. The shell corrections are calculated using the liquid drop model of the nucleus, employing experimental nucleus masses. The effective correction for even-odd differences in the level density is determined by fitting the calculated dependencies of the number of levels on the excitation energy to experimental data on discrete levels. Here we can see the advantages of the generalized superfluid nucleus model. On the one hand, the value to be obtained is slightly dependent on the assumed value of the asymptotic level density parameter and the discrete level schemes available can be used in those cases where no data on the neutron resonance density is available. On the other hand, the values obtained are satisfactorily described the simple systematics in [11] and, for nuclei, where we have no discrete level scheme or it is insufficiently reliable, these systematics may be used. The second generalized superfluid nucleus model parameter is satisfactorily systematized by the dependency $\tilde{a} = 0.073A+0.115A^{2/3}$, and we may expect that the estimate of this value will be satisfactory for nuclei on which no experimental data on the level density is available and for which it is unlikely such data will become available in the near future. The reliability of the LDPL-98 fission fragment data is discussed below.

RADIATION STRENGTH FUNCTIONS. For the majority of fission fragments no experimental photoabsorption cross-sections are available and in calculations the systematics of the parameters of the giant dipole resonance have to be used. The available data on the energies E_r, widths Γ_r and maximum cross-sections σ_r [15]; derived from a description of

experimental data on photoabsorption cross-sections using the Lorentz formula, are shown in Fig. 1. These parameters are satisfactorily described by the formulae:

$$\begin{aligned} \sigma_r &= 0.085 \cdot A^{5/3}, \text{ mb} \\ E_r &= 51/A^{1/4}, \text{ MeV} \\ \Gamma_r &= 6.1 - 0.012 \cdot A, \text{ MeV}. \end{aligned} \qquad (3)$$

Resonance splitting for highly deformed nuclei was not taken into account when obtaining these formulae. The available data can clearly be described using the simple equations in expression (3), with an accuracy of at least 50%. Thus, the strength functions in the 10-20 MeV energy may be calculated with approximately the same level of accuracy using expression (3).

The discharge of excited nuclei produces a large quantity of soft (ε_γ = 1-3 MeV) photons and we must extrapolate the strength functions obtained for the giant resonance region (10-20 MeV) to this energy region. The estimates yielded by the various methods for calculating f_{E1} for low energies may differ by orders of magnitude, even when the same giant dipole resonance parameters are used. The peculiarity of the KMF-PT method proposed in [16] is that the parameter T is selected in such a way as to reproduce the maximum values of f_{E1} observed in the characteristics of the transitions between discrete levels. It is assumed that it is precisely the most intensive transitions which generate the spectra observed in the reactions. The reasons for the existence of a distinct “step” in the maximum values of the observable strength functions at $E_\gamma < 2$ MeV, which differ according to the nature of the nuclei (superallowed transitions) [16], remains uncertain.

The distributions of the experimental strength functions of the dipole transitions obtained in [16] using the data from [17] for various mass number ranges are shown in Fig. 2. For all emitter nuclei mass ranges and both types of transition, there is a clear upper limit for the values of $f_{E,M1}$ - the superallowed dipole transitions. Transitions with different mean strength function logarithms also occur - a peculiar splitting of the distribution which grows as the mass number increases. The statistically significant values of $f_{E,M1}$ lie within the range 10^{-15}-10^{-8} MeV^{-3}. In this case, any form of averaging of the gigantic differences leads to a situation where the average values $\langle f_{E,M1} \rangle$ are close to the maximum values $f^{max}_{E,M1}$. In this article, we will use the KMF-PT method which describes the observable f^{max}_{E1} values.

2. NEUTRON EMISSION

Neutron spectra are clearly reproduced in the statistical model of nuclear reactions if the reaction passes through a compound nucleus, i.e. there are no links between the entrance and exit channels of the reaction, apart from those links that are determined by the laws of conservation of energy, total angular momentum and parity. From this point of view, we may assume that the formation process for fragments and the generation of their properties fully meets the requirements for application of the statistical model of nuclear reactions.

In normal nuclear reactions (such as (n...α,xn)), the excitation energy of the neutron-emitting nucleus is determined with great accuracy. In fission, the excitation energies of fragments may have a wide range of values from 0 to 50 MeV. Therefore, the first step in using the statistical model of nuclear reactions is therefore to determine the mean excitation energies of the fragments.

EXCITATION ENERGIES OF FRAGMENTS. Information on the excitation energies of fission fragments prior to neutron emission may be derived from data on the mean numbers of neutrons, assuming that the neutrons are emitted by fully accelerated and formed fission product nuclei [8]. The reliability of the data obtained using such an approach is determined by the fact that the number of neutrons is unambiguously dependent on the excitation energy of a given nucleus. In order to demonstrate typical dependences of the number of neutrons emitted ν on the excitation energy of the nucleus U, nuclei were selected corresponding to the fission fragments of ^{252}Cf with the largest (^{121}Cd) and smallest (^{130}Sn) multiplicities of neutrons, and the maximum yield (^{140}Xe) and a value of ν corresponding to the ν(U) dependence plateau (Fig. 3). The maximum error in determining the excitation energy may be 2-3 MeV and is due to the fact that the ν(U) dependence contains plateaux for the values ν=1 (Fig. 3). Indeed Fig. 3 shows that, if the number of neutrons is equal to 1, then the inaccuracy in the derived excitation energy is 2-3 MeV. This inaccuracy will drop if, in the procedure, we use the dependence not for one nucleus, but an averaged dependence for several fragments.

For four fissile systems - fission of ^{233,235}U and ^{239}Pu nuclei by thermal neutrons and spontaneous fission of ^{252}Cf, the probabilities of emission of different numbers of neutrons by fission fragments at excitations of up to 80 MeV were calculated. Calculations were carried out for product nuclei with A=70-160 with yields of at least 0.1 of the maximum yield of fragments with a specific mass. Source data from the LDPL-98 level density parameter library were used. The distributions of the yields of fragments of a particular mass and charge Y(Z,A) were calculated using the model in [18] based on experimental data. The dependence ν(Z,A,U) were averaged with weighting of yields and then, by comparing the calculated values of ν(A,U) and the experimental values of <ν(A)> [18-20], the values of <U> were determined. Fig. 4 shows the mean fission fragment excitation energies obtained and the mean neutron multiplicities used [18-20] relative to the fragment masses. Clearly, the sawtooth structure of <ν(A)> must be and is repeated in the dependences <U(A)>. It is important to emphasize that the experimental values of <ν(A)> are often insufficiently accurate. Thus, for example, for ^{252}Cf in the region A = 120 the accuracy is 15%, and for ^{235}U in the mass region A=115-125 the variation in the data given by different authors is 40% [18].

The dependences of the derived mean excitation energies of fragments with different masses on the mean number of neutrons are shown in Fig. 5. In addition, data from [21] for the various total kinetic energies of the fragments are used. It should be noted that, in seven cases, the <U>(ν) dependences obtained are very similar. Moreover, they can all be described using the formula:

$$<U>=5+4\nu+\nu^2. \qquad (4)$$

The non-linearity of function (4) shows that the mean energy removed by the neutrons increases as their number grows as the residual nucleus approaches the stability line. In subsequent calculations, the mean energies obtained for fragments with specific masses at mean total kinetic energies were used, and the mean square deviation of the Gaussian distribution was assumed to be equal to 5 MeV, based on the fact that the dispersion of full kinetic energies is approximately 10-12 MeV and the width of the distribution has a slight influence on the derived mean excitation energies.

ENERGY BALANCE. The procedure for deriving the mean excitation energies of fragments does not take into account the fission energy balance; therefore the results may be verified by comparing the values of the total mean energies of additional fragments $<U(A_L,A_H)> = <U(A_L)>+<U(A_H)>$ with the free energy $TXE(A_L,A_H)$ calculated as follows:

$$TXE(A_L, A_H) = Q(A_L, A_H) - TKE(A_L, A_H), \qquad (5)$$

where Q is the reaction energy, TKE is the total kinetic energy, and A_L and A_H are the masses of the light and heavy fragments respectively. In the calculations experimental values for $TKE(A_L,A_H)$ from [19, 22] were used and nucleus binding energies from [23]. The comparison of $<U(A_L,A_H)>$ and $TXE(A_L,A_H)$ is shown in Fig. 6 for fission of ^{252}Cf and ^{235}U nuclei. The satisfactory level of agreement of the values shows, firstly, that the procedure for deriving the mean excitation energies of fragments does not contradict the law of conservation of energy and, secondly, that the free fission energy is almost completely converted into the excitation energy of the fragments. The fact that $TXE(A_L,A_H)$ is about 10 MeV higher than $<U(A_L,A_H)>$ for ^{235}U in the mass-symmetric fission region may be explained by the considerable inaccuracies in $<\nu_{exp.}>$.

The verification of the energy balance would be incomplete if we did not break down the energy received by the fragments into the components removed by neutrons and γ-rays. On the one hand, the widely held assumption that the γ-ray energy E_γ constitutes approximately half the neutron binding energy $E_\gamma \approx B_n/2$ may be verified and, on the other hand, the method in [8] for deriving the mean excitation energies of fragments may be verified once again.

Using multidimensional calculation matrices for the neutron spectrum $S_n(Z,A,U,\varepsilon_n)$ and the γ-ray spectrum $S_\gamma(Z,A,U,\varepsilon_\gamma)$, we can obtain theoretical values for any of the observable characteristics of fragments [8]. In particular, the energy removed by neutrons and γ-rays may be calculated as follows:

$$\left.\begin{array}{c} E_n = \nu(<\varepsilon_n> + <B_n>) \\ E_\gamma = \mu <\varepsilon_\gamma> \end{array}\right\}, \qquad (6)$$

where the mean energies ($<\varepsilon_n>$ and $<\varepsilon_\gamma>$) and multiplicities (ν and μ) are obtained from the corresponding spectra.

Thus, comparing $<U(A)>$ with (E_n+E_γ) and $E_{\gamma\,calc.}$ with c $E_{\gamma\,exp.}$ we can demonstrate that, in the approach used, all the energy emission channels are in fact correctly taken into account.

Fig. 7 compares the fragment excitation energies with the energy removed by neutrons and γ-rays for fragments in the four fissile systems. Clearly, the balance of the energy received by the fragments during fission and the energy removed during the discharge of these fragments is maintained, as was to be expected. A few comparatively small discrepancies may be explained by the fact that the energy balance is checked using mean values.

The γ-rays emitted by fission fragments remove up to 50% of the excitation energy (Fig. 7), and therefore it is very important to check that the description of the radiation discharge channel in the theoretical model is correct. The experimental mean γ-ray energies in [24, 25] are compared with the calculated values in Fig. 8 for fragments generated by fission of ^{235}U and ^{239}Pu nuclei by thermal neutrons. A satisfactory level of agreement is achieved between $E_{\gamma\ calc.}$ and $E_{\gamma\ exp.}$, although the structure in $E_{\gamma\ exp.}(A)$ is not reproduced in the calculation. Curiously, E_γ constitutes between 20 and 90% of the neutron binding energy.

LEVEL DENSITY. The derived values of <U(A)> are dependent on the parameters of the models used to calculate the neutron and γ-spectra, primarily on the level density parameters. Where the neutron spectra in the calculations are poorly reproduced, the values of the mean excitation energies will be heavily distorted. Consequently, it is both important and interesting to verify the description of the fission fragment neutron spectra. The nuclear reactions calculated using the statistical model and employing the parameters from the LDPL-98 library [8] are compared with the experimental neutron spectra [26], in Fig. 9. The satisfactory level of agreement between the spectra indicates that the data in the LDPL-98 library are correct and that the statistical model of nuclear reactions may be used successfully to describe the emission properties of fission fragments.

The LDPL-98 parameters may be indirectly verified by comparing them with the empirical values obtained from the neutron spectra in [19, 26] (Fig. 10). The most convincing evidence of the predictive capabilities of the level density model in [11] used to create the LDPL-98 library is the detailed reproduction of the shell structure for fragments with A=130. The shortcomings of the method for deriving the level density parameters used in [19, 26] should be noted. Firstly, data are obtained for the neutron-emitting nuclei, whereas it is well known that the spectra are determined by the parameters of the residual nuclei; secondly, a procedure exists for deriving the absolute value of the level density from the emission spectra [27], but it was not used; and thirdly, in the expression $U=at^2$ used to obtain the parameter “a” the temperature “t” does not correspond to the value derived from the spectra using the Le Couteur-Lang equations [28].

NEUTRON MULTIPLICITIES. The correlations between the excitation energies were obtained for the mean values of the total kinetic energies of pairs of additional fragments. Since experimental data on $\nu_{exp.}(TKE,A)$ are available [19, 20, 29], we can verify these correlations over a wider excitation range. Since the $TXE(A_L,A_H)$ values are the sum of the excitation energies of two fragments, the distribution of this energy between the fragments will influence the calculated dependences $\nu_{calc.}(TKE,A)$. In the calculations, the excitation energy for a given fragment is taken to be equal to:

$$U(A_{L,H}) = [Q - TKE(A_L, A_H)] \frac{< U(A_{L,H}) >}{< U(A_L, A_H) >}, \quad (7)$$

i.e. proportional to the correlation obtained above for the mean kinetic energies. The experimental [19] and calculated values of ν(TKE,A) are compared in Fig. 11 for six pairs of additional fragments generated by spontaneous fission of ^{252}Cf, four light fragments and mass-symmetrical fission. The level of agreement between the $\nu_{exp.}$(TKE,A) and $\nu_{calc.}$(TKE,A) dependences is suitably convincing over a wide range of total kinetic energies. The excitation energies of individual fragments also vary in the range from 0 to 40 MeV. Some discrepancies in the absolute values are due to differences in TXE and <U> (see Fig. 6). A similar comparison of the data from [29] with the calculation results for ^{235}U is shown in Fig. 12. Since the data in [20] were used to derive the mean energies and the $\nu_{exp.}$(TKE,A) values are taken from [29], the calculated dependences had to be renormalized to take account of the differences in <ν> in Refs [20] and [29]. For six pairs of additional fragments generated by fission of ^{235}U by thermal neutrons, agreement was achieved between the calculated and experimental values of ν(TKE,A) over a wide range of total kinetic energies (150-190 MeV) and fragment masses (90-146) (Fig. 12). We may therefore conclude that, in the vast majority of cases, fission fragments emit neutrons while in a state of equilibrium deformation. The sharp reduction in the $\nu_{exp.}$(TKE,A) values at TKE< ~150 MeV (Fig. 11), shows that, for some reason, the fragments receive less excitation.

Given the satisfactory description of the neutron spectra and multiplicities, and the high level of agreement of the level density parameters for fragments with A≈130, the almost twofold divergence in mean neutron energies $<\varepsilon_n>$ for masses ranging from 125 to 135 is unexpected (Fig. 13). In this connection, the experimental values of $<\varepsilon_n>$≈1.5-1.8 MeV at emitter nuclei excitation energies of 5-7 MeV seem unjustifiably large. For fragments with other masses, the level of agreement of $<\varepsilon_n>_{exp.}$ and $<\varepsilon_n>_{calc.}$ is entirely acceptable.

THERMODYNAMIC EQUILIBRIUM. If we know the mean excitation energies of additional fragments, we can verify the energy condition for splitting of a fissile nucleus, i.e. answer the question as to what proportion of the free fission energy is passed on to a given fragment and/or in what proportions this energy is divided between additional fragments. The thermodynamic equilibrium condition is often used to answer this question, i.e. the fact that the temperatures of the light t_L and heavy t_H fragments is the same at the point of splitting. From this condition it follows that the excitation energy of a given fragment will be equal to:

$$U_{L,H} = U/(1 + a_{H,L}/a_{L,H}), \quad (8)$$

where U is the total excitation energy of the additional fragments and *a* is the level density parameter. Since in the level density model in [11] the parameter *a* is dependent on the excitation energy, an iterative procedure was used to solve equation (8).

Fig. 14 compares the "true" excitation energies of fragments (Fig. 6) and the values obtained using expression (8), with $U=<U(A_L,A_H)>$, for the four fissile systems. The distributions of the $U_{L,H}$ values are similar to the <U(A)> distributions because the level

density parameters are dependent on the excitation energy and shell corrections. As was to be expected, using formula (8) for spontaneous fission is not acceptable because the fissile nucleus is in the ground state. For induced fission the results are incomparably better, despite the fact that the excitation energy of the compound nucleus attributable to a single fragment (3-4 MeV), comprises a small part of its total excitation energy.

3. γ-RAY EMISSION

The first peculiarity of the experimental γ-ray spectra of fragments generated by spontaneous fission of ^{252}Cf, which is discussed in detail in [30], is the major difference in the shape of the spectrum for fragments with A=126-136 from the shape of the spectra for fragments with other masses (Figs 15 and 16). Indeed, in the spectra of fragments in the vicinity of the doubly-magic nucleus ^{132}Sn there is a significant surplus of γ-rays with energies in the 3-8 MeV range. An explanation of this fact is given in [19], based on an analysis of neutron spectra, from which it appears that the level density parameters of nuclei in the vicinity of the doubly-magic nucleus ^{132}Sn have a clearly defined shell structure (see Fig. 10). The second characteristic feature of the measured spectra is the essential similarity in the shape of the spectra of heavy and light fragments (Fig. 17), apparently caused by the fact that the radiation source is ambiguously identified in the measurements [30].

In this paper we are primarily interested in the level of agreement of the slope of the experimental γ-spectra [30] and the calculated spectra, which were obtained using two methods for calculating the strength functions of electric dipole transitions - the KMF-PT method and Lorentz dependence method. Figs 15 and 16 compare the results spectrum calculations employing experimental data from [30] for various mass ranges of heavy and additional light fragments. Clearly, the change in the method for calculating the strength functions yields a more acceptable level of agreement in the slopes of the spectra, especially for heavy fragments. The most representative changes are those for the A=126-130, 142-146, 138-142 and 146-150 ranges. It is noteworthy that, for the A=126-130 and 130-134 ranges in the vicinity of the doubly-magic fragment, with no extra effort, the surplus of γ-rays with energies of 3-8 MeV is well reproduced.

Taking into account the aforementioned peculiarity of the measurement method, we will conduct our subsequent analysis by comparing the data for additional fragments with the corresponding calculated spectra obtained as mean values with weighting of yields of heavy and light fragments (Fig. 17). In this comparison, there is an additional uncertainty caused by possible differences in the observable and calculated dependences of the γ-ray multiplicities on the fragment mass, in other words uncertainties in the normalization coefficients for the calculated spectra. Fig. 17 shows that a satisfactory description has been achieved for the observable γ-spectra for all fragment masses in the $E_\gamma \geq 1$ MeV energy range. What differences there are may easily be eliminated by varying the normalization coefficients for the calculated spectra of the additional fragments, since the required shapes are to be found in the components comprising the total spectra (see Figs 15 and 16).

It should be noted that, for all cases (Figs 15 to 17), the calculated spectra are always lower than the experimental values at low radiation energies $E_\gamma < 1$ MeV. If, despite the

complex dependence of the detector efficiency on the energy in this range, the experimental data are accurate, analysis of the divergences may provide interesting information on the properties of excited states of fission fragments. For example, we will be able to evaluate the contribution of the rotational degrees of freedom to formation of the initial fragment spins, since the most natural explanation for the observed divergences may be the failure to take account in the calculations of the enhanced probability of γ-decay during transitions between members of rotational bands. In this connection, it would be useful to increase the mass resolution of the spectra in [30]. Fig. 18 shows the effect of the method for calculating f_{E1} on the calculated γ-spectra for the fission of ^{235}U by thermal neutrons. The γ-ray emitted by fragments with masses of A=80-160 were taken into account in the calculations. Clearly, the description of the experimental data in [31] is significantly improved by using the KMF-PT method [16], which is therefore used in the calculations. The reasons for and possible ways of eliminating the discrepancies in the calculated and experimental spectra for the energies $E_\gamma \leq 1$ MeV are discussed in [8] and in connection with the situation shown in Fig. 19.

γ-RAY MULTIPLICITIES. The experimental γ-ray multiplicities $\mu_{exp.}$ in [24, 25] relative to fragment mass have a "sawtooth" structure similar to the dependence $<\nu(A)>$ (Fig. 19). The calculations do not reproduce this dependence. The reason for the discrepancies may be that, in the calculations, the radiation mechanism, for the transitions between the members of rotational bands of excited nuclei was not taken into account. A qualitative corroboration of this assumption may be the characteristic rise in the number of γ-rays emitted as we move further away from the spherical fragment with A=130 towards the deformed fragments with A=140-150 (Fig. 19).

Let us continue our analysis of the possible reasons for the discrepancies between the calculations and the experiment by comparing the energies removed by γ-rays relative to the total kinetic energy of pairs of additional fragments. In the calculations, the excitation energy of a fragment was correlated with the total kinetic energy of the pair in the same way as for neutrons, i.e. using formula (7). Figs 20 and 21 compare the experimental data in [24, 32] and the calculated data for fragments of various masses in two fission systems. The calculated dependences $E_\gamma(A,TKE)$ have a characteristic wave-form structure caused by the fact that the opening and subsequent increase in strength of the neutron channel as the excitation energy of the emitter nucleus increases (reduction in TKE) causes a decrease in strength in the radiation discharge channel. The dependencies $E_{\gamma\ calc.}(A,TKE)$ were not averaged with respect to the distributions of the total kinetic energies and therefore the structure in these functions emerges very clearly. The averaging process will smooth $E_{\gamma\ calc.}(A,TKE)$ and facilitate a more representative comparison of the experimental and calculated dependences. Nevertheless, a number of conclusions may be drawn. Despite the divergences in the experimental and calculated multiplicities, the total γ-ray energies for a pair of additional fragments are sufficiently well reproduced for fission of ^{235}U by thermal neutrons (Fig. 20). The picture is different for spontaneous fission of ^{252}Cf (Fig. 21): there are several pairs of fragments (A=108, 111, 114, 117) where the slope of the calculated curve contradicts the experimental data. These discrepancies may have the same origin as the differences in the γ-ray spectra in the soft portion (Figs 15-18) and the differences in the mean γ-ray multiplicities (Fig. 19).

Thus, the description of the observable characteristics of fission fragment emission properties using the statistical model of nuclear reactions, shows that the model reproduces the experimental data over a wide range of total kinetic energies and fragment masses. The next stage of this investigation of the emission properties of fragments using the statistical model of nuclear reactions and cascade-evaporation model is to study the population of the isomeric levels of fragments.

4. ISOMERIC RATIOS

Currently, the method in [35] is used to calculate the isomeric ratios of independent yields [33, 34]; this method is based on the assumption that the population distribution of an isomeric nucleus with respect to the total angular momentum J is proportional to the spin distribution of the density of excited levels:

$$W(J) = Const \cdot (2J+1) \cdot \exp\left(-\frac{(J+1/2)^2}{2\sigma^2}\right), \qquad (9)$$

where σ^2 is the spin dependence parameter. According to [35], population of the isomeric state occurs via a number of γ-transitions the probability of which is determined by the level density of the final states. It is also assumed that the parameter σ is not dependent on the excitation energy and there is no energy dependence of the radiation strength functions. The method was verified using experimental isomeric ratios for the radiative capture of thermal and resonance neutrons, and isomeric ratios for the (γ,n) reaction in several nuclei. By varying within reasonable limits the number of γ-rays μ emitted to populate the isomeric state and the value of the parameter σ, an acceptable description was produced of the data available at that time for 28 nuclei in the (n,γ) reaction. The situation in photonuclear reactions is different. For example, to describe the experimental data for the ^{115}In(γ,n) reaction, we had to assume that $\sigma \to \infty$.

The physical basis of the method in [35] is the assumption that the isomeric ratio is formed by the cascade of γ-rays during decay of the isomeric nucleus. This assumption is confirmed by analysis of the isomeric cross-sections of many reactions [4-7]. For example, even for the (n,γ) reaction with 14 MeV neutrons, direct population of the isomer by a neutron emission is insignificant, i.e. the main contribution to the isomeric ratio comes from γ-cascades which remove the remaining excitation after emission of a neutron [6]. However, the shape of the distribution population prior to the γ-emission which leads to formation of the isomer may differ significantly from expression (9), if the states of the isomeric nucleus are formed by neutron emission and if the compound nucleus has high excitation levels. In this case, the derived parameter σ will be overestimated, as demonstrated in [35]. Since the fission fragments prior to neutron emission may have significantly high (up to 50 MeV) excitation levels, use of the method in [35] to analyse the isomeric ratios of independent yields would not be appropriate.

The most consistent method of calculation for isomer formation cross-sections and isomeric ratios is by using the statistical model of nuclear reactions and the

cascade-evaporation model [1-3], as has been demonstrated in a large number of papers. An acceptable description of the experimental data can be obtained for a wide spectrum of incident particles (from photons to alpha-particles), a wide range of nucleus mass numbers (from 20 to 240) and a wide range of energies (from thermal to 40 MeV). However, this approach has formerly not been used for the isomers formed during the fission process owing to additional complexities and uncertainties of the initial conditions, caused by the peculiarities of the fission process. Since the mean excitation energies of fragments have been established above and the library of source parameters has been tested, there are no limitations in principle on the use of the statistical model of nuclear reactions and the cascade-evaporation model.

FRAGMENT ISOMER POPULATION MECHANISM. A specific state of a fission product nucleus according to the cascade-evaporation model may be populated in the following manners: 1. - during the fission process the fragment is in this state (cold fission); 2. - following neutron emission; and/or 3. - following a γ-ray cascade. Applying this assumption regarding the isomer population mechanism, the isomeric ratios of independent yields for the nucleus (Z,A) may be calculated using the formula:

$$R = \frac{\sum_{i=0}^{n} Y_i(Z, A+i) \cdot \langle P_i \cdot r_i \rangle}{\sum_{i=0}^{n} Y_i(Z, A+i) \cdot \langle P_i \rangle}, \qquad (10)$$

where Y_i is the independent yield of the fragment (Z,A+i) emitting i neutrons; P_i is the probability of emitting this number of neutrons; and r_i is the isomeric ratio for emission of i neutrons. The summation in expression (10) is performed from zero neutrons (isomeric nucleus formed actually during fission) up to a certain number of neutrons n, following whose emission an isomeric nucleus is formed. Thus, (n+1) fission product nuclei are involved in the formation of the isomeric state. Averaging is carried out with respect to the excitation energy of the corresponding primary fragments taking into account the distribution function f(U). Apart from the distribution of the excitation energies, the original distribution of the fragment level populations must be specified with respect to the total angular momentum J when calculating P_i and r_i.

Fig. 22 shows the dependences of the values in formula (10) on the excitation energy of the corresponding nucleus during emission of a varying number of prompt neutrons leading to the formation of an isomer in the nucleus ^{123}Sn. Since the metastable state of the ^{123}Sn nucleus is low-spin (J^{π}=3/2+), an increase in excitation energy causes a decrease in the probability of population of this state in all ^{123}Sn formation channels following emission of neutrons (ν=1-4) and γ-rays (ν=0). Multiplying the function r(U) by P(U) produces "bell-shaped" functions with almost identical maxima. Finally, if we take into account the dependence Y(A+i), we obtain numerator terms in expression (10) which make it necessary to take account of emission of 4 or 5 neutrons in the calculations even where <U>=10-15 MeV. Thus, population of the isomer occurs for several channels with comparable probabilities. If

we assume that isomers can also be formed following the emission of delayed neutrons, then the calculations become so complex that further research would be required to perform them.

MEAN FRAGMENT SPINS. Use of the statistical model of nuclear reactions, taking into account the laws of conservation of total angular momentum and parity to calculate the emission properties of fission fragments requires a knowledge of the spin distributions of their populations $W_0(U,J)$ before the emission of neutrons, i.e. of their mean spin values <J> and shape of the dependence $W_0(U,J)$. In other words, when applying the statistical model of nuclear reactions consistently we must specify the dependence of the fission barrier penetrabilities on the orbital momentum of the relative movement of fragments at the time the fissile nucleus $T_f(l)$ is split. This question, which is of secondary importance when calculating the emission spectra of fragments [8], becomes one of the most important when calculating isomeric ratios. If, as is clear from [36], the value $T_f(l)$ is not dependent on the orbital momentum 1, then the dependence of the initial populations of fragments on the total momentum will take the form:

$$W_o(U,J) \sim (2J+1)\rho(U,J)\,. \tag{11}$$

The assumption in expression (11) may be verified using existing data on the mean spins <J> of fission fragments [37] (Fig. 23). Although the results in [37] are not purely experimental (the results of calculations of the mean momenta "removed" by neutrons and γ-rays were also used to produce them), they are sufficiently informative for the purposes of comparison, since the main part of the mean spin value was obtained by experiment. The calculation values of <J> in Fig. 23 were obtained using the assumption in expression (11) and the mean excitation energies of primary fragments discussed in connection with Figs 4-6, and two limit values for the moment of inertia of nuclei F - these correspond to the solid-state F_{rig} and semi-solid state $F_{rig/2}$ moments. Clearly, the data in [37] lie within the limits of the corridor defined by the calculation results. Consequently, use of the assumption in expression (11) in the calculations results in a satisfactory level of agreement between the calculated mean spins of primary fragments and the observable values.

POPULATION DISTRIBUTION WITH RESPECT TO SPIN. For the mean fragment spins, it is impossible to verify the correctness of the assumption regarding the shape of the dependence (11) on J, since different dependences may yield identical values of <J>. A broad distribution of (11) may occur if primarily the single-particle levels of a fragment are populated and they are linked to the collective levels of the rotational bands. In the opposite case, i.e. if nuclear fission causes population of the collective levels and there is no link between different kinds of level, the distribution of $W_o(U,J)$ will take the form:

$$W_o(U,J) = \delta(J - < J >)\,, \tag{12}$$

where <J> is determined using (11) or from observed values, and δ is the Dirac delta function. Fig. 23 shows that the mean fragment spins are better reproduced by calculation for $F=F_{rig/2}$, and therefore this variant will be used henceforth together with the assumption in expression (12).

The data in [38, 39] on the mean angular momenta of the rotational bands of fragments generated by spontaneous fission of ^{252}Cf, which were obtained by analysing γ-transitions, are useful for verifying the assumptions in expressions (11) and (12).

The mean spins of fragments with mass A following emission of a specific number of neutrons ν are dependent on the excitation energy of the primary fragment as:

$$J_\nu(U) = \frac{\int_0^{U-B_\nu} \sum_J J \cdot W_\nu(x, J)dx}{\int_0^{U-B_\nu} \sum_J W_\nu(x, J)dx}, \qquad (13)$$

where W_ν is the population of the nucleus following emission of ν neutrons. Integrating the dependence $J_\nu(U)$ with respect to the excitation energy of the primary nucleus with weighting of the distribution function with respect to the energy f(U) and the emission probability of a given number of neutrons $P_\nu(U)$, yields the following mean fragment spin:

$$< J >_\nu = \int_0^{U_{max}} J_\nu(U) P_\nu(U) f(U) dU \quad . \qquad (14)$$

Fig. 24 shows the mean spins of the nuclei ^{102}Zr, ^{104}Mo and ^{144}Ba - spontaneous fission fragments of ^{252}Cf formed following neutron emission. The mean spin values calculated using the assumption in expression (11) are significantly higher than the experimental values, even taking into account experimental error and inaccuracies in the main parameter of the model exerting the strongest influence on the calculated values of <J> - the moment of inertia of the nucleus. In this case it is clear that an anomalously low moment of inertia of the nucleus would be required to fit the values to $<J>_{exp.}$ On the other hand, use of the assumption in expression (12) yielded a satisfactory level of agreement with the experimental data in [38, 39]. Thus, the data on the mean total angular momenta of fission fragments shows that the spin distribution in expression (12) of the populations of primary fragments is preferable for low-energy fission.

ISOMERIC RATIOS. Experimental data on the isomeric ratios of independent yields for fission of ^{235}U by thermal neutrons [34] are available for 48 isomeric pairs of fragment nuclei with A=79-148. The main characteristics of the isomeric levels of the nuclei studied are shown in the table. It is important to note that the characteristics of the isomeric levels are not unique, i.e. the difference in the spins of the ground and metastable levels comprises, as a rule, several units $\hbar$. Therefore, at first glance, describing the isomeric ratios of independent yields for these levels should not cause significant difficulties [4-6]. The exception is the three isomeric levels of the nuclei ^{120,122,130}In which have high spins.

Fig. 25 compares the calculated (using the assumption in expression (11)) and experimental [34] isomeric ratios of independent yields. It is striking that the calculated ratios are consistently higher for levels with high spin and consistently lower for levels with low spin, irrespective of whether the level in question is ground or metastable. Attempts to change the nucleus parameters (for example, changing the spin distribution parameter corresponding

to the solid-state moment of inertia to a value corresponding to the semi-solid-state moment of inertia), or changing the method for calculating the radiation strength functions, bring about only insignificant changes in Fig. 25 but do not alter the overall picture.

Figs 26 and 27 compare the experimental isomeric ratios of independent yields and the isomeric ratios calculated using the two limit assumptions in expression (11) and (12) regarding the population distributions of primary fragments with respect to the total angular momentum. Clearly, expression (12) yields a significantly better description of the experimental data, which has not been possible using other methods for all nuclei simultaneously. Of course, a number of discrepancies still remain even using expression (12); and to eliminate these we may need to improve the description of the spectra (Figs 15-18) for soft γ-rays and/or refine the discrete level schemes of isomeric fission fragment nuclei.

The fragment spin formation conditions during the fission process and their subsequent modification during Coulomb acceleration of the fragments may differ for different fissile systems, for example in thermal neutron fission and α-particle fission. In the first instance, the excitation energy of the compound nucleus is 5-6 MeV, while in the second case it may be several tens of MeV. Obviously, if the distribution in expression (12) predominates in the (n_{th},f) reaction, the contribution of (11) must be greater in (α,f). This can be confirmed by analysing the energy dependences of the isomeric ratios of independent yields from the latter reaction. Fig. 28 shows experimental data on the isomeric ratios of eight nuclei, relative to their average mean energies <U>, obtained taking into account multichance fission and neutron emission [40]. The figure also shows the results of calculations using the two assumptions concerning the spin distribution of primary fragment populations in expressions (11) and (12). Clearly, the observed isomeric ratios of independent yields usually lie within the corridor defined by the calculated lines. As might have been anticipated, at low fragment excitation energies the “rotational” distribution (12) predominates and at high levels the “thermal” distribution (11). This conclusion is also confirmed by the data for the $^{235}U(n_{th},f)$ reaction analysed from the point of view of fragment excitation energy (Fig. 29). In fact, the greatest influence on the calculation results of substituting distribution (11) by (12), bringing them closer to the experimental data, is observed at <U>=6-10 MeV; the influence is much less at <U>=14-20 MeV.

The fission fragment spin formation mechanism may therefore consist of two processes. Rotational movement of a fragment after splitting of the fissile nucleus and internal movement of fragment nucleons. During the acceleration process, when the potential deformation energy is converted into internal energy, the initial mono-distribution (12) “blurs” to distribution (11), owing to the density of the internal non-collective movement types.

The author would like to thank the organizers and participants of the seminar on “The time-scale and dynamics of fission-fusion process in heavy and super-heavy nuclei” held at the Laboratory of Nuclear Reactions of the Joint Institute for Nuclear Research in Dubna.

Conclusion

The statistical model of nuclear reactions and the cascade-evaporation model for decay of excited nuclei are used in this paper to analyse the emission properties and isomeric ratios of fission fragments. In order to justify this approach the mean excitation energies of fragments relative to fragment mass were obtained from experimental data on the mean neutron multiplicities and verified with respect to the energy balance. The observable emission spectra from fragments of differing masses were reproduced by calculating the spectra from emitter nuclei at excitation energies equal to the mean fragment energies obtained. The experimental dependences of the neutron and γ-ray multiplicities on the total kinetic energy of additional fragments were modelled by dividing the total free fission energy between the fragments in proportion to the derived mean excitation energies. The mean fragment spin, calculated for the mean excitation energies assuming fission barrier penetrability is not dependent on the orbital angular momentum agreed with the analogous values derived from the experimental data. Two opposing assumptions regarding the nature of the distribution of the total angular momenta of fragments after full acceleration were analysed: a “rotational” distribution and a distribution corresponding to single-particle movement. It was shown that the assumption regarding the spin distribution of primary fragment populations is one of the key factors influencing the isomeric ratios of independent yields. When describing the observable isomeric ratios, it proved necessary to introduce the assumption that a component with a fixed total angular momentum value may be present in the spin distribution of primary fragment populations.

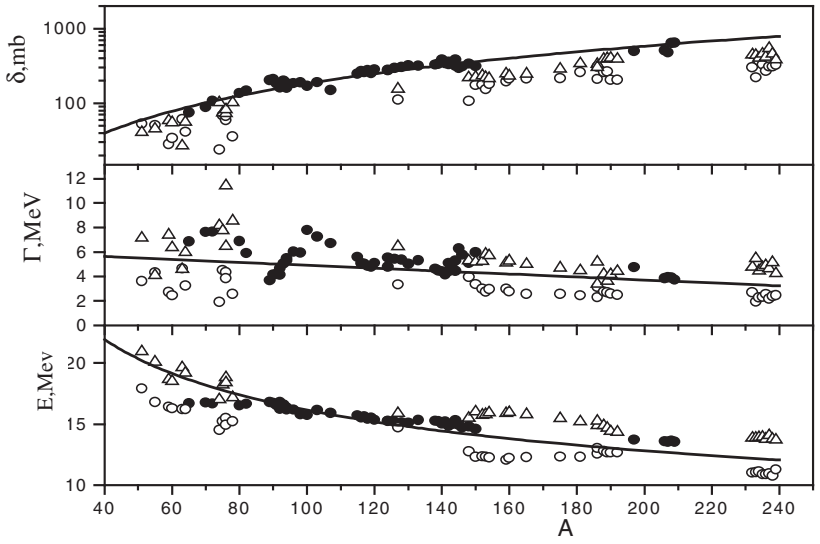

Fig. 1. Giant dipole resonance parameters of nuclei with A=50-240: energies, widths and maximum cross-sections (bottom to top). The signs indicate the results of fitting the Lorentz dependence to the experimental photoabsorption cross-sections in [15].
(•) - for monoresonances, (o) and (Δ) - for split resonances. The lines are the results of calculations using the formulae in expression (3).

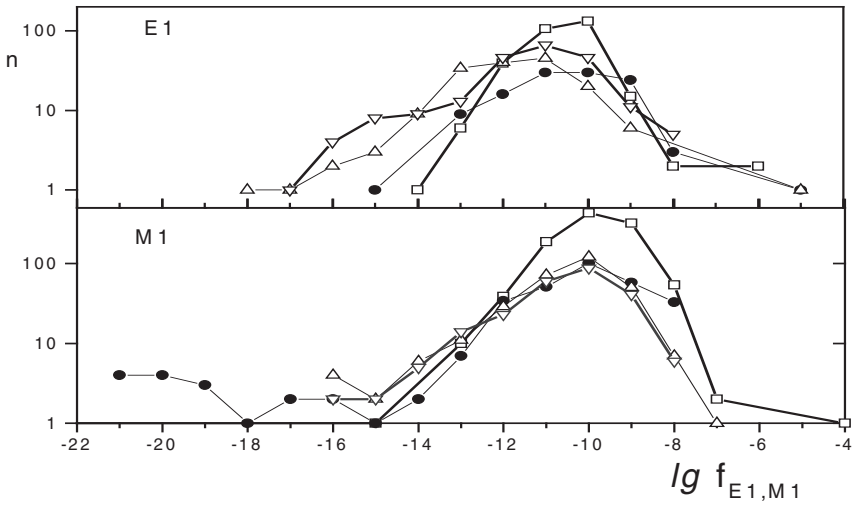

Fig. 2. Distribution of the strength functions of dipole electric (top) and magnetic transitions with energies E_γ<2 MeV. The signs indicate the data from [17] obtained in [16] for various mass number ranges: (□) - A=45-84, (•) - A=85-105, (Δ) - A=106-145, (∇) - A=145-165.

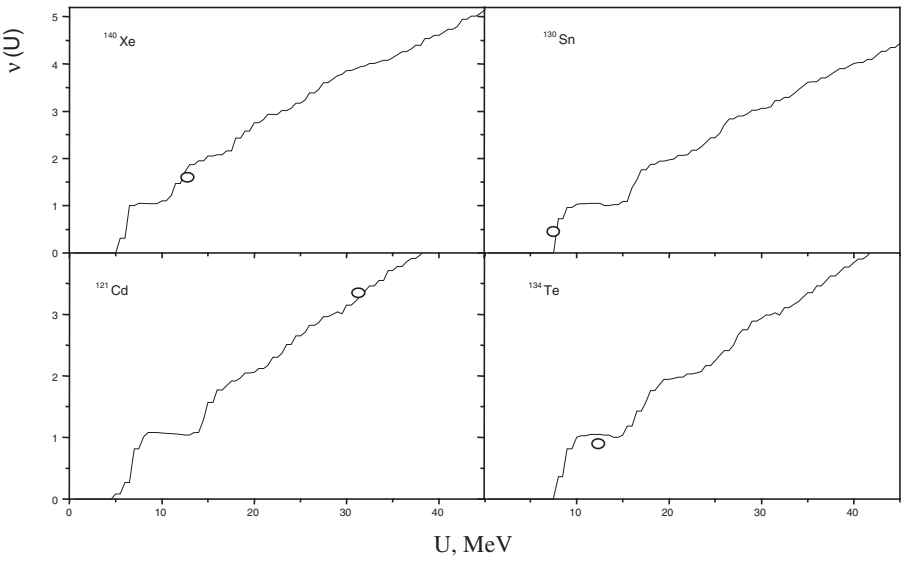

Fig. 3. Dependence of the number of neutrons on emitter nucleus excitation energy: ^{121}Cd, ^{130}Sn, ^{134}Te and ^{140}Xe. The signs indicate the experimental values of <ν> for fragments of ^{252}Cf of corresponding mass [18].

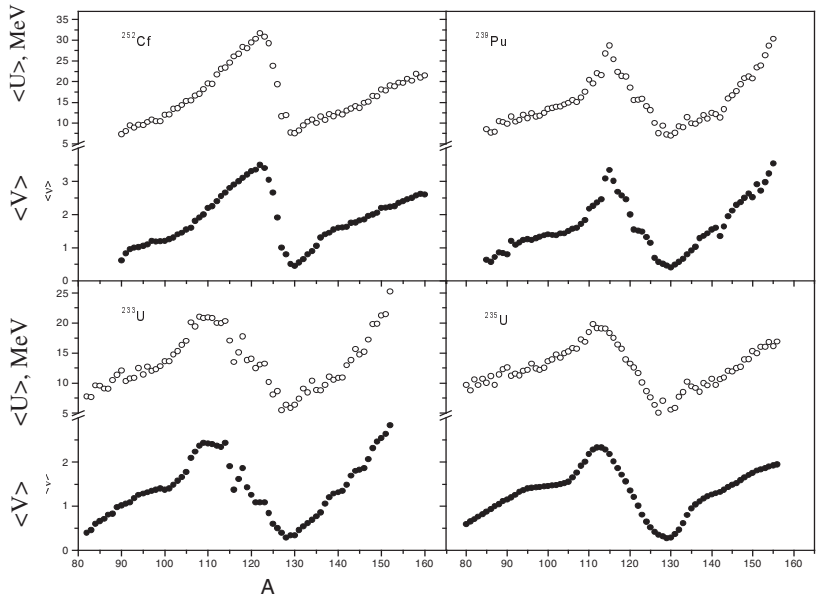

Fig. 4. Mean excitation energies and mean neutron multiplicities relative to fragment mass for fission of ^{233}U, ^{235}U and ^{239}Pu by thermal neutrons and spontaneous fission of ^{252}Cf.

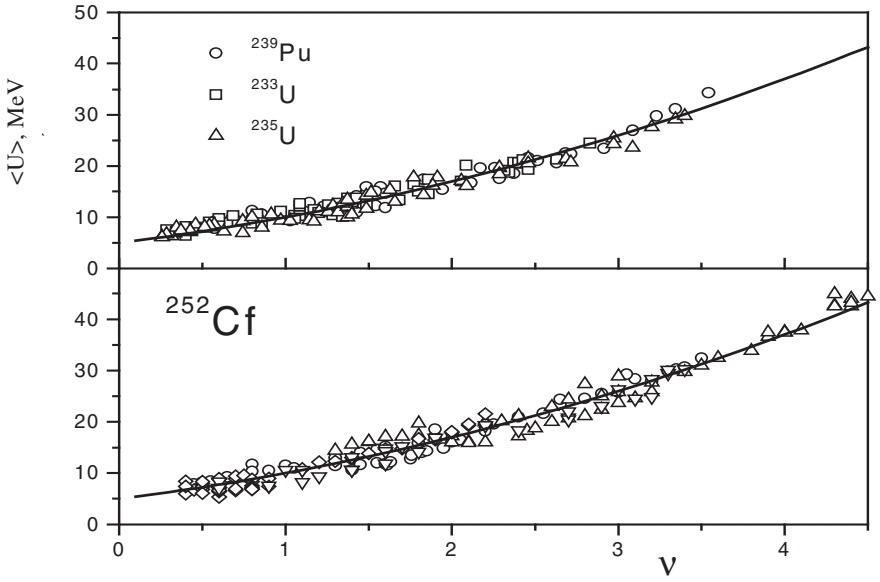

Fig. 5. Dependence of the mean excitation energy of fragments on the mean number of neutrons emitted. Top - fission of ^{233}U (□), ^{235}U (Δ) and ^{239}Pu (o) by thermal neutrons. Bottom - spontaneous fission of ^{252}Cf for various total kinetic energies of fragments: (o) – 187 MeV, (▽) – 147 MeV, (Δ) – 167 MeV and (◊) – 207 MeV. Lines - calculation using formula (4).

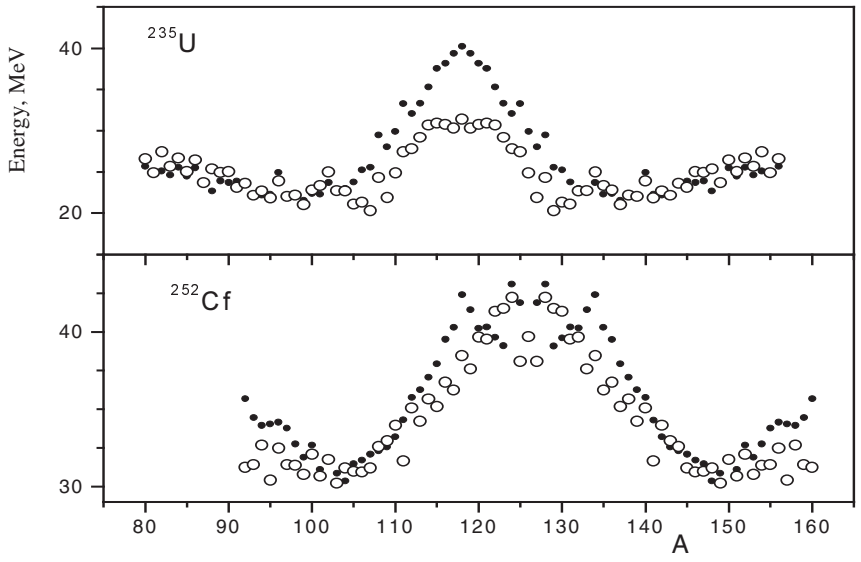

Fig. 6. Free energies TXE=Q-TKE (•) and sums of the mean excitation energies of additional fragments $\langle U(A_L,A_H)\rangle = \langle U(A_H)\rangle + \langle U(A_H)\rangle$ (o) for spontaneous fission of ^{252}Cf (bottom) and fission of ^{235}U by thermal neutrons (top), relative to fragment mass.

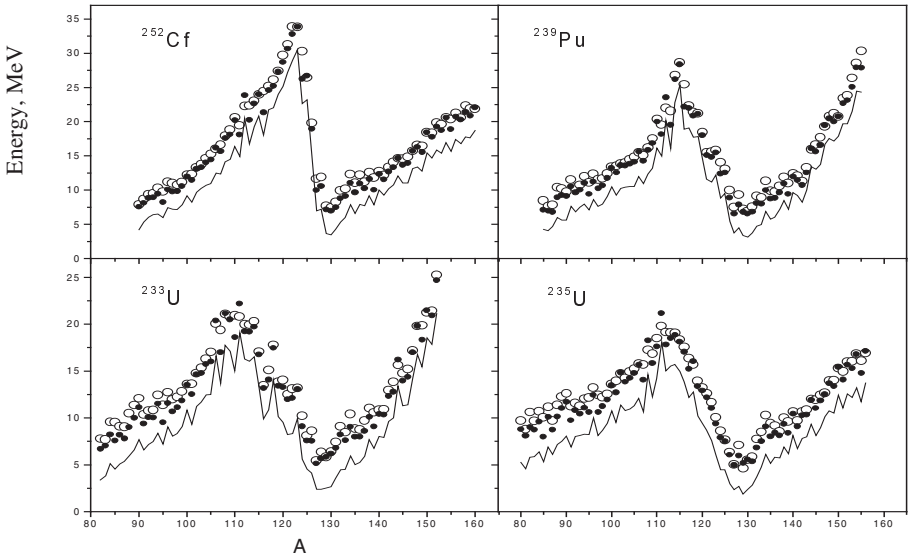

Fig. 7. Mean excitation energies of fission fragments (o), sum of mean energies removed by neutrons and γ-rays (•) and mean energies removed by neutrons (lines).

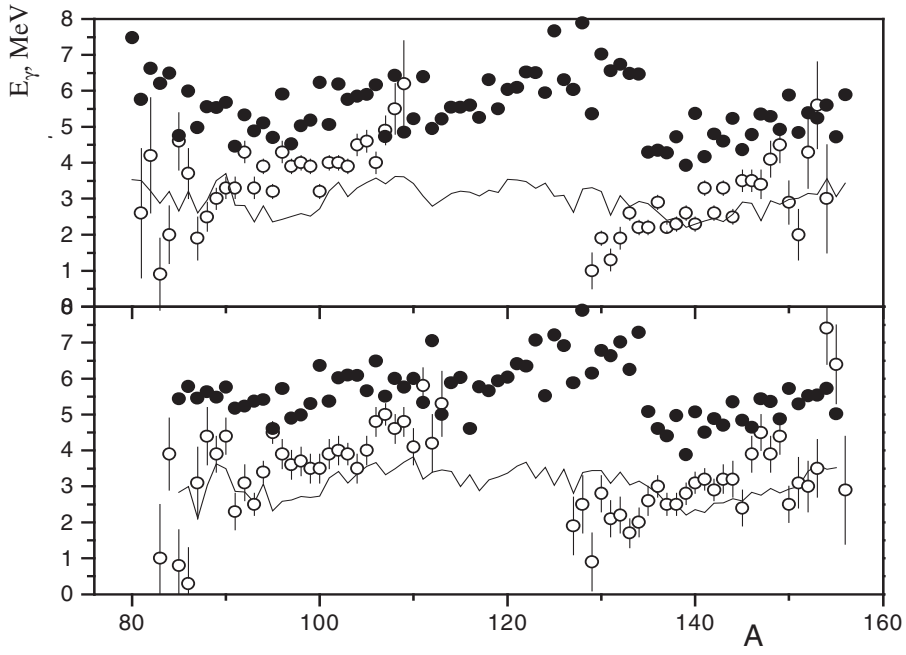

Fig. 8. Data on mean energies removed by γ-rays from thermal neutron fission fragments of ^{235}U (top) and ^{239}Pu (bottom). Empty circles - experimental data from [24, 25]; lines - calculation results; shaded circles - mean neutron binding energies in emitter nuclei.

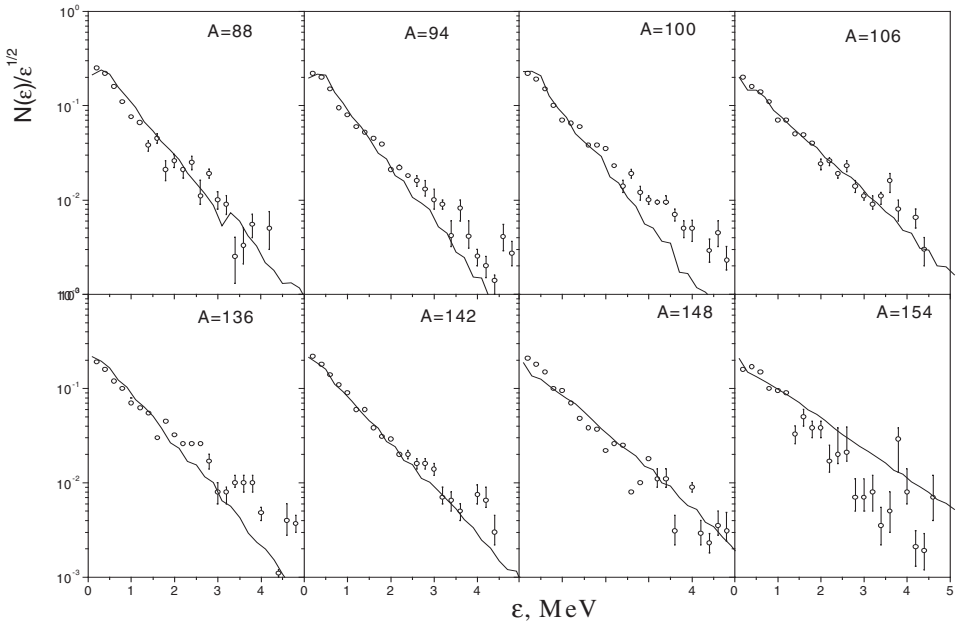

Fig. 9. Neutron spectra from thermal neutron fission fragments of ^{235}U. Signs - experimental data from [26]; lines - calculation results.

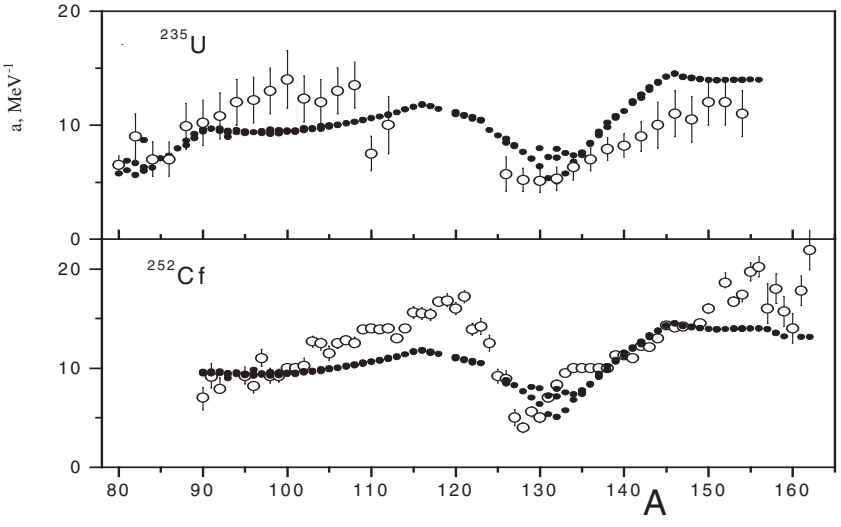

Fig. 10. Level density parameters of primary spontaneous fission fragments of ^{252}Cf (bottom) and thermal neutron fission fragments of ^{235}U (top) relative to fragment mass. The symbols indicate (o) the empirical values obtained in [19, 26] from the neutron spectra and (•) the LDPL-98 library data calculated for the mean excitation energies.

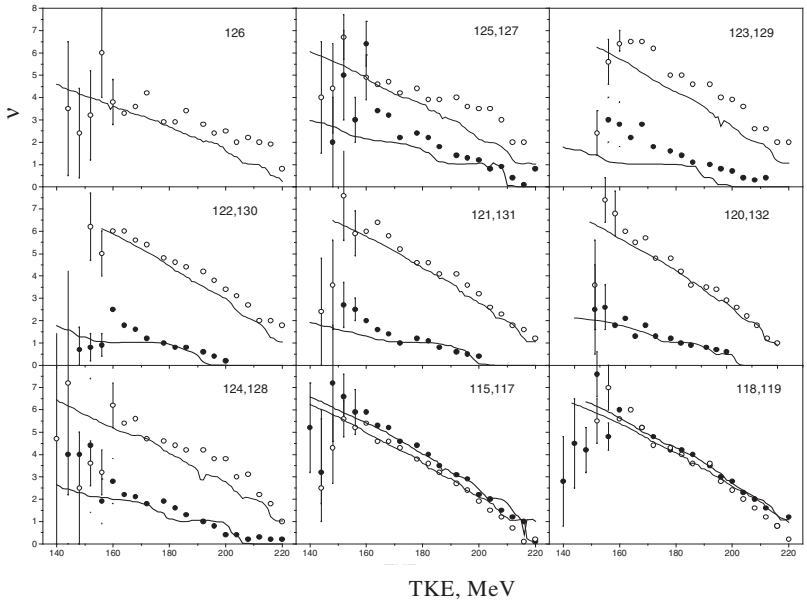

Fig. 11. Multiplicities of neutrons emitted by spontaneous fission fragments of ^{252}Cf relative to the total kinetic energy. The signs indicate the experimental data from [19]: empty circles - light fragment; shaded circles - heavy fragment. The lines show the calculation results.

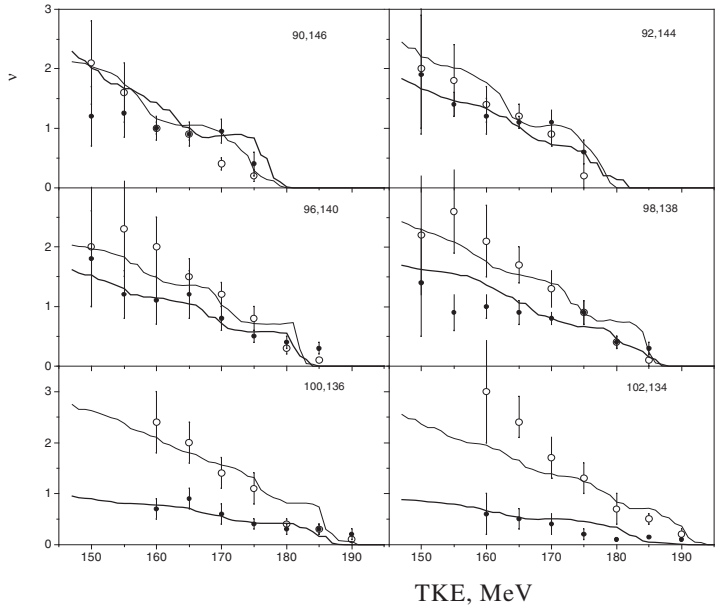

Fig. 12. As for Fig. 11, but for thermal neutron fission of ^{235}U. Experimental data from [29].

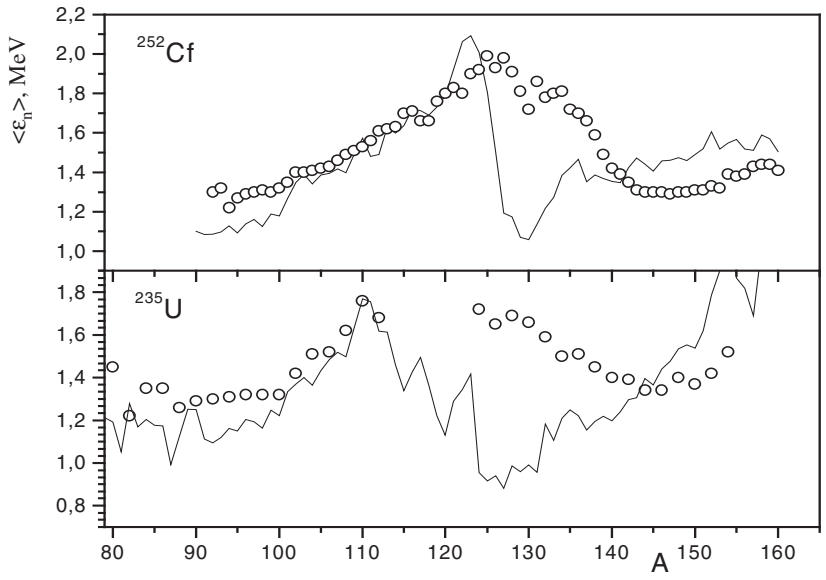

Fig. 13. Mean energies of neutrons emitted by spontaneous fission fragments of ^{252}Cf (top) and thermal neutron fission fragments of ^{235}U (bottom) as a function of primary fragment mass. Symbols - experimental data from [19, 26]; lines - calculation results.

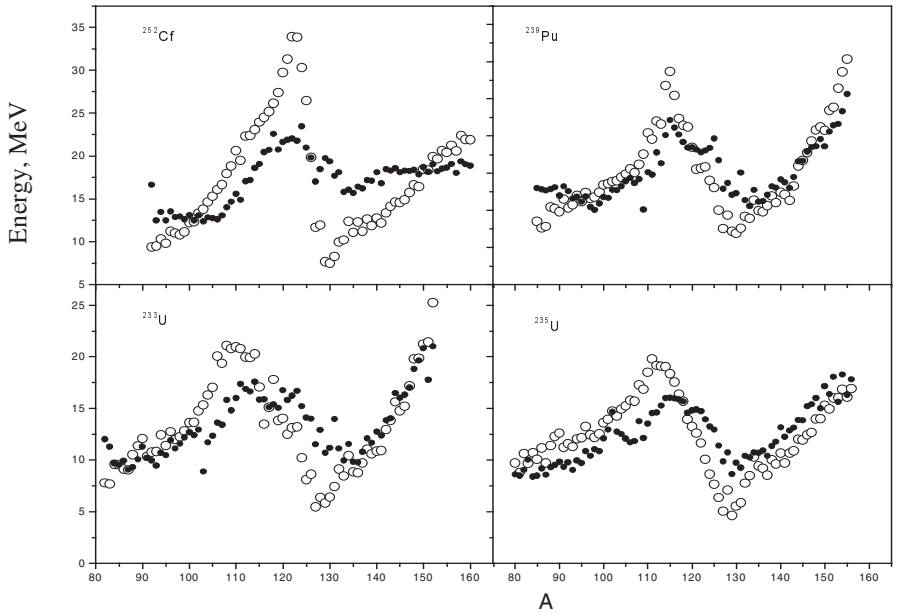

Fig. 14. Excitation energy distributions for thermal neutron fission fragments of ^{233}U, ^{235}U and ^{239}Pu and spontaneous fission fragments of ^{252}Cf. Empty circles - mean energies obtained from neutron multiplicities; shaded circles - values calculated using formula (8).

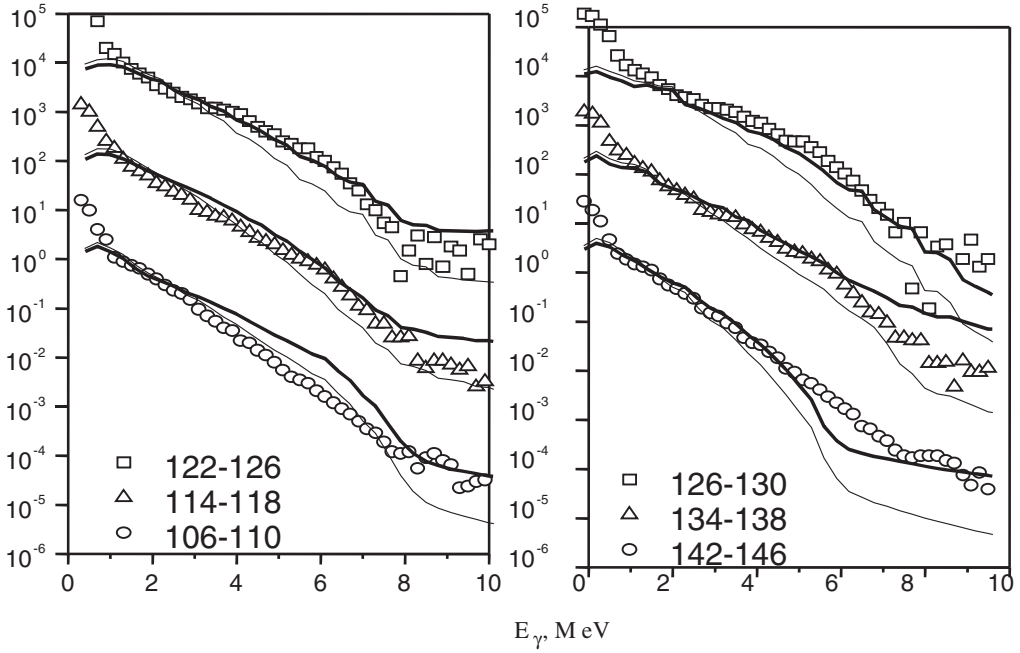

Fig. 15. ^{252}Cf spontaneous fission γ-ray spectra emitted by heavy (right) and additional light (left) fragments. The signs indicate the experimental data from [30] for the fragment mass ranges: (□) - A=126-130 (A_L=122-126), (Δ) - A = 134-138 (A_L=114-118), (o) - A=142-146 (A_L=106-110). Thick lines - results of calculations using f_{E1} values calculated according to the KMF-PT method [16]; thin lines - results of calculations using the Lorentz dependence.

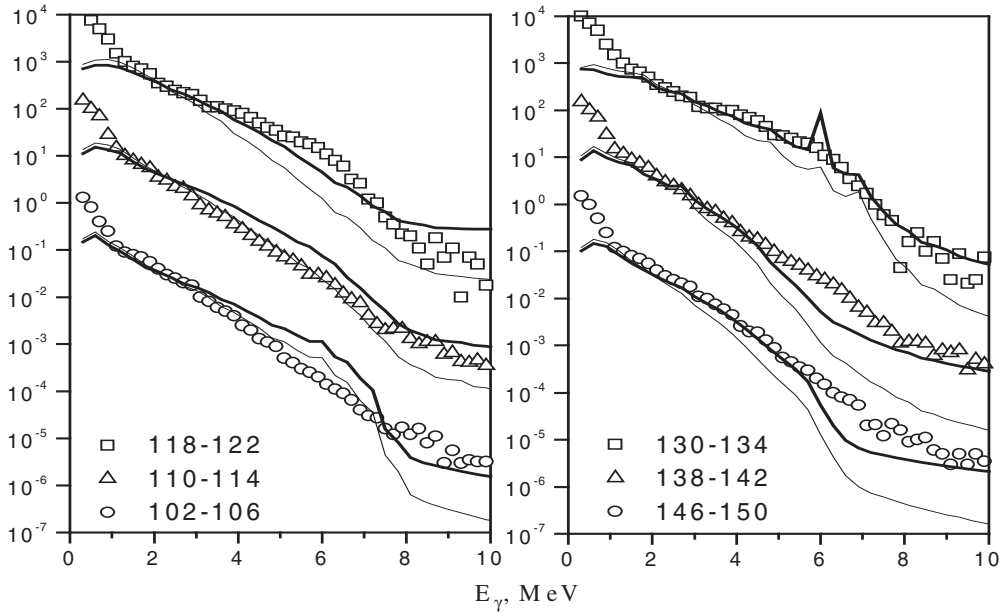

Fig. 16. As for Fig. 15, but for fragments with masses of 130-134, 138-142 and 146-150.

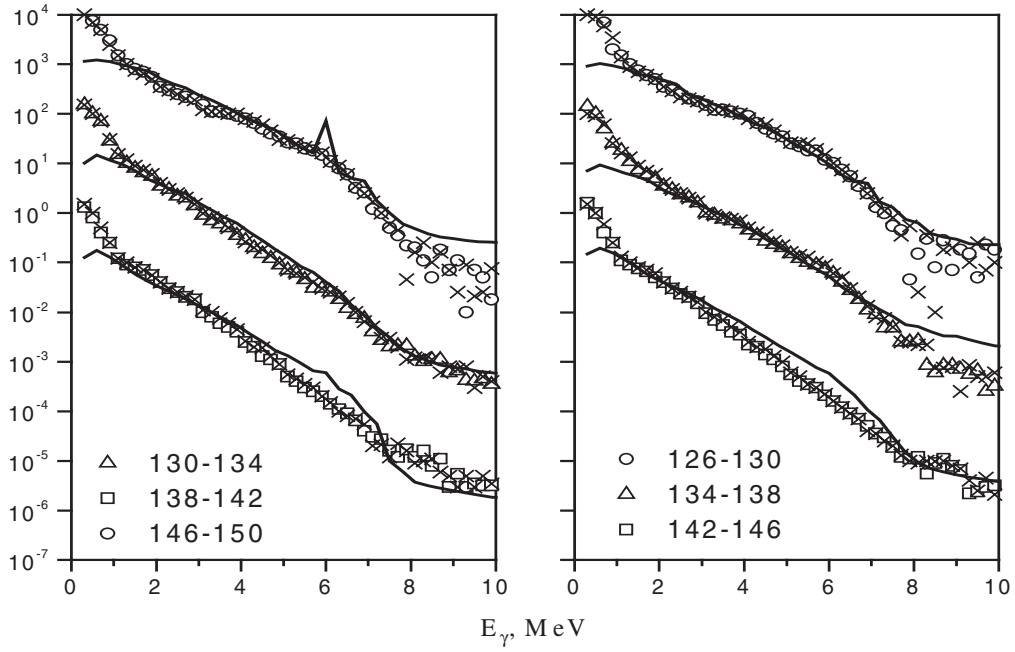

Fig. 17. Data on γ-spectra of ^{252}Cf fission fragments. The experimental data from [30] are indicated by the signs: (Δ) - A=130-134, (□) - A=138-142, (o) - A=146-150 (left); (o) - A=126-130, (Δ) - A=134-138, (□) - A=142-146 (right). The symbols (x) indicate the data for the corresponding additional light fragments. The lines are the calculation results for pairs of fragments using data from the LDPL-98 library and f_{E1} values calculated according to the KMF-PT method.

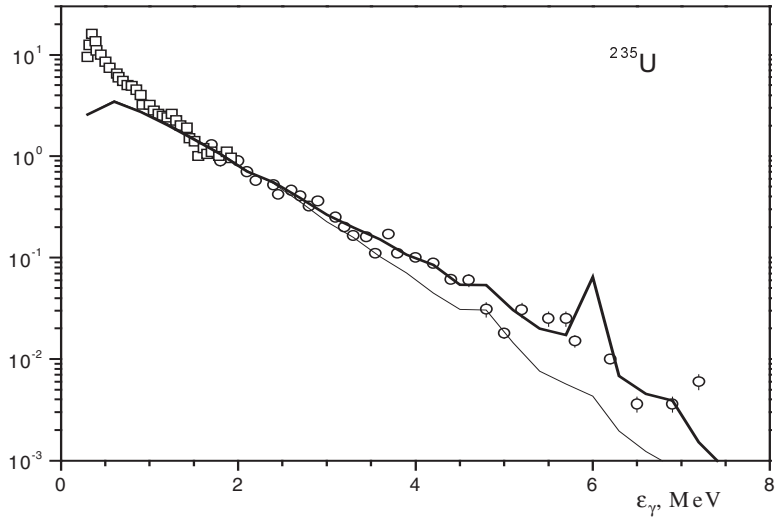

Fig. 18. ^{235}U thermal neutron fission γ-ray spectra. Signs - experimental data from [31]; lines - calculation results: thin line - using the Lorentz dependence for f_{E1}; thick line - using the KMF-PT method [16].

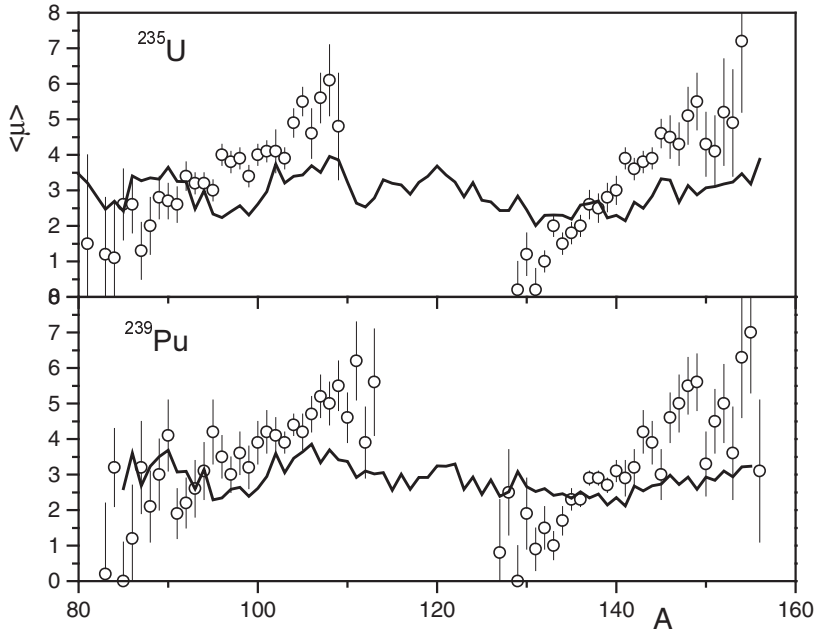

Fig. 19. Data on γ-ray multiplicities from ^{235}U (top) and ^{239}Pu (bottom) thermal neutron fission fragments. Signs - experimental data from [24, 25]; lines - calculation results.

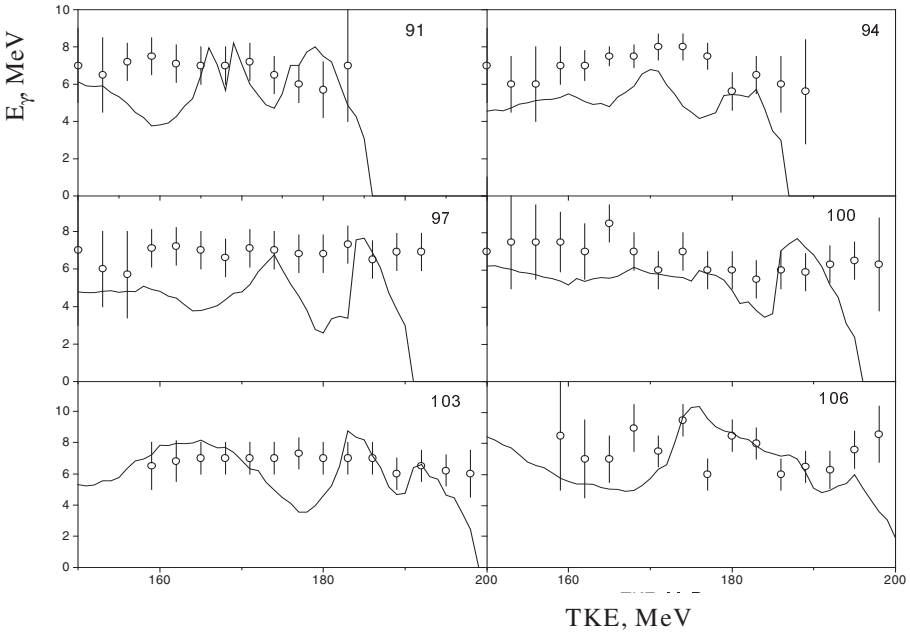

Fig. 20. Data on the dependences of the total γ-ray energies on the total kinetic energy of pairs of additional ^{235}U thermal neutron fission fragments. Dots - experiment in [24]; lines - calculation results. Masses of light fragment indicated.

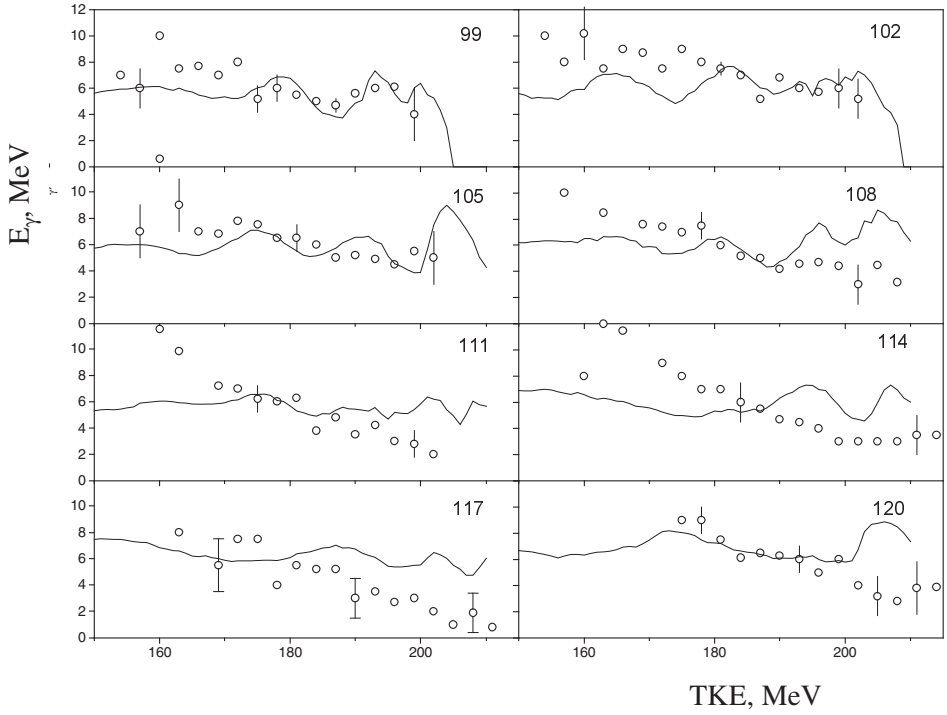

Fig. 21. As for Fig. 20, but for ^{252}Cf fission fragments. Experimental data from [32].

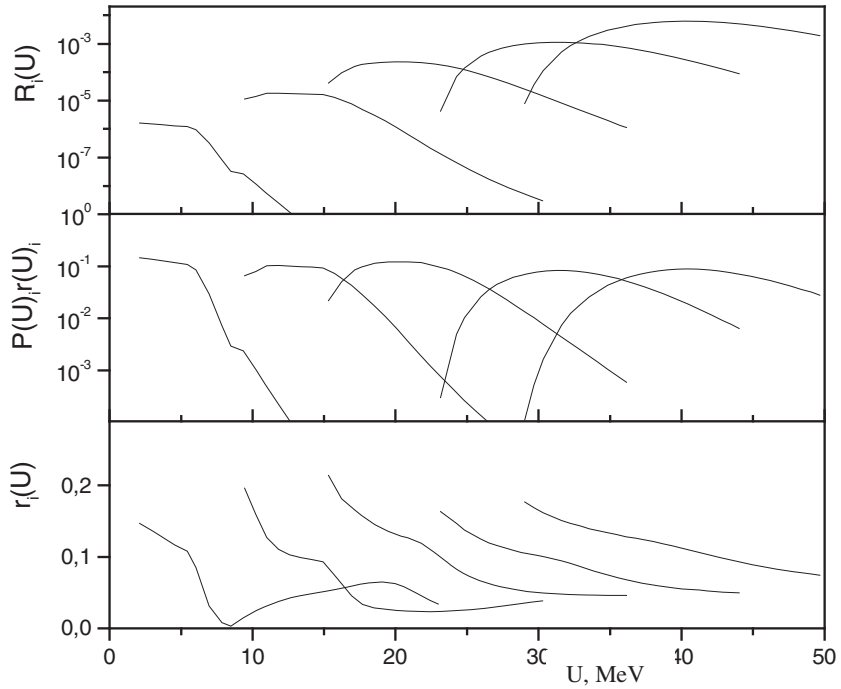

Fig. 22. Energy dependences of the isomeric ratios $r_i(U)$ (bottom), population probabilities $r_i(U)xP_i(U)$ (middle) and yields $R_i(U)$ (top) of the ^{123}Sn($3/2^+$) isomer following emission of a number of neutrons ν=0-4 (left to right).

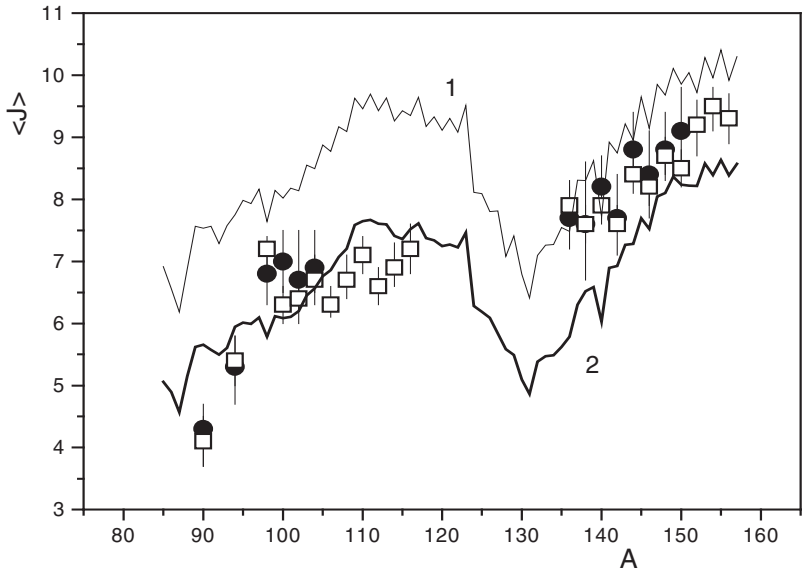

Fig. 23. Mean spins of ^{235}U thermal neutron fission fragments and ^{248}Cm spontaneous fission fragments. Signs - data from [37]; lines - calculation results: 1 - c F=F_{rig}, 2 - c F=$F_{rig/2}$.

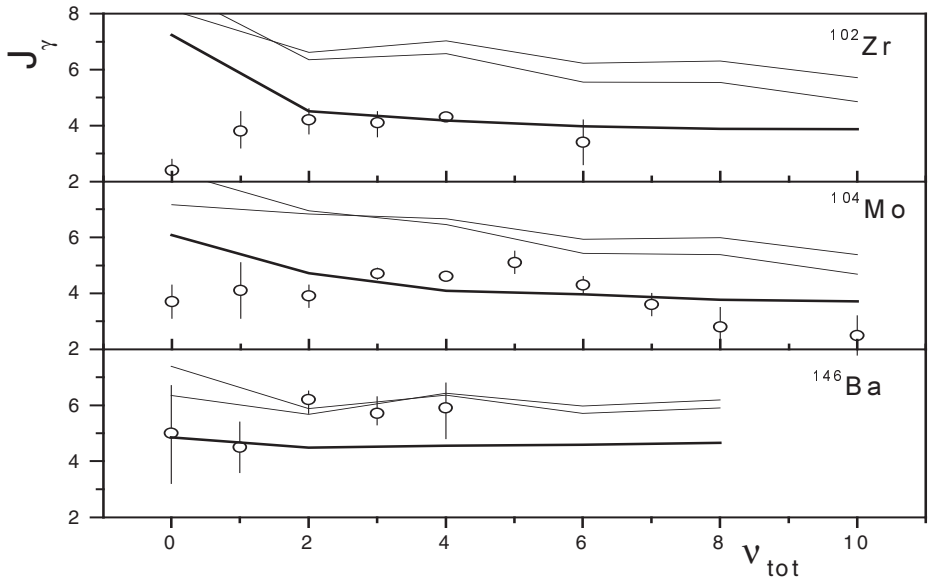

Fig. 24. Mean spins of ^{102}Zr (top), ^{104}Mo and ^{146}Ba (bottom) - spontaneous fission products of ^{252}Cf - as a function of the number of neutrons emitted by a pair of additional fragments. Symbols - experimental data from [38, 39]. Lines - calculation results: thin and dotted lines - using the distribution in expression (11) with the parameters σ^2_{rig} and $\sigma^2_{rig/2}$ respectively; thick lines - using the distribution in expression (12) with $\sigma^2_{rig/2}$.

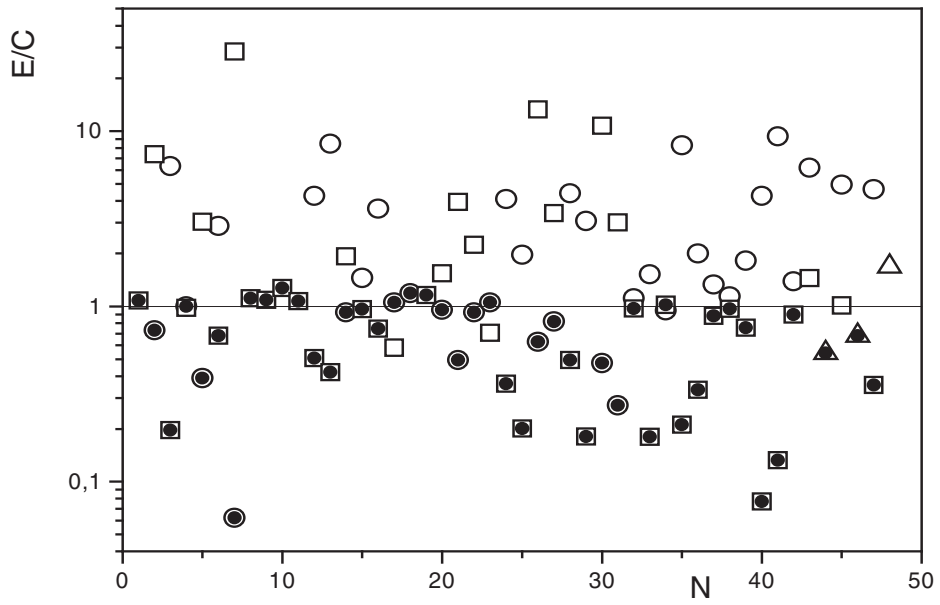

Fig. 25. Relation of the experimental [34] and calculated (using the assumption in expression (11)) isomeric ratios of independent yields of ^{235}U thermal neutron fission fragments. (o) - ground states, (□) - first metastable levels, (Δ) - second metastable levels. (•) - data for states with a larger spin.

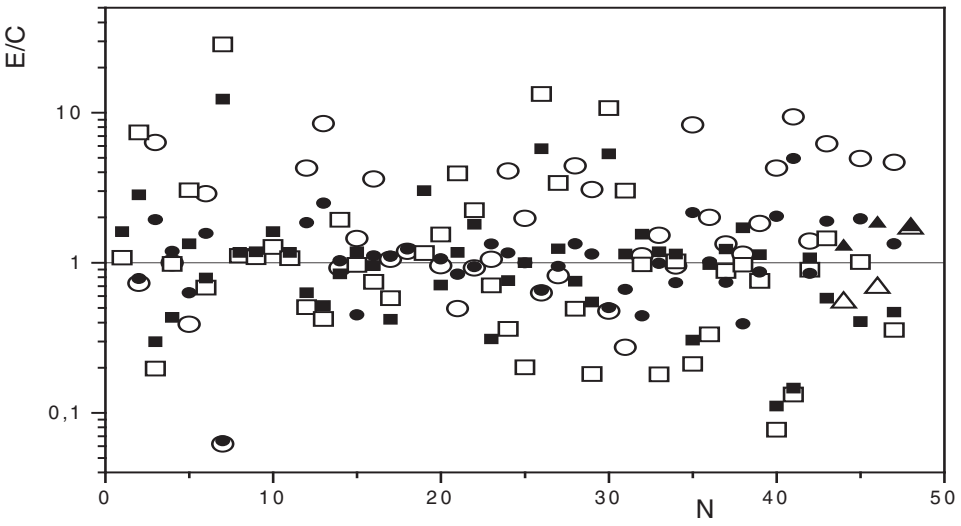

Fig. 26. Relation of the experimental [34] and calculated isomeric ratios of isomeric pairs of ^{235}U thermal neutron fission fragments. Empty signs - data calculated using the distribution in expression (11); shaded signs - data calculated using the distribution in expression (12).

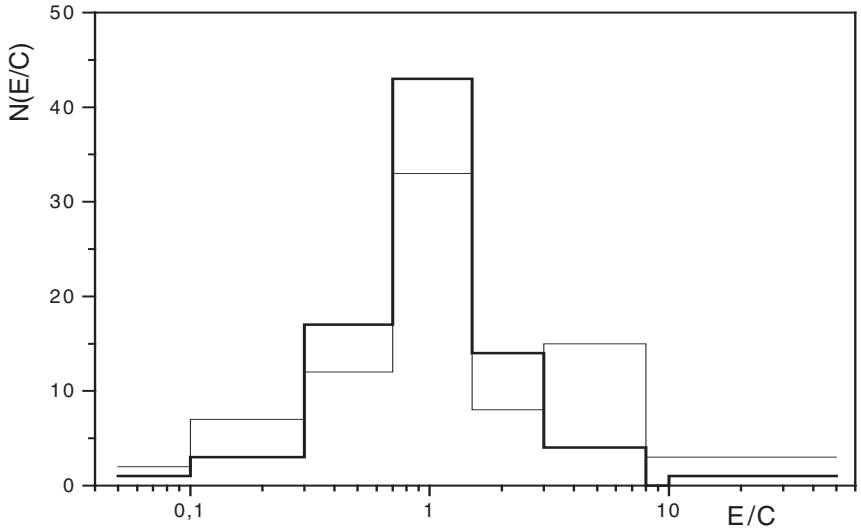

Fig. 27. Distribution of the divergences in the relations of the experimental and calculated isomeric ratios of independent yields for ^{235}U thermal neutron fission fragments. Thick line - results of calculations using the assumption in expression (12); thin line - results of calculations using the assumption in expression (11).

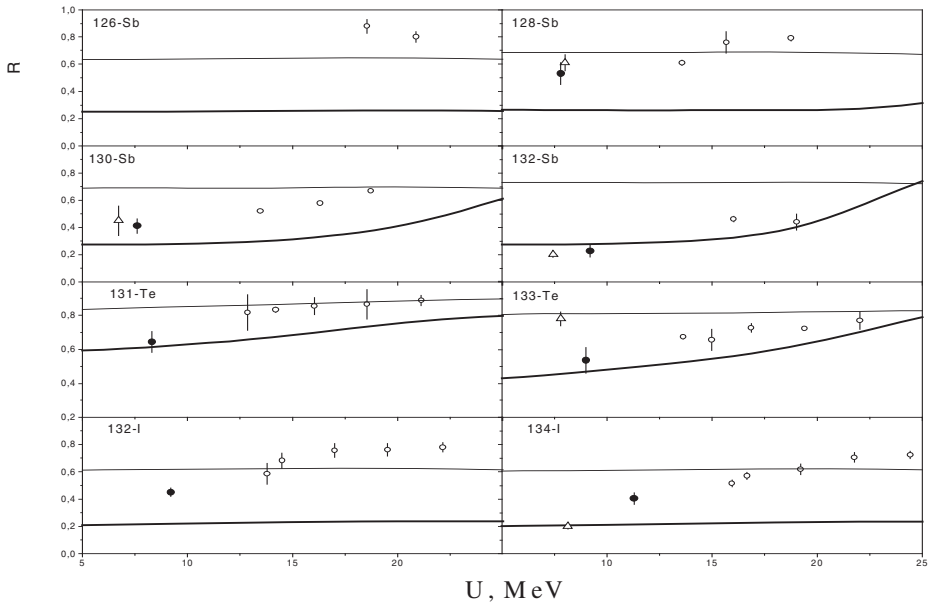

Fig. 28. Data on the isomeric ratios of the product nuclei from the reaction $^{238}U(\alpha,f)$ (o), $^{241}Pu(n_{th},f)$ (•) [40] and $^{235}U(n_{th},f)$ (Δ) [34]. The lines show the calculation results: thick lines - using the assumption in expression (12); thin lines - using the assumption in expression (11).

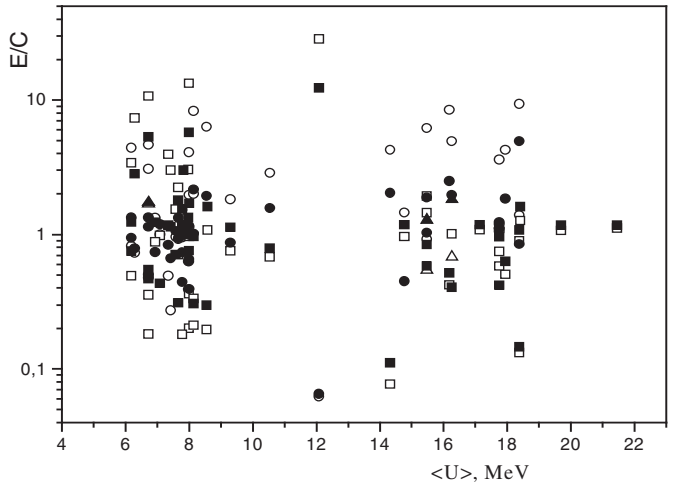

Fig. 29. As for Fig. 26, but relative to the mean fragment excitation energy.

Characteristics of the isomeric levels of ^{235}U thermal neutron fission product nuclei whose isomeric ratios are measured in [34]. The spins and parities J^{π} of the ground and metastable levels and the energy of the metastable level E_m are shown

No.	nucleus	J_g^{π}	J_m^{π}	E_m, MeV	No.	nucleus	J_g^{π}	J_m^{π}	E_m, MeV
1	^{79}Ge	1/2-	7/2+	0.188	2	^{81}Ge	9/2+	1/2+	0.679
3	^{82}As	1+	5-	0.022	4	^{83}Se	9/2+	1/2-	0.231
5	^{84}Br	5-	2-	0.048	6	^{90}Rb	1-	4-	0.107
7	^{99}Nb	9/2+	1/2-	0.367	8	^{113}Ag	1/2-	7/2+	0.046
9	^{115}Ag	1/2-	7/2+	0.043	10	^{116}Ag	2-	5+	0.083
11	^{117}Ag	1/2-	7/2+	0.022	12	^{118}Ag	1+	5+	0.130
13	^{119}Cd	1/2+	11/2-	0.149	14	^{120}Ag	5+	0+	0.205
15	^{121}Cd	1/2+	11/2+	0.149	16	^{123}Cd	3/2+	11/2+	0.149
17	^{123}In	9/2+	1/2-	0.322	18	^{123}Sn	11/2-	3/2+	0.027
19	^{124}In	3+	8-	0.192	20	^{125}In	9/2+	1/2-	0.182
21	^{126}In	6+	3+	0.152	22	^{127}In	9/2+	1/2-	0.162
23	^{127}Sn	11/2-	3/2+	0.070	24	^{128}In	2+	7-	0.192
25	^{128}Sn	0+	7+	2.093	26	^{128}Sb	8-	5+	0.107
27	^{129}In	9/2+	1/2-	0.200	28	^{129}Sn	3/2+	11/2-	0.037
29	^{130}Sn	0+	7-	1.949	30	^{130}Sb	8-	5+	0.0220
31	^{132}Sb	4+	8-	0.022	32	^{133}Te	3/2+	11/2-	0.336
33	^{133}I	7/2+	19/2+	1.636	34	^{133}Xe	3/2+	11/2-	0.235
35	^{134}Sb	0-	7-	0.020	36	^{134}I	4+	8-	0.318
37	^{135}Xe	3/2+	11/2-	0.529	38	^{136}I	2-	6-	0.642
39	^{138}Cs	3-	6-	0.082	40	^{146}La	2-	6-	0.022
41	^{148}Pr	1-	6-	0.092	42	^{148}Pm	1-	6-	0.140
43	^{120}In	1+	3+	0.200	44	^{120}In	1+	8-	0.302
45	^{122}In	1+	4+	0.102	46	^{122}In	1+	8-	0.222
47	^{130}In	1-	10-	0.052	48	^{130}In	1-	5+	0.402

References

[1] W. Hauser, H. Feshbach, Phys. Rev., V. 87 (1952) p. 366.
[2] P.A. Moldauer, Phys. Rev., V. 135 (1964) p. 642.
[3] E.S. Troubetzkoy, Phys. Rev., V. 122 (1961) p. 212.
[4] S.M. Qaim, A. Mushtag, M. Uhl, Phys. Rev., V. C38 (1988) p. 645.
[5] M.B. Chadwick, P.G. Young, Nucl. Sci. Eng., V. 108 (1991) p. 117.
[6] O.T. Grudzevich, Yadernaya fizika, V. 61 (1998) p. 29.
[7] O.T. Grudzevich, Nuclear Physics (in print).
[8] O.T. Grudzevich, Yadernaya fizika 2000, V. 63 (2000) p. 503.
[9] P.G. Young, E.D. Arthur, Los Alamos National Laboratory report LA-6947 (1977).
[10] M. Uhl, B. Strohmaier, Report IRK 76/01, Vienna (1976).
[11] O.T. Grudzevich, A.V. Ignatyuk, V.I. Plyaskin, Proc. of Int. Conf. on Nuclear Data for Science and Technology, 1988, Mito, Japan, p. 1221.
[12] D. Wilmore, P.E. Hodgson, Nucl. Phys., V. 55 (1964) p. 673.
[13] Handbook for calculations of nuclear reaction data, IAEA-TECDOC-1034, Vienna (1998).
[14] NUDAT database, version (23 February 1996), maintained by the National Nuclear Data Center, BNL, USA.
[15] S.S. Dietrich, B.L. Berman, Atomic Data and Nuclear Data Tables, V. 38 (1988) p. 199.
[16] O.T. Grudzevich, Yadernaya fizika, V. 62 (1999) p. 227.
[17] ENSDF, produced by INSDDN, maintained by NNDC, BNL, USA (file as 1996).
[18] A.C. Wahl, At. Data and Nucl. Data Tables, V. 39 (1988) p. 1.
[19] C. Budtz-Jorgensen, H.H. Knitter, Nucl. Phys. A490 (1988) p. 307.
[20] J.W. Boldeman, A.R.L. Musgrove, R.L. Walsh, Aust. J. Phys., V. 164 (1967) p. 1520.
[21] I. During, V. Jahnke, H. Marten, In Proc. of the Workshop on Nuclear Fission and Fission-Product Spectroscopy, Grenoble, France (1994) p. 202.
[22] H.H. Knitter, F.J. Hamsch, C. Budtz-Jorgensen, Z. Naturforsch., V. 42a (1987) p. 786.
[23] G. Audi, A.H. Wapstra, Nucl. Phys., V. A595 (1995) p. 409.
[24] F. Pleasonton, R. Ferguson, H.W. Schmitt, Phys. Rev. C6 (1972) p. 1023.
[25] F. Pleasonton, Nucl. Phys. A213 (1973) p. 413.
[26] K. Nishio, I. Kimura, Y. Nakagome, ISINN-7, Dubna (1997) p. 325.
[27] H. Vonach, Proc. IAEA Advisory Group Meeting, New York (1983) p. 247.
[28] K.J. Le Couteur, D.W. Lang, Nucl. Phys., V. 13 (1959) p. 32.
[29] M.S. Samant, R.P. Anand, R.K. Choudhury, et al., Phys. Rev. C51 (1995) p. 3127.
[30] F.J. Hambsch, J. Aarle, R. Vogt, Proc. of XIII Meeting on Physics of Nuclear Fission, Obninsk (1995) p. 27.
[31] Nuclear Fission Physics (V.S. Stavinsky, Ed.), Moscow, Gosatomizdat (1963).
[32] H. Nifenecker, C. Signarbieux, M. Ribrag, et al., Nucl. Phys., V. A189 (1972) p. 285.
[33] D.G. Madland, T.R. England, NSE, V. 64 (1977) p. 859.
[34] G. Rudstam, Proc. of a Specialists' Meeting on Fission Product Nuclear Data, Tokai, Japan (May 1992) p. 271.
[35] J.P. Huizenga, R. Vandenbosch, Phys. Rev., V. 120(4) (1960) p. 1305.
[36] A.L. Barabanov, W.I. Furman, Proc. XIII Meeting on Physics of Nuclear Fission, Obninsk (1995) p. 52.

[37] J.L. Durell, In Proc. of 3rd Intern. Conf. “Dynamical Aspects of Nuclear Fission”, 1996, (J. Kliman, Ed.), Dubna (1996) p. 270.
[38] G.A. Popeko, et al., In Proc. of Int. Conf. on Fission and Properties of Neutron-Rich Nuclei, Florida, USA (1997) p. 645.
[39] G.M. Ter-Akopian, et al., Flerov Laboratory of Nuclear Reactions, Scientific Report 1995-1996, Dubna (1997) p. 81.
[40] H. Naik, et al., Nucl. Phys. A 648 (1999) p. 45.

UDC 539.173

SEMIMICROSCOPIC TREATMENT OF NUCLEAR FISSION BARRIERS

S.G. Yavshits, S.A. Pakhomov
V.G. Khlopin Radium Institute, St. Petersburg, Russia

O.T. Grudzevich
Institute of Nuclear Power Engineering, Obninsk, Russia

SEMIMICROSCOPIC TREATMENT OF NUCLEAR FISSION BARRIERS. The model is proposed to calculate the fission barriers of heavy nuclei with account of their possible dependence on excitation energy. The model is based on the shell correction method for calculation of potential energy of deformation with nuclear shape parameterization in the lemniscate coordinates.

The development of reliable fission barrier systematics is one of the main points in the development of fission cross-section systematics itself especially in the fields where calculated results cannot be compared with experiments directly. Besides, the well-known semiempirical systematics of fission barriers [1] includes only range of traditional nuclei at low excitation energy while the development of new nuclear accelerator-driven systems (ADS) requires to expand the systematics in order to include neutron deficient nuclei with sufficiently high excitations.

The Strutinsky method [2] of shell correction was used as a base for the new systematics. The necessary single-particle level schemes were calculated with the DIANA code [3]. The calculation of smooth “liquid drop” part of deformation energy is based on the improved Yukawa potential (Yukawa-plus-exponential model [4]).

We used Cassini ovaloids as a basis for the description of nuclear shape defined in the lemniscate coordinates [5]. The deviations of nuclear shapes from the basic figures which define high deformation modes are described by coefficients at corresponding Legendre polynomials. So, the configuration of the fissioning system is defined by the following parameter set:

$$\{\alpha_f\} = (A, Z, \varepsilon, [\alpha_m], T), \tag{1}$$

where A, Z are mass and charge numbers, ε is the deformation of the basic figure, $[\alpha_m]$ are coefficients at polynomials and T is the temperature of the fissioning nucleus.

The transformation of the (R,x) point in the lemniscate coordinate system to the cylindrical coordinates is as follows:

$$\begin{aligned} r &= 2^{-1/2} [R^4 + 2 S R^2 (2x^2 - 1) + S^2)^{1/2} - R^2(2x^2 - 1) - S]^{1/2}, \\ z &= 2^{-1/2} \, \mathrm{sign}(x) \, [R^4 + 2 S R^2 (2x^2 - 1) + S^2)^{1/2} + R^2(2x^2 - 1) + S]^{1/2}, \end{aligned} \tag{2}$$

$$S = \varepsilon R_0^2$$

where S and R are

$$R(x) = R_0(1 + \sum_{m=1}^{N} \alpha_m P_m(x)) \quad (3)$$

and P_m are Legendre polynomials.

In this model the parameter ε can be considered as a fission coordinate. At ε=0 (and $[\alpha_m]$=0) the nucleus has the spherical shape. At 0<ε<0.4 the shape is close to an ellipsoidal one. At 0.5<ε<1 the neck arises and develops and at ε=1 the neck radius is equal 0, i.e. nucleus is divided in two fragments:

$$S = \varepsilon R_0^2 , R_0 = r_0 A^{1/3}. \quad (4)$$

It is commonly used to restrict the set of deformation parameters by degree N=4. Then the coefficient α_1 defines fragment mass asymmetry, α_2 is correlated with ε and can be omitted, α_3 defines octupole deformation and α_4 defines hexadecapole deformations.

The different fission stages for ^{240}Pu are presented in Fig. 1 vs. parameter ε where ε varies in the diapason 0-1 with step 0.1 and α_1= 0.06, α_3= 0 and α_4= 0.016. This set of parameters corresponds to the formation of pair fragments ^{100}Y and ^{140}Cs.

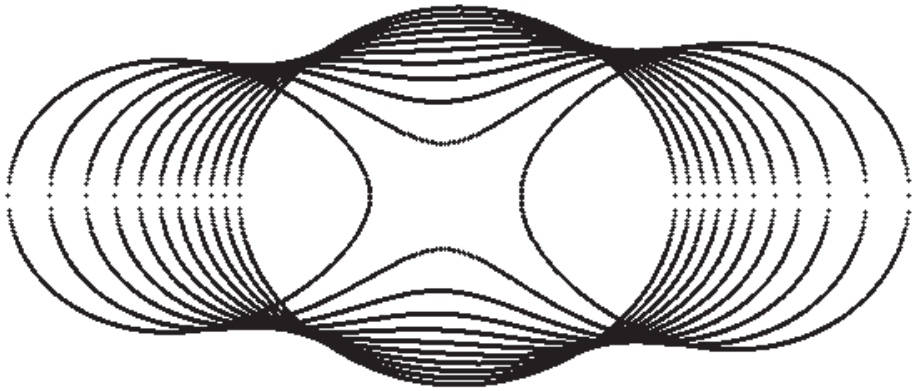

Fig. 1. Different ^{240}Pu fission stages.

The potential energy of deformation at the ground state in the shell correction method has the following form:

$$E=E_{coul}+E_{nuc}+\delta U_n+ \delta U_p + Ep_n + Ep_p, \quad (5)$$

where E_{coul} is the coulomb energy of the charged liquid drop, E_{nuc} is the nuclear part (surface energy), δU_n, δU_p and Ep_n, Ep_p are shell corrections and pairing energies for neutrons and protons correspondingly.

The shell corrections as well as the pairing energies have been calculated on the base of single-particle spectra obtained by means of the DIANA code in the deformed Woods-Saxon well V({α_f}).

According [4] the value of coulomb energy for axially symmetrical and uniformly charged the liquid drop can be presented by the integral:

(6)

$$E_{coul} = \pi \rho^2 \int_{Z1}^{Z2} dz \int_{0}^{r(Z)} dr \int_{Z1}^{Z2} dz' \{[r^2(z') - r^2(z) - (z-z')^2 + \frac{dr^2(z')}{dz'}(z-z')]F(a,b) + E(a,b)\},$$

where ρ is the charge density, F(a,b) and E(a,b) are the complete elliptical integrals of the first and second kinds, correspondingly, and the value of the parameters a and b are defined by equations:

$$a(r,z) = \sqrt{(r + r')^2 + (z' - z)^2}, \quad b(r,z) = \sqrt{(r' - r)^2 + (z' - z)^2}, \tag{7}$$

The nuclear part of energy in the Yukawa+exponential model [4] has the following form:

$$E_{nuc} = c_S /(4\pi r_0^2) \int_{Z1}^{Z2} dz \int_{Z1}^{Z2} dz' \int_{0}^{2\pi} d\varphi \{2 - [(\sigma/a)^2 + 2\sigma/a + 2] e^{-\sigma/a}\} r(z)[r(z) - r(z')\cos(\varphi) - r'(z)(z-z')]r(z') - r(z)\cos(\varphi) - \frac{dr(z')}{dz'}(z'-z)]/\sigma^4, \tag{8}$$

where $\sigma = [r^2(z) + r^2(z') - 2\, r(z)\, r(z') \cos(\phi) + z^2 + z'^2 - 2\, z\, z']^{1/2}$;
c_s is the effective constant of surface energy, $c_s = a_s[1 - k_s (N-Z)^2/(N+Z)^2]$;
a_s is the constant of surface energy (a_s = 21.7 MeV);
k_s is the constant of isospin asymmetry (k_s = 3.0);
a is the radius of improved Yukawa potential (a = 0.65 fm);
r_0 is the nuclear radius constant (r_0 = 1.18 fm).

The example of deformation energy calculation is shown in Fig. 2 where the curves of potential energy and its components for fission of ^{240}Pu are presented as follows: liquid drop part E_{lq} ($E_{lq} = E_{coul} + E_{nuc}$), shell correction E_{sc} ($E_{sc} = \delta U_n + \delta U_p$) and pairing energy Ep ($Ep = Ep_n$ and Ep_p) as a function of parameter ε. The heights of fission barriers are shown in the same Figure.

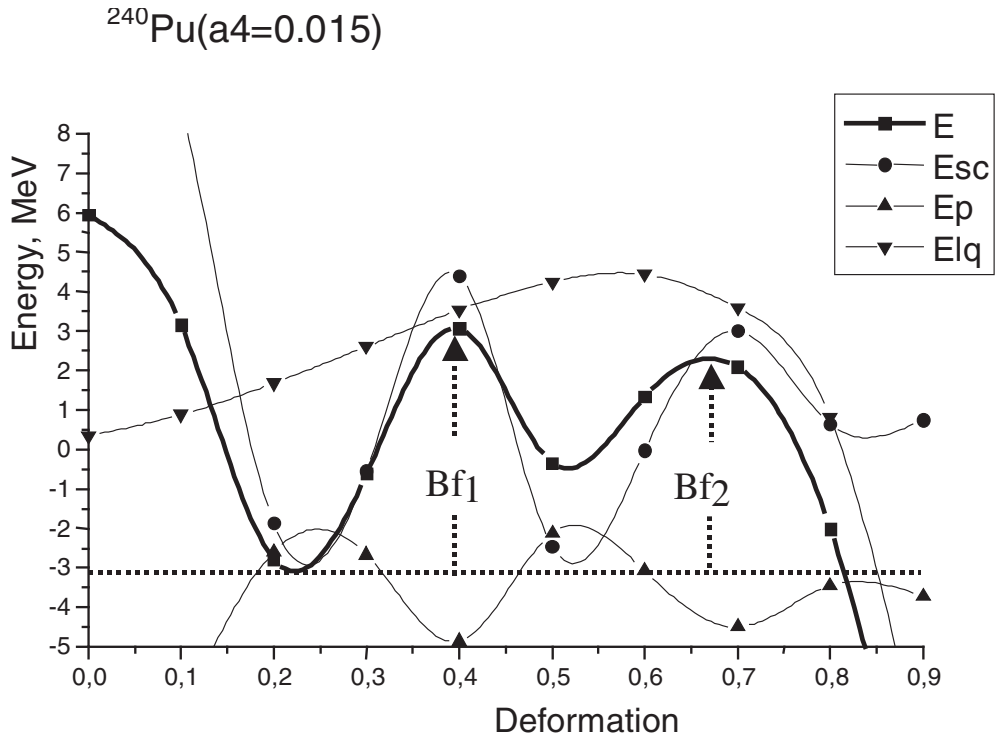

Fig. 2. Deformation energy E and its components E_{lq}, E_{sc} and Ep for ^{240}Pu fission vs. deformation and fission barriers Bf_1 and Bf_2.

The parabolic approximation near maximums was used for the evaluation of fission barriers Bf_1 and Bf_2 as well as to estimate barriers curvatures as a second derivative of deformation energy E at the barrier top (C) which is necessary for the calculation of frequencies ω:

$$\omega = k \sqrt{C / B} \ , \tag{9}$$

$$B = 3m/(4\pi)\ r_0^2\ A^{5/3}\ /2, \tag{10}$$

where k is the fitting coefficient, B is the hydrodynamic mass parameter and m is the nucleon mass.

The potential energy E at each stage of fission has to be minimal on all deformation parameters [α_m]. For the definition of the optimal set of these parameters, the effective routine of the multidimensional optimization has been developed which is based on the complex algorithm [6]. However, in practice, there is no possibility to achieve the satisfactory agreement between calculated fission barriers with known semiempirical systematics [1]. The possible reason of this disadvantage may be due to the used shape parameterization which is the main problem in the description of the fission evolution.

Such a circumstance forces to use some parameterization of deformation parameters in the ground state of fissioning nucleus {α_m} by some smooth functions which depend in their turn on the mass and the charge numbers of nucleus or fissility parameter Z^2/A. The example

of barriers behavior as functions of α_1, α_4 fixed along fission path is presented in Fig. 3 (A,B) for the case of ^{240}Pu.

The coefficient α_1 is connected with the formation of the fragment mass distribution. In the actinide region the peak of the mass distribution of the heavy fragments is situated around $A_H \approx 140$ a.e.m. and the asymmetry parameter can be fixed (from 0.12 up to 0.05 for transition from Th to Cf). It is seen in Fig. 3 that the variation of α_4 coefficient from –0.05 up to 0.1 leads to the monotonous increase of the heights for both barriers Bf_1 and Bf_2.

Other important values which define barriers heights are surface energy parameter C_S and coulomb radius R_0 (Fig. 3 C,D).

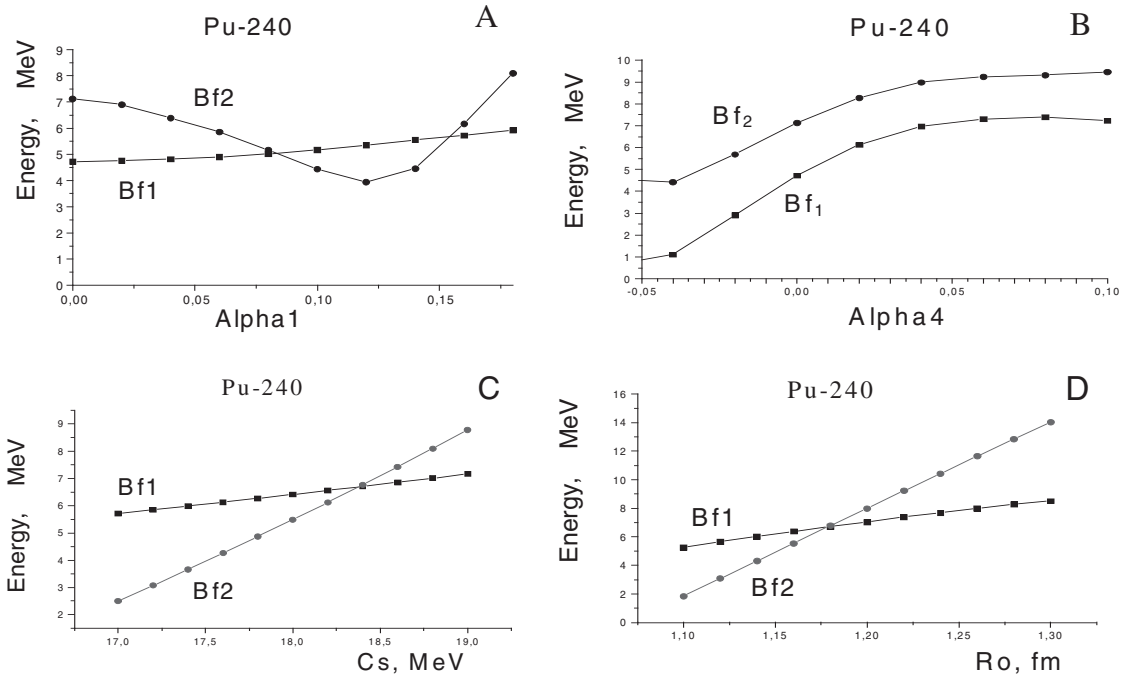

Fig. 3. The fission barriers heights vs. deformation parameters α_1, α_2, α_3, α_4 and parameters C_S, R_0.

We used the parameters Cs and α_4 as fitting parameters to construct the systematics. In order to check the possible odd-even effects, the actinide region has been divided in three groups: even group ^{232}Th, ^{234}Th, ^{236}U, ^{240}U, ^{240}Pu, ^{244}Pu, ^{250}Cm; odd-even group ^{229}Th, ^{233}Th, ^{235}U, ^{239}U, ^{239}Pu, ^{243}Pu, ^{245}Cm, ^{249}Cm, ^{253}Cf; even-odd group ^{232}Pa, ^{234}Np, ^{236}Np, ^{238}Np, ^{240}Am, ^{242}Am, ^{244}Am, ^{250}Bk; and odd-odd group of nuclides ^{231}Pa, ^{235}Np, ^{239}Np, ^{243}Am, ^{247}Am, ^{249}Bk. These nuclides uniformly cover the tables of the known fission barrier systematics.

We defined the optimal set of parameters Cs and α_4 from the condition of the best concurrence with Back systematics [1]. The analysis of the results has not revealed any odd-even staggering in the behavior of parameters. Such a circumstance allow to use the same functions Cs(N,Z) and α_4(N,Z) for the whole table. The values of parameters obtained from fitting as well as their parameterization are presented in Table 1. The quality of these parameterizations is sufficiently high – the deviations from data obtained with fitting on barrier systematic are less than 2%.

Table 1

Values of C_s and α_4 and their (N,Z) dependencies

Nuclides	Cs	α_4	Nuclides	Cs	α_4
Th232	17.65	0.055	Cf253	18.9	-0.065
Th234	17.3	0.08	Pa232	18.01	0.046
U236	17.9	0.04	Np234	18.41	0.029
U240	17.55	0.035	Np236	18.15	0.029
Pu240	18.25	0.02	Np238	18.15	0.024
Pu244	17.85	0	Am240	18.24	0.022
Cm250	18	-0.035	Am242	18	0.015
Th229	17.85	0.06	Am244	17.91	0.005
Th233	17.4	0.065	Bk250	18.49	-0.035
U235	17.85	0.048	Pa231	18.07	0.05
U239	17.35	0.07	Np235	18.29	0.033
Pu239	18.05	0.04	Np239	17.9	0.024
Pu243	17.9	0.01	Am243	18.03	0.008
Cm245	18	0.005	Am247	17.97	-0.006
Cm249	17.95	-0.026	Bk249	18.29	-0.024
$C_s = 20.54\,(1 - 2.58\,(N-Z)^2/A^2) - 6.72 + 0.185\,Z^2/A$					
$\alpha_4 = 1.162 - 0.0036\,Z - 0.0033\,A$					

The obtained function Cs(N,Z) now contains two terms: the first one is close to the function used in [4] $(21.7\text{-}3(N\text{-}Z)^2/A^2)$; the appearance of the coulomb parameter Z^2/A in the second term is probably connected to the necessity to improve the coulomb part of the Nix and Sierk model [4]. The hexadecopole deformation falls as mass number of nuclide growths and values of α_4 are close to the commonly used ones (see, for example [6]).

The comparison of the calculated barriers with values given by Back values [1] is presented in Table 2 and Fig. 4. The quite satisfactory results have been obtained as it can be seen in the presented data.

Table 2

The heights of Bf_1 and Bf_2 and the values of $h\omega_1$, $h\omega_2$ (MeV)

	Bf_1 (calc.)	Bf_1 (Back)	$h\omega_1$(calc.)	$h\omega_1$ (Back)	Bf_2 (calc.)	Bf_2 (Back)	$h\omega_2$(calc.)	$h\omega_2$ (Back)
Th229	6.82	(6.02)	0.89	(0.9)	7.21	6.30±0.20	0.49	-
Th230	6.33	-	0.88	-	6.7	6.5±0.3	0.52	-
Th231	6.37	(6.02)	0.9	(0.9)	6.76	6.22±0.20	0.55	0.52±0.10
Th232	5.89	<5.50	0.88	-	6.34	6.15±0.20	0.58	0.50±0.10
Th233	5.91	(6.02)	0.91	(0.9)	6.38	6.28±0.20	0.63	0.45±0.10
Th234	5.51	6.15±0.20	0.88	1.00±0.10	6.06	6.52±0.20	0.66	0.75±0.10
Pa231	6.64	5.75±0.30	0.9	(0.8)	6.64	5.85±0.30	0.56	(0.45)
Pa232	6.67	5.75±0.30	0.91	(0.6)	6.76	6.10±0.30	0.6	(0.45)
Pa233	6.22	5.85±0.30	0.9	(0.8)	6.34	6.00±0.30	0.63	(0.4)
U232	6.2	5.54±0.20	0.86	0.80±0.10	5.99	5.45±0.20	0.58	0.55±0.10
U234	5.97	6.20±0.25	0.88	1.00±0.10	5.81	5.95±0.25	0.64	0.65±0.10
U235	6.17	6.10±0.30	0.93	(0.85)	5.91	5.65±0.30	0.68	(0.5)
U236	5.81	5.70±0.20	0.9	0.90±0.10	5.69	5.68±0.20	0.7	0.50±0.10
U237	6.07	6.35±0.30	0.93	(0.85)	5.86	5.95±0.30	0.74	(0.55)
U238	5.7	5.90±0.20	0.9	1.00±0.10	5.6	6.12±0.20	0.74	0.62±0.10
U239	5.93	6.55±0.30	0.93	(0.9)	5.76	6.30±0.30	0.77	(0.65)
U240	5.52	5.75±0.20	0.89	1.00±0.10	5.41	5.95±0.20	0.76	0.70±0.10
Np234	6.57	5.35±0.30	0.91	(0.6)	6.07	5.00±0.30	0.65	(0.42)
Np235	6.26	5.60±0.30	0.91	(0.8)	5.79	5.20±0.30	0.68	(0.55)
Np236	6.49	5.70±0.30	0.96	(0.6)	5.91	5.20±0.30	0.72	(0.42)
Np237	6.13	5.70±0.30	0.92	(0.8)	5.74	5.50±0.30	0.73	(0.55)
Np238	6.36	6.00±0.30	0.95	(0.6)	5.89	6.00±0.30	0.77	(0.42)
Np239	6.01	5.85±0.30	0.92	(0.8)	5.67	5.50±0.30	0.77	(0.55)
Pu238	5.83	5.90±0.20	0.9	0.80±0.10	5.19	5.20±0.30	0.72	0.55±0.10
Pu239	6.13	6.43±0.20	0.93	1.00±0.10	5.41	(5.5)	0.75	(0.55)
Pu240	5.88	5.80±0.20	0.91	0.82±0.10	5.23	5.45±0.20	0.74	0.60±0.10
Pu241	6.16	6.25±0.20	0.93	1.10±0.10	5.46	(5.5)	0.76	(0.55)
Pu242	5.86	5.60±0.20	0.89	0.82±0.10	5.22	5.63±0.20	0.74	0.59±0.10
Pu243	6.1	6.05±0.20	0.91	0.80±0.10	5.38	(5.6)	0.74	(0.55)
Pu244	5.81	<5.6	0.87	-	5.12	5.35±0.20	0.72	0.57±0.10
Pu245	6.06	5.72±0.20	0.88	0.90±0.10	5.33	(5.45)	0.72	(0.55)
Am240	6.32	6.35±0.20	0.94	0.70±0.10	5.36	(4.8)	0.77	(0.42)
Am242	6.33	6.38±0.20	0.93	0.50±0.10	5.37	(4.8)	0.76	(0.42)
Am243	6.1	5.98±0.20	0.91	0.75±0.10	5.14	(4.8)	0.73	(0.55)
Am244	6.31	6.18±0.20	0.92	0.50±0.10	5.3	(4.8)	0.73	(0.42)
Am245	6.02	5.88±0.20	0.88	0.85±0.10	5.02	(4.8)	0.7	(0.55)
Am247	5.83	5.60±0.20	0.85	0.90±0.10	4.73	(4.8)	0.65	(0.55)
Cm244	5.98	6.12±0.20	0.9	0.90±0.10	4.65	<4.9	0.67	-
Cm245	5.4	6.38±0.20	0.8	0.65±0.10	4.84	(4.2)	0.67	(0.55)
Cm247	6.41	6.20±0.20	0.89	0.70±0.10	4.93	(4.2)	0.65	(0.55)
Cm248	5.97	6.15±0.20	0.85	0.90±0.10	4.47	<4.6	0.62	-
Cm249	6.13	5.80±0.20	0.85	0.75±0.10	5.78	(4.2)	0.7	(0.55)
Cm250	5.79	5.15±0.20	0.82	0.72±0.10	3.84	3.90±0.30	0.37	0.69±0.10
Bk249	6.28	6.05±0.20	0.87	0.80±0.10	4.23	(4.2)	0.61	(0.55)
Cf253	6.7	5.60±0.30	0.85	1.10±0.10	3.46	(4.2)	0.42	(0.55)

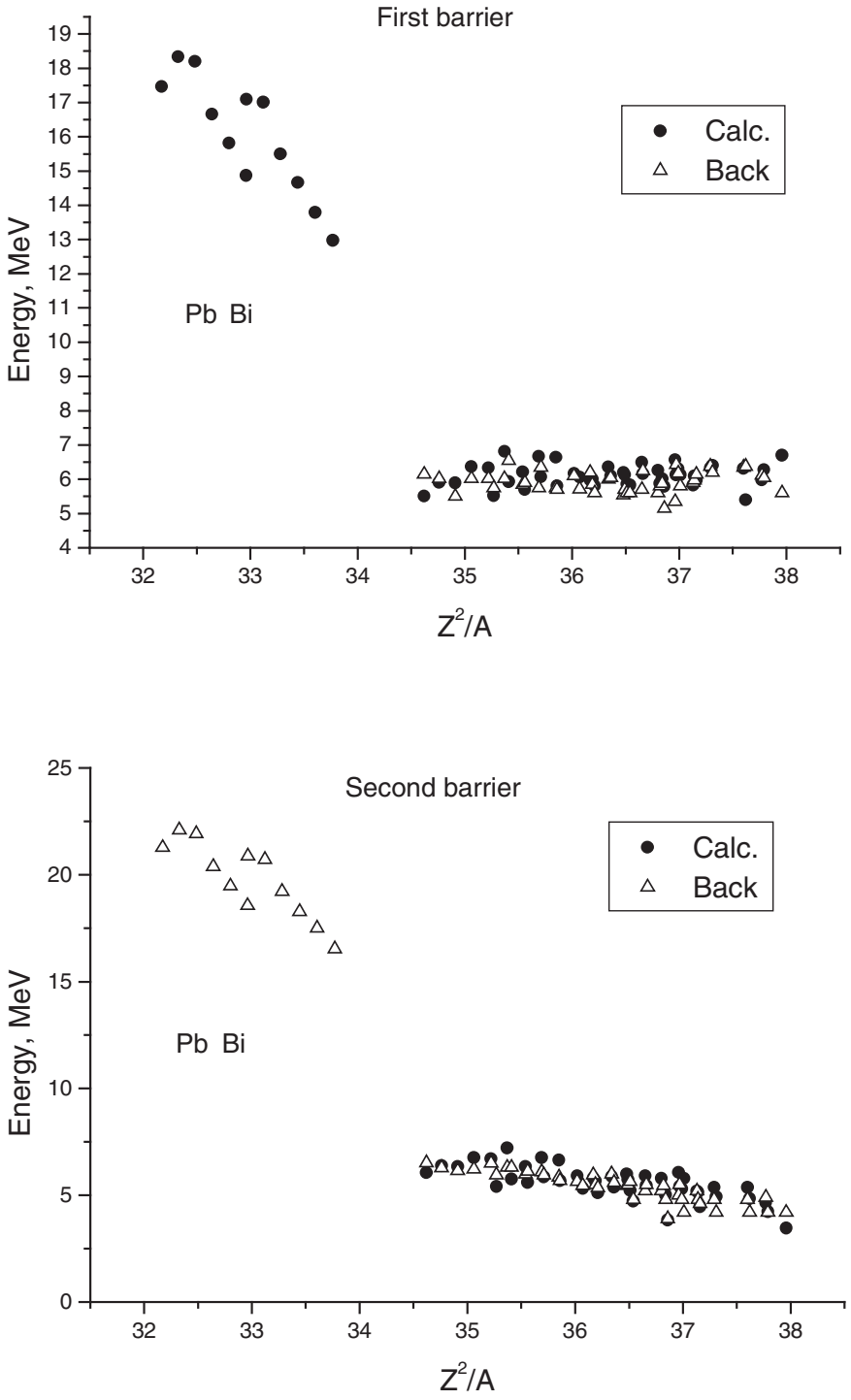

Fig. 4. The comparison of our results with data of Back [1].

The left part of the figures ($Z^2/A < 34$) presents the data obtained for nuclides which are very important for ADS technologies, i.e. isotopes of Pb and Bi (^{204,205,206,207,208,209}Pb and ^{204,205,206,207,208,209}Bi) where fission barriers are poorly investigated. The barriers in these cases were calculated for $\alpha_1=0$ (symmetric fragment mass distribution). It is seen from the data that the barrier heights decrease for more neutron-deficient isotopes.

The interaction of high-energy particles (up to 1 GeV for ADS) with target nuclei leads to the formation of high and very high excited nuclei which can undergo the fission. It is necessary for these reactions to include the dependence of fission barriers on excitation energy (or nuclear temperature T) into consideration. We use a simple model to demonstrate this kind of dependence, $E = E_{lq} + (E_{sc} + E_p) \cdot \exp(-T/T_{cr})$, where T_{cr} is the parameter. The dependence of deformation energy for the case of ^{240}Pu on the temperature for T_{cr} = 0.75 MeV is shown in Fig. 5 along the fission axes. The degeneration of structure effects with temperature growth is clearly seen in the figure. At T ≥ 2 MeV the barrier is only defined by liquid drop nuclear properties.

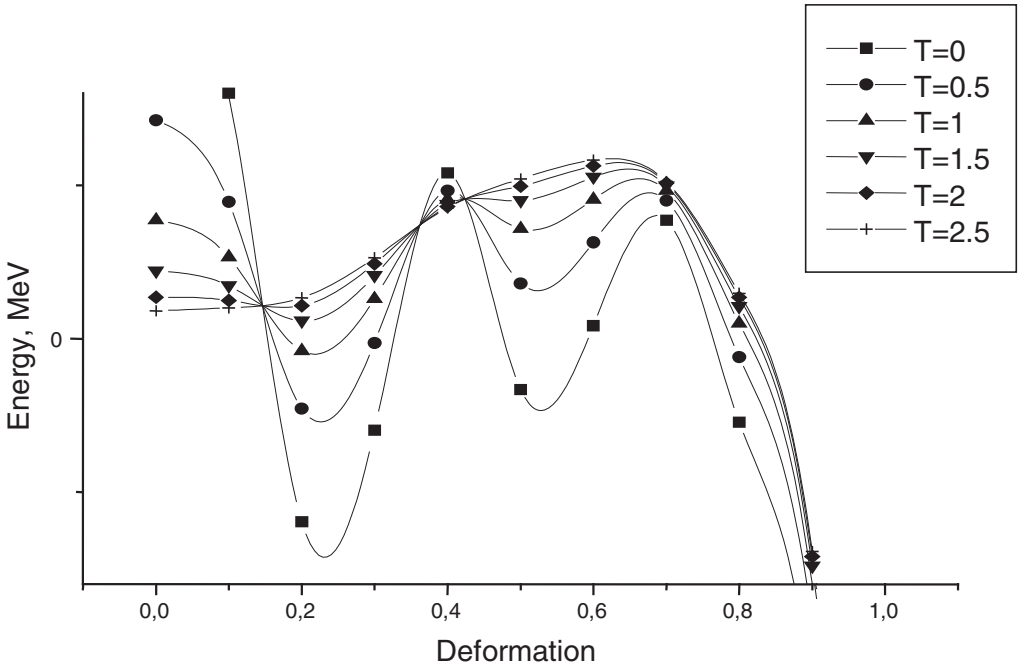

Fig. 5. The temperature dependence of deformation energy.

So, the semimicroscopic model is proposed in this work which allows to calculate the fission barriers of heavy nuclei with account of their possible dependence on excitation energy.

References

[1] J.E. Lynn, Report AERE-R7468 (1974); B.B. Back et al., Phys. Rev. C9, 1924 (1974); B.B. Back et al., Phys. Rev. C10, 1948 (1974); T. Ohsawa, IAEA-TECDOC-483, p. 134 (1988).
[2] V.M. Strutinsky, Nucl. Phys. A122, 1 (1968).
[3] V. Pashkevich, V. Rubchenya, Bull. of Nuclear Data Center LINP, 3 (1976).
[4] H.J. Krappe, J.R. Nix, A.J. Sierk, Phys. Rev. C20, 992 (1979).
[5] V.V. Pashkevich, Nucl. Phys. A169, 275 (1971).
[6] P. Moller, J.R. Nix, W.D. Myers, W.J. Swiatecki, At. Data and Nucl. Data Tables 66, 131 (1997).

UDC 539.173

MULTICONFIGURATION FISSION CROSS-SECTIONS AT TRANSITIONAL ENERGY REGION 20-200 MeV

S. Yavshits, G. Boykov, V. Ippolitov, S. Pakhomov, A. Roschin
V.G. Khlopin Radium Institute, St. Petersburg, Russia

O. Grudzevich
Institute of Nuclear Power Engineering, Obninsk, Russia

MULTICONFIGURATION FISSION CROSS-SECTIONS AT TRANSITIONAL ENERGY REGION 20-200 MeV. The new approach to the calculation of nucleon induced fission cross sections at 20-200 MeV is presented. The cross sections of multiconfiguration fission (MCF) is calculated as a mixture of (Z,A,p,h,U) configurations formed as a result of fast stage of fission reaction with weights defined by the population probability Y of (Z,A) nucleus in the (p,h) particle-hole state at the excitation energy U. We use the intranuclear cascade model to compute the probability Y and the precompound-statistical model for calculation of fission and de-excitation cross section from state (Z,A,p,h,U). Calculated results are presented for two absorption cross sections obtained with two optical model parameter sets. Up to 15 fissioning nuclei in 10 (p,h) states at the wide excitation region were taken into account in the calculation.

Introduction

The development of the future nuclear power energetics with application of hybrid technologies using accelerator-based incineration systems requires a knowledge of data library on cross-sections of nuclear reactions in a wide energy range of incident particles (from very slow particles up to beams with energy of a few GeV). The systematic experimental research for such wide energy range is complicated and for many targets in principle impossible. Therefore a key role for the development of the required nuclear data library has a model calculations which should have a sufficient predicting force for the description of fission cross-sections and cross-sections of other competing nuclear reactions with necessary accuracy. At the present time there are a lot of experimental data and rather reliable codes for the calculation of fission cross-sections at incident particle energies up to 20 MeV. At energies of particles about several hundreds MeV (from 200 MeV and higher), rather reliable evaluations can be obtained by means of codes based on the most modern versions of an intranuclear cascade model. At the same time, in an energy range from 20 up to 200 MeV there is a lack of experimental data which are frequently not agreed among themselves and the agreement of results of the best modern model codes is not better than within a factor of 2 or more. Besides, in this energy range, the significant variation of cross section values is observed for both beam energy growth and a transition from nucleus to nucleus.

The energy region of 20-200 MeV is a transitive one from well investigated low-energy nuclear physics to the physics of intermediate energy. It is possible to divide the existing

model codes used for calculation of the reaction cross-sections in this transition region into two basic classes:

- Codes for the description of low energy reactions (up to several MeV) using the statistical model based on the Hauser-Feshbach theory and the pre-equilibrium emission model with total angular moment conservation (codes STAPRE, GNASH and others);

- Codes for the calculation of cross-sections at intermediate energies from several hundreds MeV up to tens of GeV using the various versions of the intranuclear cascade model (cascade-emission model of Ilyanov-Mebel, cascade-exiton model of Toneev-Mashnik and others).

Unfortunately in the transition energy region where the contributions of pre-equilibrium and direct emission, various fission chances, structures of fission barriers and low-energy states are essential, the predicting ability of these model approaches is rather low due to a wide and not always reasonable variation of model parameters for the description of experimental data. The basic problems which need to be solved for this energy region are the description of the entrance channel, the correctness of non-equilibrium process calculations and the systematic of fission barriers including their energy dependence.

The example of fission cross-section description with both, the pre-equilibrium-statistical model (STAPRE code) and the intranuclear cascade-exciton model (code CEM95) with default parameters (i.e. without input parameters fitting) are shown in Figs 1 and 2 for ^{232}Th(n,f) and ^{239}Pu(n,f) reactions in comparison with experimental data. The crucial discrepancy between the results of two model calculations and between the calculated and experimental data is clearly observed.

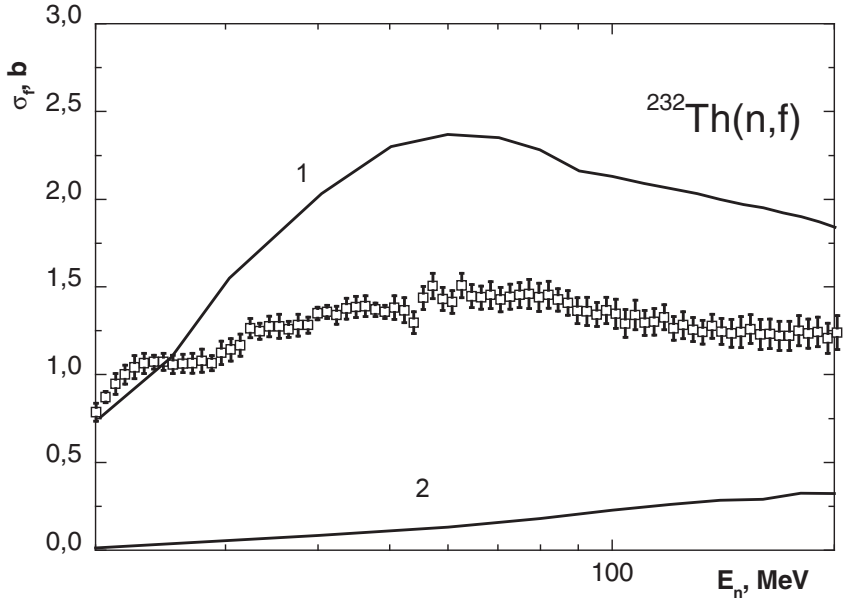

Fig. 1. Comparison of the default versions of CEM95 and STAPRE codes for ^{232}Th(n,f) reaction. The points are the experimental data. Curve 1 is the STAPRE result, curve 2 is the CEM95 result. See text for details.

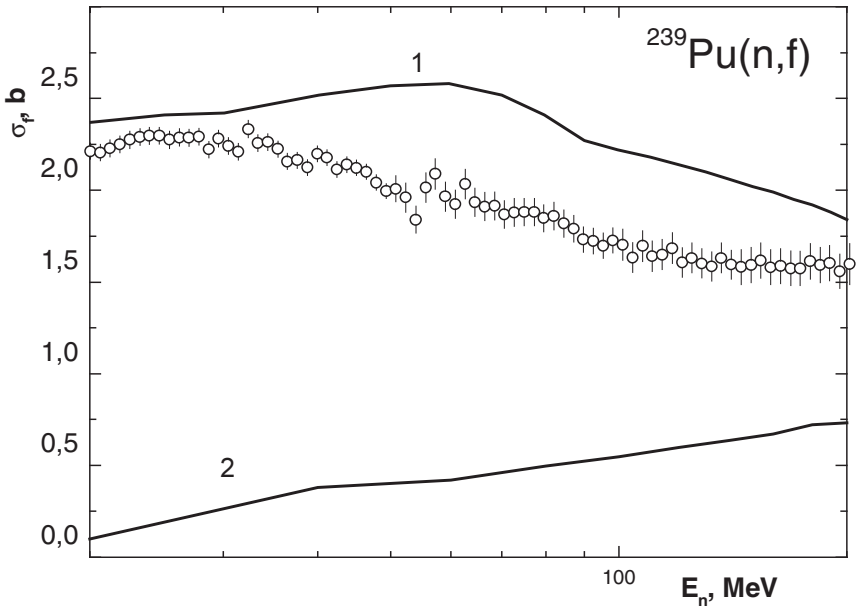

Fig. 2. The same as in Fig. 1, but for ^{239}Pu(n,f) reaction.

1. Optical model calculation of reaction cross-sections for deformed targets

The realistic description of the entrance channel (i.e. calculation of the probability for nucleon to penetrate inside nucleus) is the significant part of any nucleon-induced fission cross-section calculations. The reaction cross-section calculation (absorption) for incident particles at all energies is defined under consideration by nucleon transmission coefficients. Moreover, transmission coefficients define decay widths of intermediate nuclear states at pre-equilibrium and evaporation stage of disintegration of excited nucleus. This is a reason why the reliability of the calculation of the transmission coefficient effects on an accuracy of fission cross-section calculations.

At present the main (and unique) method for this kind of calculations is the optical model of nuclear reactions. For spherical nuclei the calculations can be done with the well-known code SCAT2 [1]. However, as a rule, fissioning nuclei are strongly deformed in their ground states and also have a number of collective low energy excited states. The connection with these states modifies the wave function of the nuclear system rather significantly. The consideration of this modification requires the application of the generalized optical model which has been formulated in the coupled channel method [2] and developed in the works of T. Tamura et al. [3]. On the basis of the Tamura approach, the code ECIS was developed by J. Raynal [4] which allows to calculate the cross-sections of nuclear reactions in the wide energy region [5].

The rotational model level schemes presented in the RIPL library [8] and relativistic kinematics are used in the calculations. The coupling of only three channels are taken into account because the account of more numbers of channels modifies results less than 1%.

On the base of this kind of calculations, the library of proton- and neutron-induced total and reaction cross-sections for 35 nuclei (^{208}Pb, ^{209}Bi, ^{227}Ac, ^{228,229,230,232}Th, ^{232,233,234,235,236,238,239}U, ^{237,238,239}Np, ^{238,239,240,242}Pu, ^{242,243}Am, ^{243,244,245,246,247,248}Cm, ^{247}Bk, ^{248,249,250,251,252}Cf) is developed for energies up to 220 MeV.

In Fig. 3 the results of total cross-section calculations are presented for ^{235}U + n reaction in the case of two optical model parameter sets (OMPS) – by Young [6] and by Konshin [7] in comparison with experimental data (the Young potential has a restricted energy interval of application, so results of calculations are shown up to 100 MeV). In both cases, our results describe the experimental data quite well. But, as it can be seen in Fig. 4, the reaction cross-sections are more sensitive to the choice of the potential: absorption cross-sections of neutron by ^{238}U are very different (up to 15% around 30 MeV). Due to the lack of the experimental data on reaction cross-sections, the choice between OMPS is difficult and we carried out the calculations for both cases. For the fission cross-section calculation, we used OMPS [7] where the picture of the gross structure in the reaction cross-section is reproduced more reliably in the whole energy region under consideration.

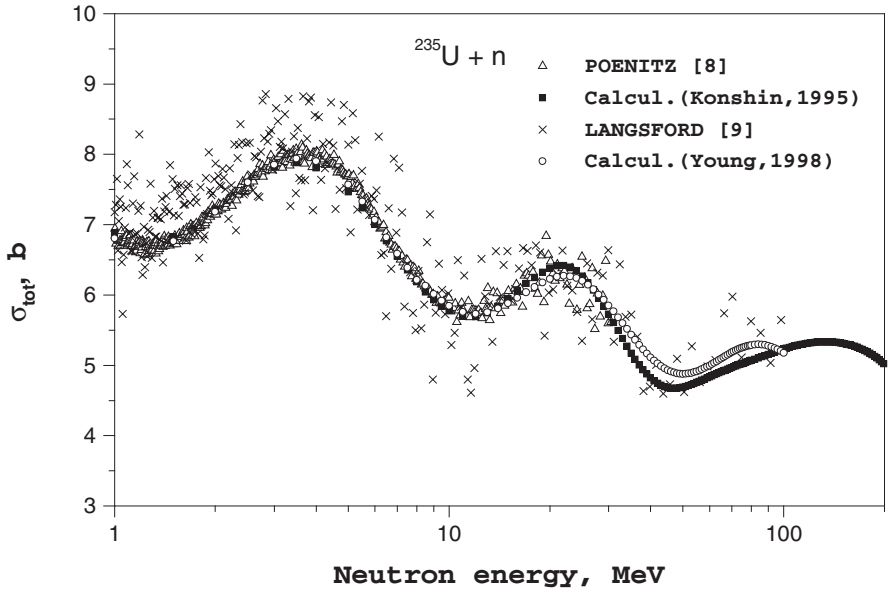

Fig. 3. Total neutron cross section for ^{238}U+n. Experimental data [8,9], curves are results of OM calculations with OMPS [6] and [7].

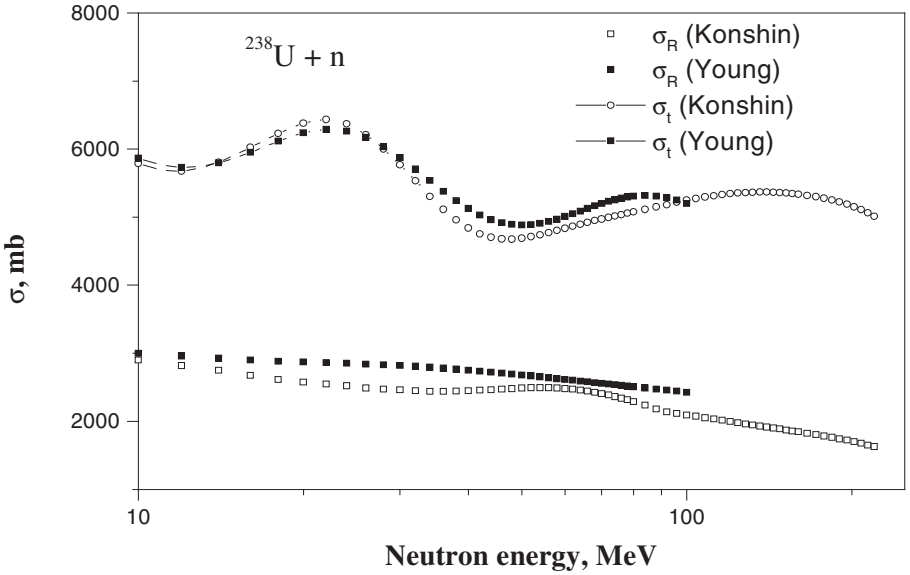

Fig. 4. Calculated cross-sections for ^{238}U+n: σ_R is the reaction cross-section, σ_{tot} is the total cross-section.

2. Simulation of entrance channel of fission reaction with intranuclear cascade model

We use the intranuclear cascade model for the description of the direct processes on the first stage of fission reaction as it is realized in the CEM code [10] where the so-called "cascade-exciton" model of nuclear reactions has been formulated.

It is assumed in this model that the nuclear reaction goes on three main stages. The first one is the intranuclear cascade where primary particle may undergo a number of re-scattering before its absorption or escape from nuclear volume occurs. The significant point of this scenario is a formation after the cascade stage of excited residual nuclei in different particle-hole configurations which serve as a start for the second pre-equilibrium reaction stage which can be treated in the framework of the standard exciton model. And the third stage is the particle evaporation and/or fission from the equilibrium state of the final nuclear system. The important point of the CEM model is the substantial difference of particle-hole configurations (characterized by exciton number $n=p+h$, where p and h are the numbers of particles and holes, correspondingly) as well as excitation energy after completion of the first direct reaction stage from the starting configurations of ordinary exciton models. Numerous calculations show that the distributions of residual nuclei after the cascade stage are rather wide on *n, p, h* and energy.

All calculations of intranuclear cascades are performed in the three-dimensional geometry. The nuclear density distribution is described by the Fermi distribution with parameters taken from the experimental data on electron-nucleus scattering. The target nucleus is divided by concentric spheres at 7 zones where the nuclear density is assumed to be a constant. The diffusiveness of nuclear density and potential edge is taken into account. For intranuclear collisions of nucleons, the Pauli principle forbids the collision with energy of secondary particles less than Fermi energy.

The main condition of the intranuclear cascade model applicability is the smallness of the length of de Broglie waves for all interacted particles; the wave length must be less than the average distance between intranuclear nucleons ~1 fm. In this case, the picture of the interaction is approximately the semiclassical one and it is possible to say about the particle trajectories and two-particle collisions inside nucleus. This condition restricts the energy region of incident particles above 50 MeV. Such a limitation is a significant point of the model. However, in order to improve it, the way out of the frameworks of intranuclear cascade is necessary with the description of reaction mechanism in the terms of rather strict quantum-statistical approach. Practically the low limit of applicability of intranuclear cascade can be established in the analysis of calculation results for the given case.

The results of our calculations for main characteristics of residual nuclei formed after the cascade stage are presented in Figs 5-8 for ^{232}Th in the transitive energy region 20-200 MeV. The yields of residual nuclei are presented in Figs 5-6 for protons and neutrons in the entrance channel. The presented results show that at low energies almost all incident particles are absorbed by target nucleus with formation of compound nucleus. For higher energies the yield of compound nucleus falls down significantly. The maximal yield in this case corresponds to the escape of one neutron or proton from target nucleus.

The yields in the direct reactions ^{232}Th(n,2n)^{231}Th and ^{232}Th(n,n')^{232}Th with formation of ^{231}Th and ^{232}Th in two particle-hole configurations are shown in Figs 7-9 as a function of excitation energy for the given residual nucleus. As it can be seen, the configurations with the low exciton number (p+h) have significantly higher yields as compared with the configurations characterized by large exciton numbers. Nevertheless, these configurations have a similar contribution to the fission cross-sections due to high excitation energies of high-exciton configurations (Fig. 5).

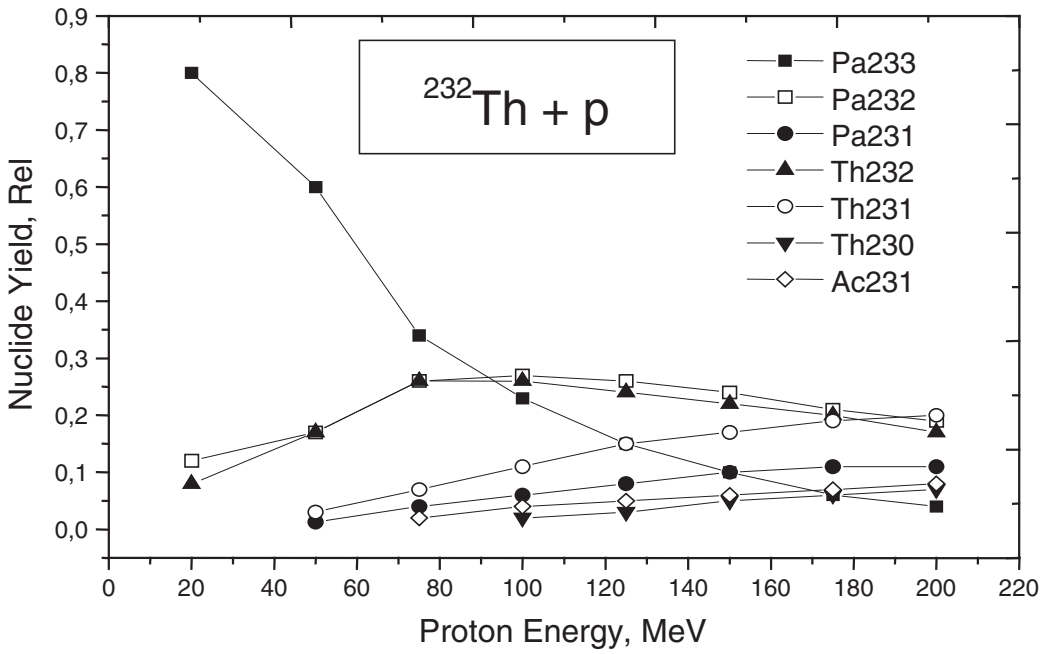

Fig. 5. The yield of residual nuclei after the cascade stage for ^{232}Th+p reaction.

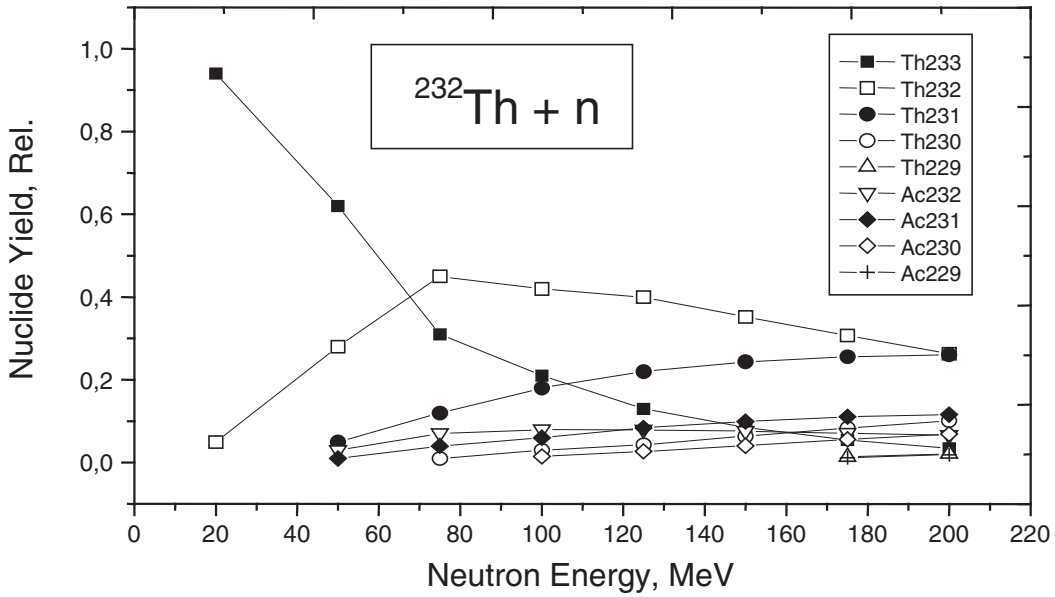

Fig. 6. The same as in Fig. 5 but for ^{232}Th+n reaction.

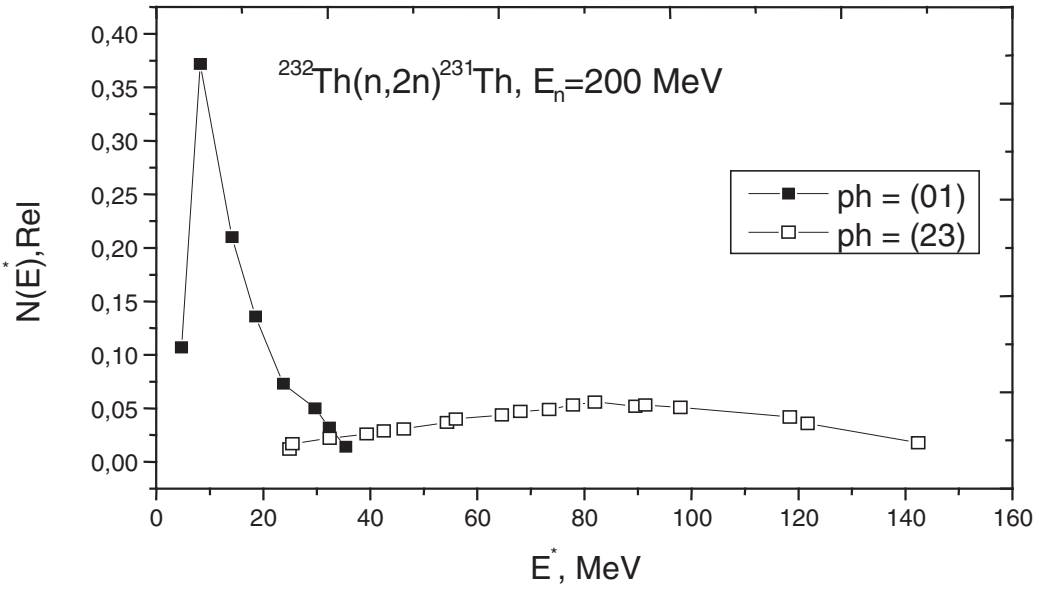

Fig. 7. The configuration yields in the direct reaction ^{232}Th(n,2n) as a function excitation energy.

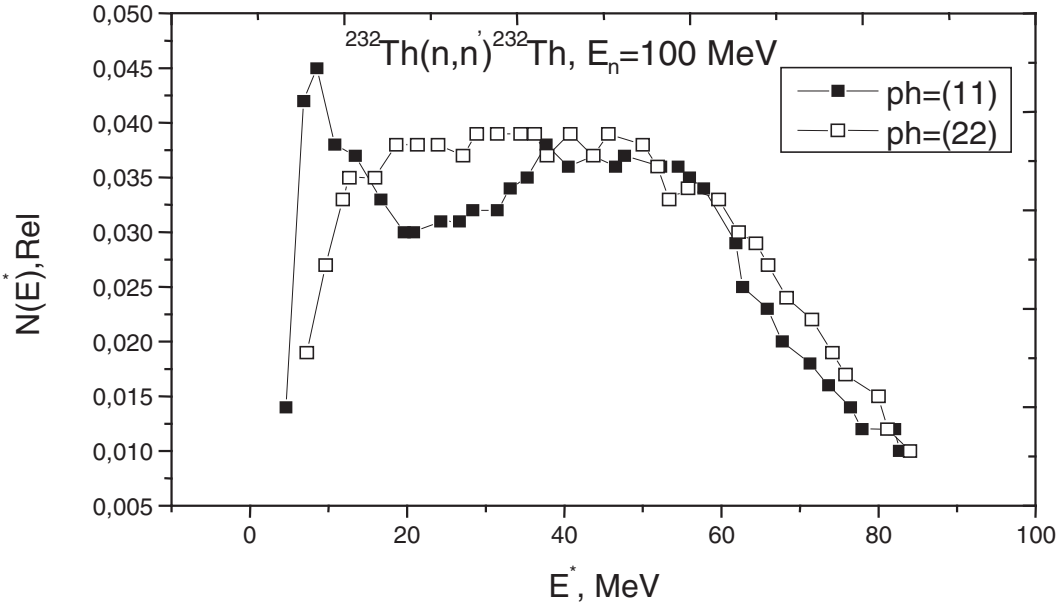

Fig. 8. The same as in Fig. 7 but for the direct reaction ^{232}Th(n,n').

The modification of the CEM95 code has been necessary for these kind of calculations. The block of intranuclear cascade has been separated from the code and the new module has been written down for the data acquisition in the output file. The necessary accuracy is achieved when 500 000 histories are taken into account. The configurations with yields more than 1% are only taken into consideration.

This kind of results serves as an input data for the calculations of pre-equilibrium and equilibrium decay of excited nuclei (code STAPRE). For each configuration, it is necessary to carry out the calculations of particle emission and fission cross-sections which further are summed with corresponding weights.

3. Calculation of multiconfiguration fission cross sections

The STAPRE code [11] was developed for the calculation of cross sections of reactions caused by particles with a competition of several particles, γ-quanta and fission in the assumption of sequential evaporation.

Each step of evaporation is described by the statistical model of nuclear reactions in a Hauser-Feshbach-Moldauer formalism [12,13] which take into account the conservation laws of the total angular momentum and parity. For the first particle the opportunity of pre-equilibrium decay is taken into account.

The code provides that in entrance and in exit channels of reaction, there can be neutrons, protons, alpha-particles and deuterons. There is an opportunity to set any particle or nucleus in the entrance channel. The way of definition of nuclei which fission is in question is thus realized.

During the 25 years of the code usage, a lot of changes and improvements were included. Some special efforts were done for calculations of fission cross sections in the 20-200 MeV region. For the calculation of the particles emission and fission with particle energies up to 200 MeV, the adaptation of the block of the statistical model of the STAPRE code was executed:

- Additional (up to 30) cascades of the particle emission to cover the whole energy range are included. The appropriate files are extended;

- The energy bin of integration is decreased from 2.5 up to 0.5 MeV to get necessary accuracy of calculations for the near threshold energy. In the current version, the whole energy region is divided into 380 bins;

- The doubled precision (REAL*8) for the maintenance of the protection from machine overflows is added.

The usage of the statistical model of nuclear reactions in the STAPRE code leads to the necessity to provide the large number of the input data: level density of the exited nuclei, characteristic of discrete levels (energy, spin and parity), fission barriers, particle binding energies, etc. It should be stressed that the large work on the preparation of the input data for calculations of nuclear reaction cross sections with theoretical models is done by the experts under the IAEA co-ordinated research program [14]. Unfortunately, in a part of level density the attention is only given to nuclei close to the stability valley, and there are mistakes in files of discrete levels.

The following work has been done in order to satisfy the input data needs for the calculations of fission cross sections for nuclei far from a beta-stability valley:

i) compilation of the schemes of discrete levels of nuclei with A=1-260,

ii) the analysis of the schemes for the level missing,

iii) the analysis of the spins and parities of levels.

The information on the exited levels of nuclei is logically divided into two parts: discrete levels described by energy, spin and parity; and continuum, where level density for the given excitation energy is used. For the STAPRE code a LDP file containing the level density parameters within the framework of the generalized model of a superfluid nucleus and SEDL file containing the characteristics of discrete levels, 2821 nuclei were formed.

The preparation of the initial data is organized according to an output file of the intranuclear cascade code, which contains the yields Y (Z,A,p,h,U) of nucleus (Z,A) in the certain particle-hole configurations p-h distributed on the excitation energies U. Hence, all nuclei, all configurations and all excitation energies have to be included in the entrance channel for the STAPRE code. Additional feature of the initial files formation is needed to take into account all steps of the particle emission for the fission cross section calculation (the chance structure of cross sections).

The PRESTAPR code is created and tested. It uses the data files as follows: LDP - parameters of level densities, SEDL - discrete levels characteristics, BARRIER - doubled humped fission barriers, GRD - parameters giant dipole resonances, Bn_MOL - energy of separation for the neutrons, protons and alpha-particles.

The PRESTAPR code prepares initial files for the calculations of the fission cross-sections by the STAPRE code using the list of nuclei, their particle-hole configurations and excitation energies (Z,A,p,h,U) calculated by the intranuclear cascade code and using the prepared LDP, SEDL, GDR, BARRIER, Bn_MOL files of initial parameters.

The result of the STAPRE code is the file of fission cross sections for the nuclei at the given configuration with the given excitation energies for the n-th chance, i.e.:

$$\sigma_f^n(Z, A, p, h, U).$$

The processing of this file consists in calculation of fission cross sections as a multiconfigurational mixture, that is as a sum on all residual nuclei (Z,A,p,h,U) with weight Y(Z,A,p,h,U):

$$\sigma_f(E) = \sum_n \sum_{Z.A} \sum_{p,h} \int \sigma_f^n(Z, A, p, h, U) \cdot Y(Z, A, p, h, U) dU$$

The procedure of the summation according this formulae is realized in the service program PROSTAPR.

4. The results of calculations

The preliminary calculations were performed for the case of ^{232}Th and ^{239}Pu neutron-induced fission in the energy region 20-200 MeV. The analysis of the role of different residual nuclei configurations in the fission cross-section formation were carried out. Up to 11 fission chances have been taken into account.

The example of this kind of analysis is shown in Fig. 9 where fission cross-sections for different residual nuclei formed in the reaction ^{232}Th + n are presented in the units of absorption cross-section. The results show that if for low energy fission the main part of total fission cross-section is due to fission of the compound nucleus, then for higher energies the role of first residual nuclei from (n,xn) reactions increases. Such a result is directly connected with the formation probability and excitation energy distribution of residual nuclei which have been obtained in the intranuclear cascade calculation.

The total fission cross-section is presented in Fig. 10 and Fig. 11. The cross-sections have been calculated for two variants of absorption cross-section calculations, that is for Konshin and Young potentials. It is seen that even these preliminary results are able to reproduce the observed fission cross-section behavior. The Konshin potential for the absorption cross-section gives a better description of the experiment.

The results obtained are only preliminary ones because the performance of detailed calculations in a wide region of nuclei requires more accurate values of main model parameters such as optical potentials, fission barriers and their dependence on excitation

energy, level density at the saddle point and so on. The additional analysis of the role of different configurations and fission chances is necessary, too, as well as the optimization of main code routines in order to reduce computer time especially for the calculations of high energy fission.

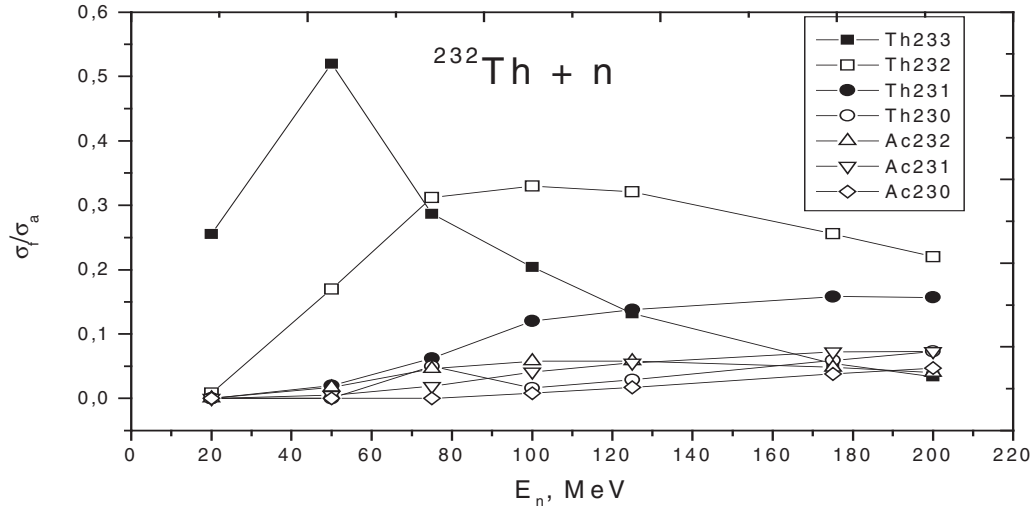

Fig. 9. Relative fission cross-sections of residual nuclei in reaction ^{232}Th+n.

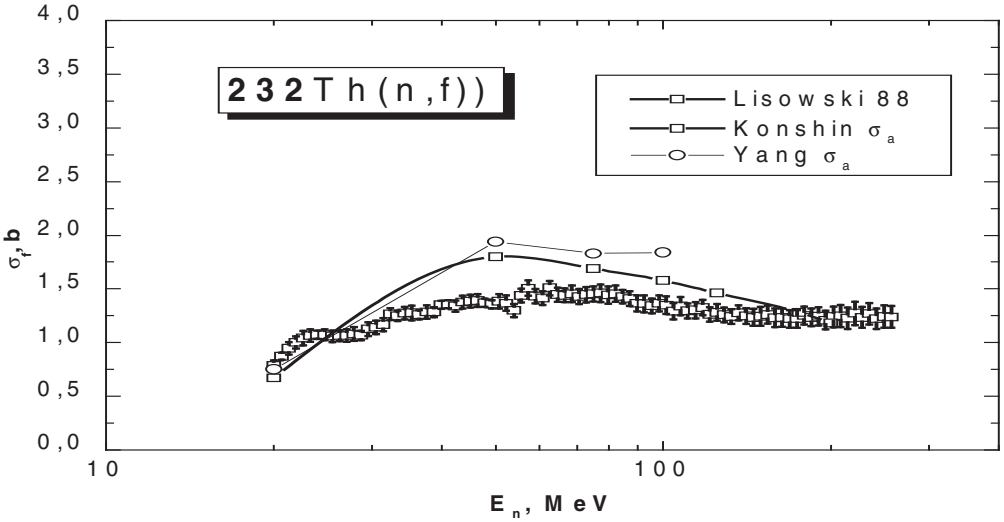

Fig. 10. Total fission cross-section for two optical potentials in comparison with the experimental data.

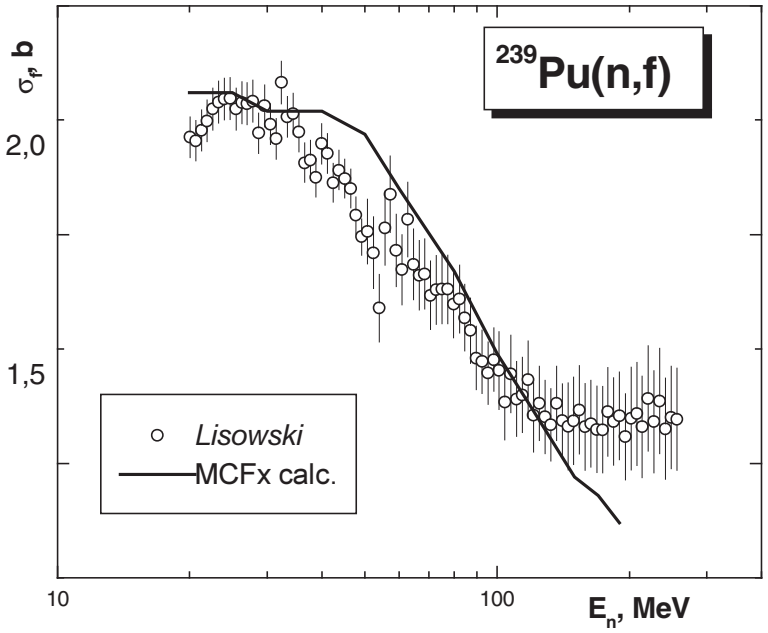

Fig. 11. The same but for ^{239}Pu+n.

References

[1] O. Bersillon, "SCAT2 – A Spherical Optical Model Code", CEA-N-2037, p. 111 (1978).

[2] A. Bohr and B.R. Mottelson, Kgl. Danske Videnskab. Selskab, Mat. Fyz. Medd. 27, No. 16 (1953).

[3] T. Tamura, Rev. Mod. Phys. 37 (1965) 679.

[4] J. Raynal, "Optical Model and Coupled-Channel Calculations in Nuclear Physics", IAEA SMR-9/8, p. 281 (1970).

[5] J. Raynal, "Nucleon-Nucleus Optical Model up to 200 MeV", Proceedings of a Specialists' Meeting, 13-15 November 1996, Bruyères-le–Châtel, France, p. 159.

[6] Young, IAEA-TECDOC, RIPL, Appendix II, 1998.

[7] V.A.P. Konshin, JAERI-Research, 95-036 (1995).

[8] J.F. Poenitz, P. Whalen, ANL-NDM-80, 8305.

[9] P. Langsford, AERE-PR/NP-9, 36, 6604.

[10] K.K. Gudima, S.G. Mashnik, V.D. Toneev, Nucl. Phys. A401 (1983) 329.

[11] M. Uhl, B. Strohmaier, Report IRK 76/01, Vienna, 1976; Addena, September 1976.

[12] W. Hauser, H. Feshbach, Phys. Rev. 1952, V. 87, p. 366.

[13] P.A. Moldauer, Phys. Rev. 1964, V. 135, p. 642.

[14] Handbook for calculations of nuclear reaction data, IAEA-TECDOC-1034, Vienna, 1998.

THE CONSTANTS AND PARAMETERS OF NUCLEAR STRUCTURE AND NUCLEAR REACTIONS

01-10118 (119) [6]
Translated from Russian

UDC 539.163

INTERACTIVE INFORMATION SYSTEM ON THE NUCLEAR PHYSICS PROPERTIES OF NUCLIDES AND RADIOACTIVE DECAY CHAINS

V.I. Plyaskin, R.A. Kosilov
Institute of Nuclear Power Engineering, Obninsk, Russia

G.N. Manturov
Russian Federation National Research Centre - Institute for Physics and Power Engineering, Obninsk, Russia

INTERACTIVE INFORMATION SYSTEM ON THE NUCLEAR PHYSICS PROPERTIES OF NUCLIDES AND RADIOACTIVE DECAY CHAINS. A brief review is given of a computerized information system on the nuclear physics properties of nuclides and radioactive decay chains. The main difference between the system presented here and those already in existence is that these evaluated databases of nuclear physics constants are linked to a set of programs, thus enabling analysis of a wide range of problems regarding various nuclear physics applications.

An interactive information system (IIS) has been set up containing comprehensive information on the characteristics of more than 2600 nuclides of the 107 chemical elements known to exist in 1999. The following characteristics are given for each nuclide: charge, mass, spin and parity of the ground state, mass excess, half-life, modes of decay and branching ratios, average decay energies of gamma-, electron-, positron- and alpha-radiation, and also the spectra of gamma and X-rays and of beta and alpha particles.

The main difference between this IIS and the widely available charts of the nuclides, Refs 1-4, reference books, Refs 5 and 6, and computerized systems, Refs 7 and 8, is that these evaluated databases of nuclear physics constants are linked to a set of programs, making it possible to:

- automatically plot and visualize radioactive decay chains;
- calculate the number of nuclei, activity and radiation energy release, for both the chain as a whole and the individual nuclides in it;

- calculate the spectra of gamma- and X-rays, and of alpha and beta particles in the chain, at a given moment in time;

- identify radionuclides from the measured gamma spectra; identification can be carried out using the half-life, gamma-radiation energy or a combination of these two parameters;

- analyse the spectra of individual radionuclides and radioactive chains, which allows radiation spectral lines to be selected for a given energy and intensity threshold.

The calculations can be made both for a "free" decay chain (for a given number of nuclei in the parent radionuclide chain at the starting point) and also when the number of nuclei in the parent radionuclide is supplemented from outside at a given rate ("target activation"). This algorithm enables the calculational capabilities of the IIS to be used in a wide range of tasks requiring analysis of radioactive decay chain parameters because it does not depend on the way in which the nuclei of the parent radionuclide are supplemented.

A user-friendly feature of the IIS is that, apart from information on nuclides and their decay chains, it also contains additional information: it gives the main physics properties of all the elements in the periodic table; fundamental physics constants; or relations between the various measurement units; information from the SI system for all the units used in nuclear physics and its applications; the binding energies for all the nuclides; and the energies and thresholds of any nuclear reaction can be calculated.

All the information in the IIS is presented in numerical or graphical form. The IIS also has a comprehensive HELP function.

1. The main principles underlying radioactive decay chain analysis and calculation

In setting up the IIS on the nuclear physics properties of radioactive chains we had to solve several important problems relating to the automatic plotting of decay chain diagrams, the calculation of radiation spectra and the determination of absorbed doses. Conventional numerical methods for computing the differential equation systems which describe radioactive decay chains, make huge demands on machine resources, even when high-speed computers are used. We describe below a calculation method which has made it possible to set up a fast-acting program package for analysing radioactive chains, and calculating the radiation spectrum and energy release.

To set up the information system we analysed all the up-to-date material and, after initial analysis, took the main data from Refs 5, 7 and 8.

1.1. Plotting radioactive decay chains

Hereafter, in accordance with the conventional notation system, we will identify nuclides by the signature Z-A-I, where Z is the nuclear charge of the nuclide, A is the mass

number and I is the isomer classification (‘g’ is ground state, ’m’,’m1’ is first excited state and ’m2’ the second, etc.).

In general terms, plotting a radioactive decay chain is formulated as follows: finding, for a given radionuclide (Z-A-I)0, all the nuclides which are formed during its decay process.

We note that, from the mathematical point of view, the decay chain is represented by a directed graph. The component nuclides of the chain are the vertices of the graph and the edges correspond to the mutual transformations of the nuclides in the decay process. A feature of this graph is that it always has one initial vertex, representing the parent radionuclide of the chain, and one or more pendant vertices, representing the stable nuclides into which the given chain decays. The edges of the graph run in the direction from the parent to the daughter nuclide and never form cycles. In this graph there is always at least one edge sequence from the initial vertex to any of the pendant vertices.

The task of plotting a decay chain is thus one of plotting this directed graph.

The algorithm for solving this task is recursive. Let us assume that we need to plot the decay chain of the nuclide Z-A-I. Each step of the recursion includes the following points:

1) Nuclide Z-A-I is added to the list of vertices already plotted; if the nuclide under investigation is stable or is already in the list, plotting is complete and we return to the previous step of the recursion;

2) If nuclide Z-A-I is unstable then, a list of daughter nuclides (for the given nuclide) is drawn up from data on its decay modes;

3) Points 1-3 are carried out for each nuclide in the list of daughter nuclides obtained in point 2.

As a result of plotting we obtain a list of graph vertices and lists of daughter nuclides for every vertex. Thus the directed graph corresponding to the decay chain of nuclide Z-A-I is fully determined. It should be noted that for point 2 of the algorithm information is needed on how to identify the daughter nuclide $(Z\text{-}A\text{-}I)_d$ from the known parent nuclide $(Z\text{-}A\text{-}I)_m$ and its decay mode. This information can be obtained from nuclear physics data on radionuclide decay.

1.2. Visualization of decay chains

The next task when plotting and calculating radioactive decay chains is placing the graph describing the chain on a plane for representation on a computer screen or printing it out in the usual way.

A fact that should be used when doing this is that a system of co-ordinates is already given for the component nuclides of the chain. This is the three-dimensional co-ordinate system (Z,A,I). Visualizing the chain is thus reduced to displaying the three-dimensional arrangement of the nuclides in the chain on a plane (X,Y).

Let us consider the algorithm below as a solution to this problem. It makes use of the fact that the range of values along the I-axis in the three-dimensional space (Z,A,I) is limited (according to available data) to three values:

(a) I='g' or is absent;
(b) I='m','m1';
(c) I='m2'.

Let us place a grid (Z,A) on the plane and arrange the nuclides in the chain in the cells. It may be that there will be two or three isomers in some of the cells. (As already mentioned, isomers are characterized by the same Z-A and their differences are shown in the I classification). In this case we will increase the width of the column and the line height of the (Z,A) grid containing the relevant cell to accommodate the number of nuclide-isomers. We will place the isomers in the cell diagonally from the bottom right to the top left-hand side starting with the lowest isomeric state number. Figure 1 gives an example of the ^{136}Te decay chain arrangement.

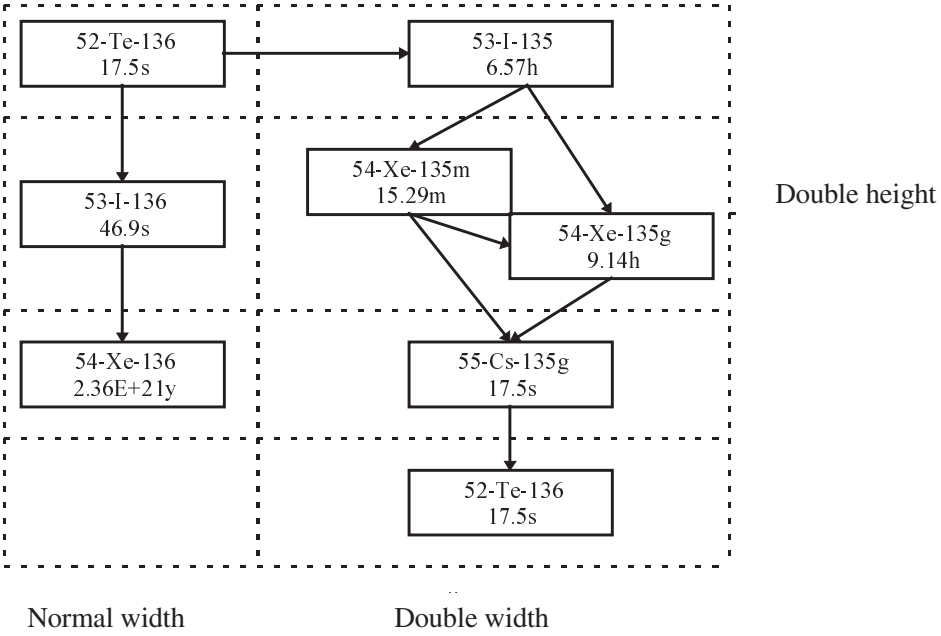

Fig. 1. Example of the Te^{136} decay chain arrangement.

1.3. Calculating the number of nuclei and the activity of the nuclides in the chain

The decay of a radioactive chain is described in general terms by the following system of differential equations:

$$\begin{cases} \dfrac{dx_1}{dt} = -S_1 x_1 \\ \dfrac{dx_n}{dt} = \sum\limits_{i \neq n} S^i_n x_i - S_n x_n, n = 2..N \end{cases} \tag{1}$$

where N is the total number of nuclides in the chain; x_n is the number of nuclei of the nth nuclide; and S_n is the decay rate of the nth nuclide. In the case of radioactive decay, $S_n = \lambda_n$ is the decay constant of the nuclide n; S^i_n is the rate at which nuclide n is formed from nuclide i. If nuclide n is not the daughter for i, then $S^i_n = 0$, if n is the only daughter nuclide of i, then $S^i_n = \lambda_i$, otherwise $S^i_n = \lambda_i k^i_n$, where k^i_n is the branching coefficient for decay of the parent nuclide i, leading to nuclide n.

The initial conditions for this system are written as:

$$\begin{cases} x_1(0) = x_{1,0} \\ x_n(0) = 0, n = 2..N \end{cases} \tag{2}$$

We note that for a linear chain the equation system (1) becomes:

$$\begin{cases} \dfrac{dx_1}{dt} = -S_1 x_1 \\ \dfrac{dx_n}{dt} = \sum\limits_{i < n} S^i_n x_i - S_n x_n, n = 2..N \end{cases} \tag{3}$$

and has the analytical solution:

$$\begin{cases} x_1(t) = x_{1,0} \cdot \exp(-S_i t) \\ x_n(t) = x_{1,0} S^1_2 ... S^{n-1}_n \cdot \sum\limits_{j=1}^{n} \dfrac{\exp(-S_j t)}{\prod\limits_{k \neq j}^{n} (S_k - S_j)}, n = 2..N \end{cases} \tag{4}$$

This can be used in solving the general task of (1) and (2).

Assuming that we need to calculate the number of nuclei of a certain radionuclide X in the chain, then we must first identify all the possible edge sequences for getting from the parent nuclide of the chain to nuclide X. Thus, we will select all the possible linear chains leading to the formation of X. Next, for every linear chain obtained, we calculate the number of nuclei in nuclide X using the formulas in (4) and adding the results together. This method makes use of the fact that different modes of nuclide decay occur independently.

We note the singularity of solution (4) if there are two nuclides with identical decay rates (S_k=S_j) in the chain. The simplest way out of this situation is to change one of the decay rates by a negligible amount within its error margin (by say 0.01%).

Let us now consider the calculation for a chain where the number of nuclei of the parent nuclide is supplemented from outside during the decay process. A typical case in point is

where a nuclide (target) is irradiated by a particle flux and, as a result of a nuclear reaction, the parent nuclide of a chain is formed.

In this case, the equation for the first nuclide in the system (1) changes to:

$$\frac{dx_1}{dt} = \hat{S}_0 - S_1 x_1, \tag{5}$$

where $\hat{S}_0$ is the rate at which the parent radionuclide of the chain is formed when the target is activated.

The following algorithm can be used to solve this: let us add an additional abstract nuclide to the existing decay chain such that it becomes the parent nuclide of the chain. Let us set the following decay conditions for the newly introduced nuclide:

$$S_0 \to 0, x_0(0) \to \infty, S_0 x_0(0) = \hat{S}_0, \tag{6}$$

where S_0 is the decay rate of the added nuclide; and x_0 is the number of nuclei of the added nuclide.

Then the system of equations describing the task with activation is similar to the system for the task in (1) and (2), and the formulas in (4) can be used to solve it. The solution is written as:

$$x_n = \hat{S}_0 S_2^1 ... S_n^{n-1} \sum_{i=0}^{n} \frac{\exp(-S_i t)}{\prod_{k \neq i}^{n} (S_k - S_i)}, n = 1..N \tag{7}$$

This result has singularity for stable nuclides in the chain, since in this case the product in the denominator for the two terms vanishes. (S_0=0 by definition, S_n=0, since the nuclide is stable).

Once the uncertainty has been resolved, the solution to the task for a stable nuclide in the chain is written as:

$$x_n = \hat{S}_0 S_2^1 ... S_n^{n-1} \left[\sum_{i=1}^{n-1} \frac{\exp(-S_i t)}{\prod_{k \neq i, k=1}^{n-1} (S_k - S_i)} + \frac{t}{\prod_{k=1}^{n-1} S_k} - \frac{\sum_{k=1 l \neq k, l=1}^{n-1} \prod^{n-1} S_l}{\prod_{k=1}^{n-1} (S_k)^2} \right] \tag{8}$$

If it is necessary to find a solution when activation has continued for a given time T_A, but then the chain has decayed without activation, the solution may be obtained from the following algorithm: up to the moment $t=T_A$ the problem is solved using activation (1, 5) and (2), and after the moment $t=T_A$ the problem is solved with (1), (without an additional nuclide), with the initial conditions obtained at the moment $t=T_A$ and for the time $\tau=t-T_A$.

It is obvious that when the target is activated under non-zero initial conditions, in (1, 5), we may obtain the solution as the sum of solutions to the task with activation and zero initial conditions and the task without activation with the given initial conditions.

From the number of nuclei calculated for a nuclide it is easy to obtain its activity by using the well-known expression:

$$A(t) = \lambda x(t), \tag{9}$$

where λ is the nuclide decay constant.

When the initial conditions for nuclides *2…N* are not zero, the solution may be obtained from the following algorithm: for each nuclide in the initial chain a decay chain is plotted (which is a part of the initial chain) and tasks (1) and (2) are solved. The results obtained are summed.

1.4. Calculating radiation energy release

If the average energies per radionuclide decay are known we can calculate the energy release *D* from radionuclide decay using the following formula:

$$D(t) = K\overline{E}\int_0^t \lambda x(\tau)d\tau\,, \tag{10}$$

where *x* is the time dependence of the number of nuclei of the radionuclide; λ is the decay constant of the radionuclide; $\overline{E}$ is the average energy, released by a single radionuclide decay; and *K* is the coefficient, depending on the choice of measurement units. If $\overline{E}$ is in MeV and *D* is in Gy, then $K = 1.602\cdot10^{-13}$.

Henceforth, for reasons of simplicity, we shall consider the task of calculating the energy release of ionizing radiation from the decay of one nuclide in the chain. The radiation energy release from the decay of all the nuclides in the chain can be obtained by adding the energy release of the separate nuclides.

It is obvious that an analytical expression for the radiation energy release can be obtained by integrating the expressions for *x(τ)*. In particular, for a simple decay chain (1) with initial conditions (2), the radiation energy release from decay of the *n*th nuclide is:

$$D_n(t) = K\overline{E}\lambda_n\int_0^t x_n(\tau)d\tau = K\overline{E}_n\lambda_n\cdot x_{1,0}S_2^1\ldots S_n^{n-1}\sum_{i=1}^{n}\frac{1-\exp(-S_i t)}{S_i\prod\limits_{k=1,k\neq i}^{n}(S_k - S_i)} \tag{11}$$

The problem of obtaining the radiation energy release values for non-zero initial conditions is solved in a similar way as for the number of nuclei: the total energy release is obtained by summation of the values obtained by solving independent tasks with initial conditions (2) for each nuclide in the chain.

Target activation is a rather more complex matter. In this case, the analytical expression for energy release takes the form:

$$D_n(t) = K\overline{E}\lambda_n \int_0^t x_n(\tau)d\tau = K\overline{E}_n\lambda_n \cdot \hat{S}_0 S_2^1 ... S_n^{n-1} \sum_{i=0}^{n} \frac{1-\exp(-S_i t)}{S_i \prod_{k=0,k\neq i}^{n}(S_k - S_i)} \tag{12}$$

This formula has a singularity, – uncertainty of the form $\frac{0}{0}$.

To exclude the uncertainty it is sufficient to expand the exponent containing S_0 in series up to terms of the first order of an infinitesimal and replace S_0 with zero:

$$D_n(t) = K\overline{E}_n\lambda_n \cdot \hat{S}_0 S_2^1 ... S_n^{n-1} \left[\frac{t}{\prod_{k=1}^{n}(S_k)} + \sum_{i=1}^{n} \frac{1-\exp(-S_i t)}{S_i \prod_{k=0,k\neq i}^{n}(S_k - S_i)} \right] \tag{13}$$

The power of radiation energy release is a simpler matter:

$$\dot{D} = \frac{dD}{dt} \tag{14}$$

From formula (10) and determination of activity *A(t)*, we obtain:

$$\dot{D}(t) = K\overline{E}\lambda x(t) = K\overline{E}A(t) \tag{15}$$

Obviously, the radiation energy release may be obtained for tasks using any combination of activation and simple decay with different initial conditions by “joining together” the tasks described above.

1.5. Calculating the radiation spectrum of the chain

The radiation spectrum of the chain is the sum of the radiation spectra of its component nuclides. On that basis, let us consider the question of obtaining the spectrum of an individual nuclide in the chain at an arbitrary point in time. If we know the spectral energies of the nuclide radiation and their intensity we can obtain the spectrum by using the following formula:

$$B_k(E_k, t) = \lambda x(t) \frac{I_k(E_k)}{100}, \tag{16}$$

where E_k is the energy of the *k*th line of radiation (or particle); I_k (E_k) is the radiation intensity of the *k*th line (in %); $B_k(E_k,t)$ is the number of quanta (or particles) emitted with an energy of E_k at the time of *t* per second.

It should be pointed out that a large computer memory is needed to calculate radiation spectra because of the large volume of data on the spectral lines of nuclide radiation and the need to calculate the spectrum of complex chains with a large number of nuclides. In order to reduce the volume of information in the proposed information system, radiation lines with an intensity of less than 1% of the maximum line intensity in the given spectrum are sifted out.

2. Identifying gamma-emitting nuclides

We know that we can identify radioactive nuclides from the energy, gamma radiation intensity and half-life values. Despite the fact that modern nuclear spectrometry methods enable us to determine with a rather high level of accuracy the above-mentioned parameters for the radiation under investigation, identification of the nuclides (especially for complex mixtures) is a very laborious task. The main difficulty lies in interpreting the experimental results with respect to known nuclear decay characteristics which, in the available reference literature, are dispersed, firstly, over the nuclides (more than two thousand nuclides) and, secondly, over the gamma-transition energies (the known number of gamma-lines exceeds 60 000).

The proposed computerized information system has the following algorithm for identifying gamma-emitting nuclides. All the radionuclides are broken down into 13 groups according to their half-lives. In each half-life range the gamma lines of the radionuclides present are broken down into energy groups. Having selected the half-life range of interest and, subsequently, the gamma-radiation energy range, the user of the computerized system obtains a table of energies and intensities of the selected gamma-lines with an indication of where every line belongs. The data given in the table may be represented graphically. Moreover, the data in the table can be used to identify radiation lines which exceed the given intensity threshold and/or to select radiation lines in a narrower energy and half-life range.

Conclusion

The IIS is intended for use by a wide range of specialists at different levels (students, post-graduate students, engineers and scientists), who need reliable information (as of 1999) on stable and radioactive nuclides. The main difference between the IIS described above and existing charts of the nuclides, reference books and computerized systems is that the evaluated databases of nuclear physics constants are linked with a set of programs enabling analysis of a wide range of problems in various nuclear physics applications. This work is supported by a grant from the Russian Fund for Fundamental Research (project No. 00-07-90376).

References

[1] F. Walker, B. Wiliam, et al., Chart of the Nuclides, Knolls Atomic Power Lab: Naval Reactor, V.S. Department of Energy, 1988.

[2] V. Yoshizawa, et al., Chart of the Nuclides, Science Eng. Research Lab: Waseda University, Tokio, 1988.

[3] I.P. Selinov, Tables of atoms, atomic nuclei and subatomic particles, Annex to the book "Stroenie i sistematika yader", Moscow: Nauka, 1990.

[4] M.S. Antony, Chart of the Nuclides, Centre de Recherches Nucléaires and Université Louis Pasteur, Strasbourg, 1993.

[5] E. Browne, R.B. Firestone, Table of Radioactive Isotopes (V.S. Shirley, Ed.), N.Y., John Wisley and Sons, 1996.

[6] T.V. Goloshvili, V.P. Chechev, A.A. Lbov, Reference book of the nuclides, Moscow: Central Scientific Research Institute of Management, Economics and Information (ATOMINFORM), 1995.

[7] Evaluated Nuclear Structure Data File - a computer file of evaluated experimental nuclear structure data maintained by National Nuclear Data Center, Brookhaven National Laboratory, (Files from March 1995).

[8] M. Konieczny, B. Potet, J. Rockey, A PC Program for Displaying Data from the Joint Evaluated File (JEF) Library, Prac. Int. Conf. on Nuclear Data Science and Technology, Gatlinburg, Tennessee, 1994, V. 2, p. 754.

NUCLEAR REACTOR DATA

01-10118 (118) [7]
Translated from Russian

UDC 621.039.58

EVALUATION OF HOW THE ACCURACY OF CALCULATIONS OF THE TEMPERATURE COEFFICIENT OF REACTIVITY AFFECTS THE SAFETY OF FAST REACTORS IN A ULOF TYPE ACCIDENT

A.V. Danilychev, D.G. Elistratov, A.A. Rinejskij, V.Yu. Stogov, V.A. Chernyj
Russian Federation National Research Centre - Institute for Physics and Power Engineering (IPPE), Obninsk, Russia

EVALUATION OF HOW THE ACCURACY OF CALCULATIONS OF THE TEMPERATURE COEFFICIENT OF REACTIVITY AFFECTS THE SAFETY OF FAST REACTORS IN A ULOF TYPE ACCIDENT. This paper provides preliminary evaluations of the possible uncertainty ranges in conventional calculation of temperature coefficient of reactivity feedback components in fast reactors. It also analyses, using point kinetics approximation, how these uncertainties affect maximum coolant temperatures during unprotected loss of flow (ULOF) type accidents.

The calculation accuracy of reactivity coefficients may become the main factor in achieving maximum self-protection in BN type fast reactors owing to the inherent feedback in the reactor through the "temperature-reactivity" channel. Perturbation theory, based on diffusion approximation, is the standard and widely used approach taken to describe the detailed spatial distributions of temperature coefficient of reactivity (TCR) components, inserted into dynamic codes. The reason for this is as follows:

- For traditional fast reactor layouts the diffusion approximation has been shown to be sufficiently accurate, Ref. 1;

- The model of the TCR from thermal expansion uses the similarity theory formulas obtained in the context of diffusion approximation, Ref. 2.

The accuracy of the values obtained by this method is questionable when there are regions adjacent to the core having very different neutron physics characteristics. For example, in prospective fast reactors with a sodium void above the core, Ref. 3, or in reactor burners with steel shielding. For such cores it has been shown, on the example of a large fast reactor loaded with plutonium, that non-diffusion description of the sodium void may lead to a change in the maximum sodium temperature during an accident of $>20^{o}$ simply on account of the sodium density of the TCR component, Ref. 4. Additional calculational investigation is given below of the effect of the limiting error of the standard TCR component calculation on an ~1300 MW(e) reactor of this type.

1. Uncertainty of the TCR_D Doppler component

Evaluations carried out using different versions of the ABBN constants and different diffusion codes for the same reactor (the BN-600, for example), have not revealed any deviations greater than ±3%, Ref. 5, in the integral value *T(MK/MT)* of the separate fuel areas. Calculations for a reactor with a sodium void which take into account corrections for non-diffusion, Ref. 4, show that the spread of *T(MK/MT)* in the context of individual constants and the program does not exceed:

- ~ 6% for integral values;
- ≤ 10% for spatial values (maximum deviations correspond to quite a narrow (<20 cm) upper layer of the core, whose contribution to the total value of *T(MK/MT)* <10%).

However, variations in the value of *T(MK/MT)* ~20% (see Table 1) were observed during international safety tests on the BN-800 type reactor with a sodium void, Ref. 6, depending on the calculation method and the nuclear data system used. In accordance with this maximum evaluation, Fig. 1 shows the sodium temperature behaviour in a ULOF accident, calculated using the point kinetics approximation.

Table 1

Doppler constant (TMK/MT)·10^{-2} in the 1500-2100°K temperature range in a BN-800 reactor (expert evaluation, Ref. 5) obtained using various programs

Unperturbed core state					
Reactor area	Russian evaluations IPPE (diffusion calculation)			ENEA**) (ITALY)	ERL**) (HITACHI)
Calculation code	CAFR*)	RHEIN*)	RHEIN**)		
Low Enrichment Zone (LEZ)	-0.406	-0.471	-0.462	-0.3746	-0.340
Medium Enrichment Zone (MEZ)	-0.176	-0.147	-0.169	-0.1916	-0.172
High Enrichment Zone (HEZ)	-0.092	-0.0843	-0.0890	-0.0767	-0.0965
Whole core	-0.685	-0.683	-0.720	-	-
Lower thermal shield	-0.075	-0.0906	-0.0852	-0.0860	-0.0761
Side shield	-0.052	-0.058	-0.0483	-0.0515	-0.0424
100% Na removal from core					
Low Enrichment Zone (LEZ)		-0.245	-0.239	-0.257	-0.222
Medium Enrichment Zone (MEZ)		-0.096	-0.0952	-0.137	-0.0959
High Enrichment Zone (HEZ)		-0.0572	-0.0520	-0.0767	-0.0507
Whole core	-0.396	-0.398	-0.338	-	-
Lower thermal shield		-0.0605		-0.0688	-0.0724
Side shield		-0.039		-0.0441	-0.0353

Note: *) calculations carried out using perturbation theory.
**) direct K_{eff} calculations.

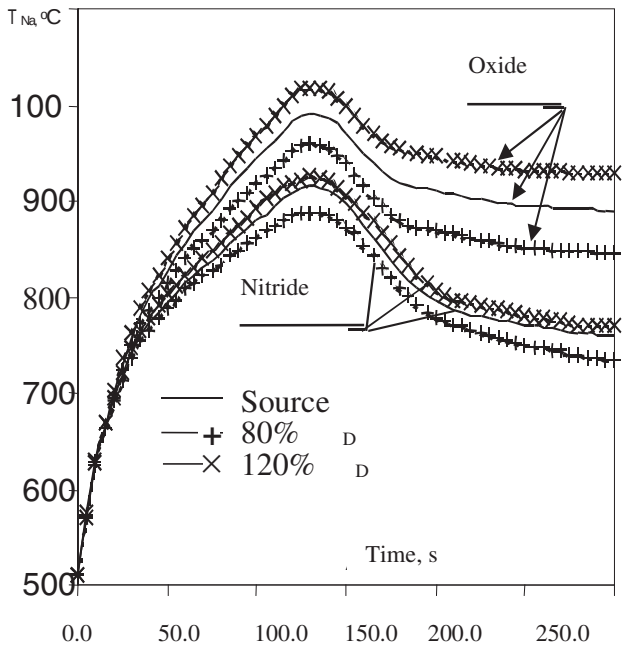

Fig. 1. Effect of a parametric change in the TCR Doppler component of ±20% from the initial value on the maximum sodium temperature in a ULOF accident (keeping the weighting contribution of the separate parts of low and high enrichment zones to the axial form-function of the Doppler constant).

Thus, variations in the integral value of the Doppler constant within the maximum possible range of its calculated error of ±20% could lead to fluctuations in the calculated sodium temperature of ~±30°C for oxide fuel and ~±20°C for nitride fuel. Proportionally, the spread of the maximum sodium temperatures on account of a similar uncertainty in the integral value *T(MK/MT)*, obtained as ~6% in diffusion programs, should not exceed ~10°, which could be negligible.

Changes in the group spectra of the flux and worth during transition to a perturbed state (with respect to temperature and density of the sodium) demonstrate their relatively weak deformation in the energy region characteristic of the Doppler effect. This means at least for the central area with a thickness which is ~40% of the height of the core, Refs 4, 6, that, for perturbations not connected with the phase transitions of materials, the initial values of *T(MK/MT)* obtained in diffusion approximation can be used.

2. Sodium density component of the TCR_{Na}

The possibility of inaccuracy in calculating the integral magnitude of TCR_{Na} for the core is illustrated using the example of nitride loading in Fig. 2. Accordingly, a magnitude of ~20% is taken as the maximum error of the integral value of this component, it being the value observed in comparison of the transport and diffusion calculations of the separate areas of a reactor with a sodium void, Refs 4, 6, shown in Fig. 2.

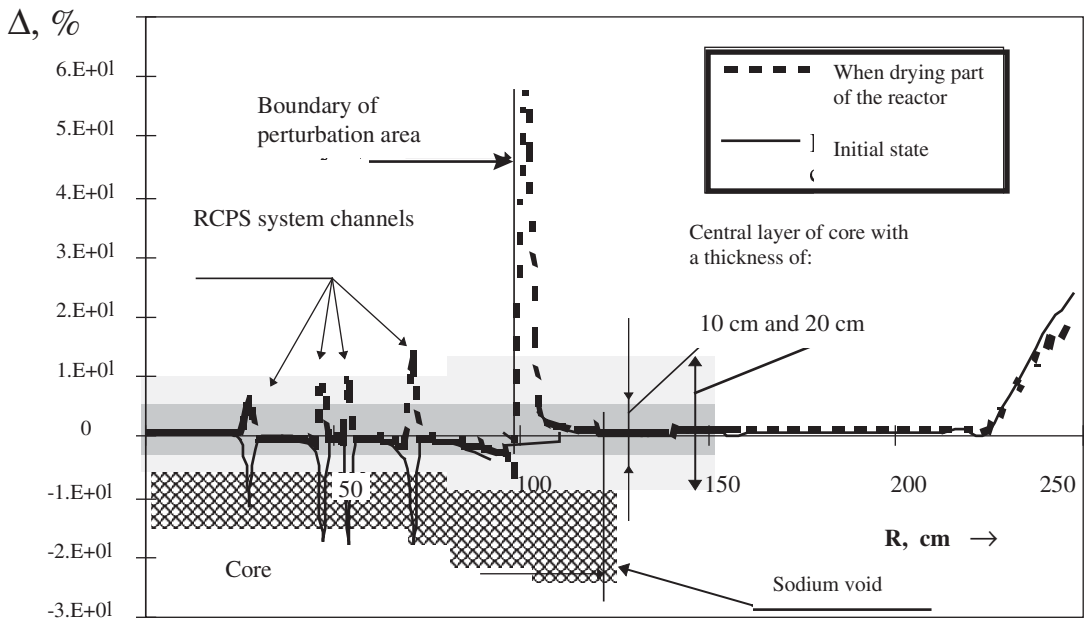

Fig. 2. Areas of maximum divergence in the efficiency distribution of 1 cm^3 of sodium, obtained from diffusion and transport (S_8-approximation) calculations.

Figure 3 demonstrates how the error assumed in the TCR_{Na} integral value for reactors with a sodium void affects change in the maximum coolant temperature and the total reactivity of the system in a ULOF accident. For these reactors, which ensure that the sodium void reactivity effect and the TCR_{Na} are non-positive because of introduction of the sodium void, the integral value of TCR_{Na} is near zero (see Table 2) and hence the uncertainty under investigation for the integral value of TCR_{Na} (±20%) is negligible and in a ULOF accident it ensures a maximum sodium temperature imbalance of only ~5°C. At the same time, the authors of Ref. 4 examined the effect of non-diffusion in the calculation model on the spatial distribution of the sodium density TCR component (especially at the **sodium void/core** boundary where there is maximum sodium heating in an accident) and found a temperature imbalance of ~20°C.

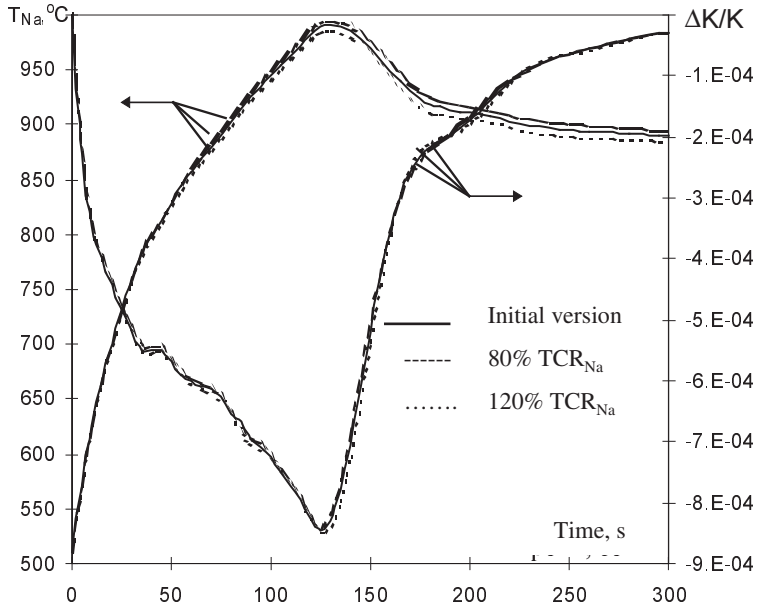

Fig. 3. Impact of a parametric change of 20% in the TCR sodium density component on the maximum sodium temperature in a ULOF accident.

Table 2

Feedback reactivity components, 10^{-5} (ΔK/K)/degrees

Reactivity components depending on:	BN-600 (UO_2)	BN-800*) (Pu-U)O_2	BN-1300*)	
			(Pu-U)N_{15}	(PuU)O_2
a) coolant temperatures:				
- sodium density	-0.12	-0.01	0.332	0.232
- radial expansion	-0.75	-0.94	-0.64	-0.70
- expansion of RCPS rods	-0.12	-0.14	-0.13	-0.13
b) fuel temperature:				
- Doppler	-1.59	-1.34	-0.804	-1.03
- axial expansion	-0.13	-0.23	-0.046	-0.052
Total TCR	-2.59	-2.52	-1.2	-1.6
Temperature effect, % ΔK/K	-0.35	-0.32	-0.22	-0.30
Power coefficient of reactivity, 10^{-6}(ΔK/K)/MW	-5.58	-3.90	-1.5	-2.6
Power effect, % ΔK/K	-0.82	-0.82	-0.48	-0.50

*) Cores with a sodium void.

3. Reactivity components from thermal expansion

These components are determined by the model adopted for thermal expansion of materials or fuel assembly bending. When there is uncertainty in such a model caused by the fuel assembly design, basic research is often limited by similarity theory formulas based on diffusion approximation, Ref. 2. Ref. 4 has demonstrated that for these formulas:

- When transport corrections are made to group fluxes and worths, the integral values of the radial expansion (TCR_R) component can vary by -1.3% from the initial magnitude;

- The analogous change in the axial expansion component (TCR_H) is ~6%.

In the upper layers of the core these corrections provide the main contribution to change in $TCR_{R,H}(z)$ and attain approximately 3% and 20%, respectively. However, the contribution of the radial expansion component itself to the total reactivity balance for a ULOF accident is large (Table 2 and Fig. 4). This forces us to look closely at possible error in its calculation.

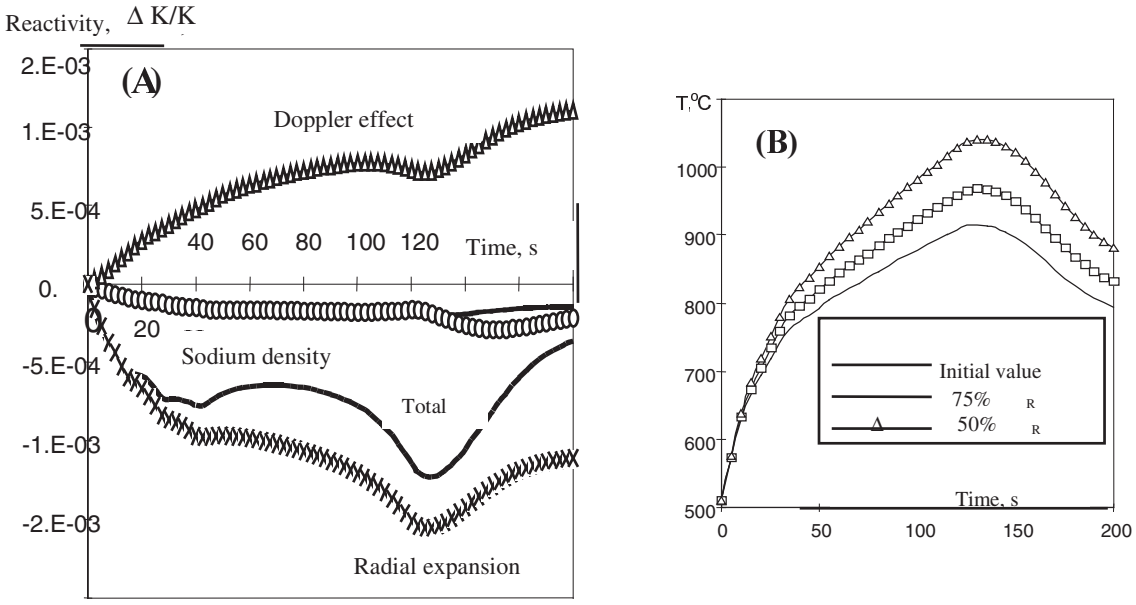

Fig. 4. Reactivity balance for a BN-1300 type reactor loaded with nitride (A) and the effect of the TCR_R magnitude on the sodium temperature in a ULOF accident (B).

The spatial distribution of $TCR_{R,H}(\vec{r})$ is such that they have a maximum contribution in peripheral areas of the core (see Fig. 5). Thus, the calculation accuracy of group fluxes and worths for TCR_R when using the standard diffusion calculation can be less accurate in the area where this component has the maximum contribution.

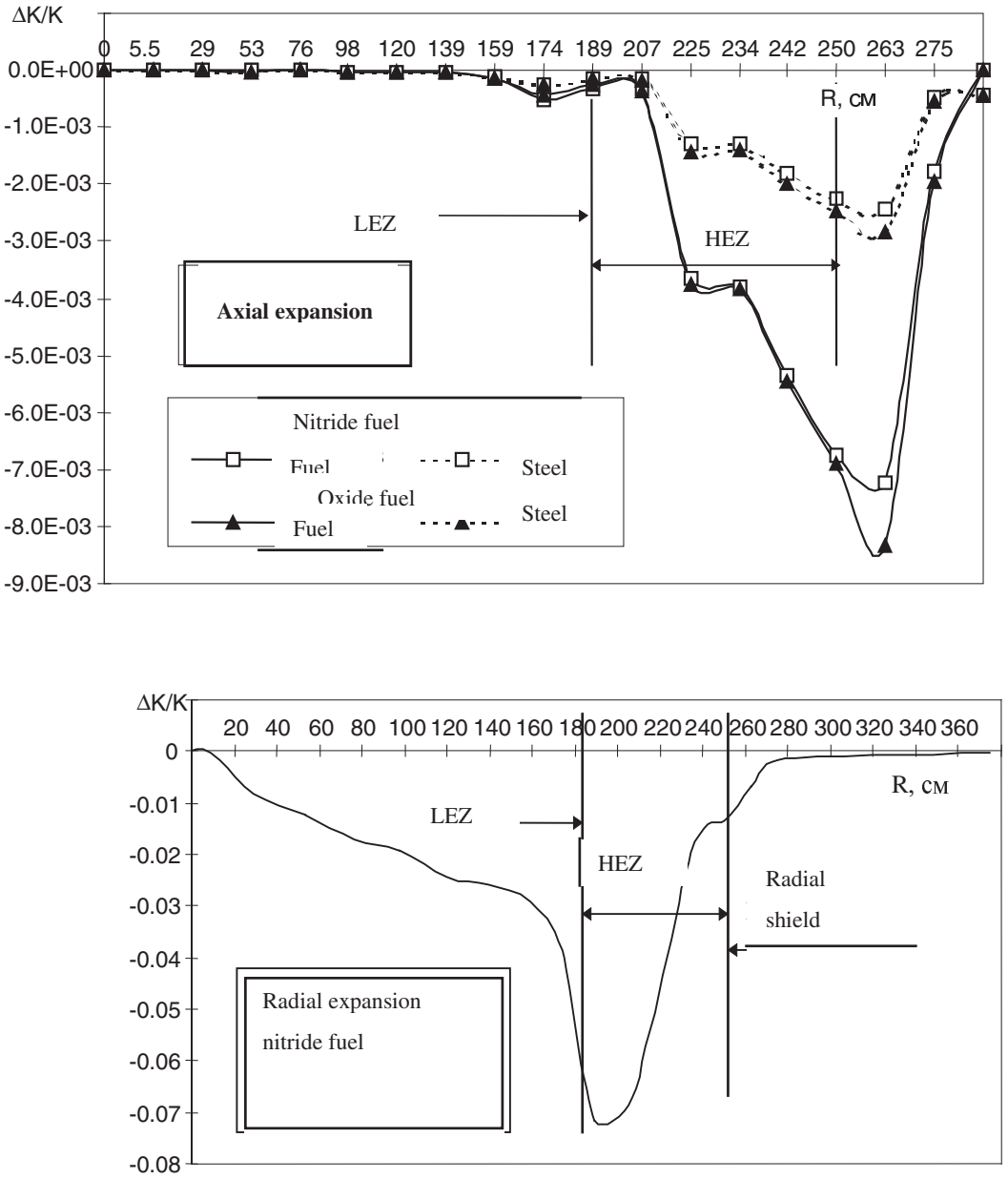

Fig. 5. Radial distribution of TCR components caused by axial and radial expansion of core materials. The integral with respect to reactor height in the bounds of the annular area of one fuel assembly row (for the conventional coefficient of linear expansion $\alpha = 1^1$/degree).

The similarity theory methods developed in Ref. 7 to evaluate the reactivity effects from temperature deformation of the core, lead to differing results being obtained in the standard diffusion model of neutron transport and the P_1-approximation of the kinetic model. The following formulas hold, Ref. 8:

Radial expansion

Diffusion approximation:

$$RE_R = -(\delta K_1 + 3\delta K_2 + \partial K_3) \times \frac{\delta R}{R}$$

P_1- approximation:

$$RE_R^* = -(\sum_1^3 \delta K_i + 2/15(4\delta K_1 + 7\delta K_2)) \times \frac{\delta R}{R}$$

Axial expansion

$$RE_Z = -2\delta K_1 \times \frac{\delta H}{H}$$

$$RE_Z^* = -(\sum_1^3 \delta K_i - 2/15(4\delta K_1 + 7\delta K_2)) \times \frac{\delta R}{R}$$

where $\delta K_1 = \frac{1}{\text{FNW}} \left\{ \int_v \sum_{k=l}^{m} 3\sigma_{tr}^{k,i} i_k(r) i_k^+(r) 2\pi r dr \right\}$ and $\delta K_2 = \frac{1}{FNW} \left\{ \int_0^H \sum_{k=l}^{m} 3\sigma_{tr}^{k,i} i_k(z) i_k^+(z) dz \right\}$ are the leakage with respect to R and Z, respectively; and

$$\delta K_3 = \frac{1}{\text{FNW}} \left\{ \int_v \left[-\sum_k \sigma_{c,f,d}^{i,k} \Phi_k(\vec{r}) \Phi_k^+(\vec{r}) + \sum_{j=1}^{k-1} \sigma_{in}^{j \to k} \Phi_j(\vec{r}) \Phi_k^+(\vec{r}) + \frac{1}{K_{eff}} \nu_f^k \sigma_f^k \Phi_k(\vec{r}) \sum_k \chi_k \Phi_k^+(\vec{r}) \right] dV \right\}$$

is the "weight" of the main numbers of the processes. FNW is the fission neutron worth (other denotations are standard, Ref. 1).

Taking this into account, Table 3 gives the change in the TCR_R and TCR_Z components. It is clear that the use of the diffusion approximation adds to the self-protection margin (P_1-approximation formulas lower the maximum sodium temperature by an estimated 10-15°C).

For TCR_R there is uncertainty in the model of its appearance (for example, the transfer to the fuel assembly bending model), and in this respect a similar margin is justified. Although both groups of formulas are valid for the homogeneous expansion of a cylinder, using them in a conical expansion model for separate axial layers and the entire core yields results which are close to the direct calculation.

The role played by thermal expansion of the RCPS drive rod, depending on its position in the core, is evaluated by lowering the maximum sodium temperature by 10-15°C (see Fig. 6).

Table 3

Change in feedback components from thermal expansion of the core when using improved similarity theory formulas in the P_1-approximation, relative units

Reactor zone	Change in TCR*) components			
	$\Delta(TCR_H)$	$\Delta(TCR_R)$	$\Delta(TCR_H)$	$\Delta(TCR_R)$
Upper shield (B4C)	3.96E-01	3.61E-01	2.54E-01	4.31E-01
Sodium void	3.90E-01	3.65E-01	2.54E-01	4.73E-01
Fuel element end pieces	2.82E-01	2.59E-01	1.42E-01	2.22E-01
Upper fuel part	2.74E-01	2.06E-01	1.50E-01	1.32E-02
Axial upper breeding zone (UBZ)	2.67E-01	2.40E-01	5.61E-02	-1.16E-02
Lower fuel part	2.83E-01	2.66E-01	1.37E-01	2.26E-01
Lower shield	3.60E-01	2.94E-01	2.50E-01	3.77E-01
Lower reflector	-6.79E-01	-6.29E-01	8.38E-01	1.60E+00

*) For the first two columns the fluxes and worths were obtained with diffusion approximation, for the third and fourth columns they were obtained with kinetic approximation using the TWODANT program.

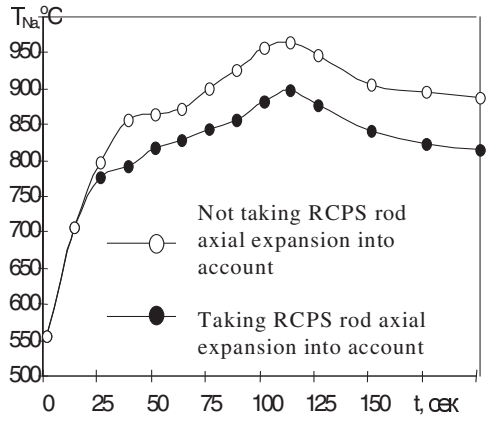

Fig. 6. Impact of taking account of thermal expansion of rods in a ULOF type accident, q_l = 320 W/cm (TCR_{RCPS} = $-0.5 \cdot 10^{-3}$ $\Delta K/K/^oC$, full reactivity for rod expansion ~ 0.1% $\Delta K/K$).

Conclusion

1. The research carried out demonstrates that diffusion approximation is not sufficiently accurate for the calculation of reactivity coefficients in reactors with zones that have sharply differing neutron physics characteristics; for example, when there is a sodium void.

2. Taking the kinetic effect into account in a single constant version and calculation code leads to changes in the TCR integral components. The Doppler constant remains more or less the same but depending on the method and accuracy with which the Doppler region is described in various programs its fluctuations are estimated to have a maximum value of <20%. The positive TCR_{Na} is reduced by ~15%. The axial fuel expansion component increases by ~6%. There is a very negligible increase in the radial expansion component (<2%). By this, the reactor self-protection is increased. The maximum change in the aforementioned components occurs in the peripheral region of the core and the sodium void where there are maximum increases in their determining temperatures in an accident. Various formulas of the similarity theory may result in an increase in the reactivity components from axial and radial expansion of up to 20-30% and 10-15%, respectively.

3. Using integral values of the TCR components (such as the Doppler effect and the sodium void reactivity effect) when comparing reactors in exploratory research does not give a true picture of the level of self-protection. Spatial distributions of the TCR components and changes in the heating of materials must be taken into account.

4. The effect of the limiting evaluated error in TCR components has been demonstrated. Its potential range in maximum evaluations corresponds to the following changes in the total sodium temperature in a ULOF accident:

-	Doppler component	-	(10-15)^{o}C
-	Sodium density component	-	(5-20)^{o}C
-	Thermal expansion of reactor	-	(10-20)^{o}C
-	Expansion of RCPS rods	-	(10-15)^{o}C

5. The estimated fluctuations in the total temperatures during an accident, related to the maximum possible error in describing the spatial distributions and integral values of the reactivity components of feedback, show the need for improved reactivity coefficient calculation codes which take their detailed spatial distribution into account. The current calculation methods used for the cores under investigation give conservative estimates.

References

[1] G. Khammel, D. Okrent, Reactivity coefficients in large fast power reactors based on fast neutrons, Moscow: Atomizdat, 1975.

[2] S.B. Shikhov, Calculating the effect of a change in dimensions on the critical mass of a fast reactor using the perturbation theory, Atomnaya energiya, Vol. 6, No. 2 (1959) pp 162-168.

[3] Evaluation of benchmark calculations on a fast power reactor core with near zero sodium void effect, IAEA-TECDOC-731, Vienna, 1994.

[4] V.A. Grabezhnoj, et al., Kinetic effects when calculating reactivity coefficients in a large fast reactor with a sodium void, Voprosy atomnoj nauki i tekhniki, Ser: Yadernye konstanty, 1996, No. 2, p. 49.

[5] A.V. Danilychev, V.Yu. Stogov, et al., How the accuracy of calculation of the TCR Doppler component affects the safety rationale for fast reactors, Collected papers for a seminar on the 30th anniversary of the BOR-60 reactor, Dimitrovgrad, November 1999.

[6] Work of IAEA/CEC Comparative Calculations for a Severe Accident (ULOF) in the BN-800/1500 MW Reactor with Zero Void Effect, - Contract CEC/IAEA B7-6340/95/191/C2.

[7] S.D. Shikhov, A.N. Shmelev, Calculating the effect of an arbitrary change in dimensions on the critical mass of a nuclear reactor using the perturbation theory, In “Fizika yadernykh reaktorov”, Moscow Institute of Physics and Engineering, Moscow, Atomizdat, 1968, pp 67-85.

[8] B.D. Abramov, Reactivity effects in kinetic and diffusion perturbation theories, Atomnaya energiya, Vol. 84, No. 2 (1998) pp 98-102.

Nuclear Data Section
International Atomic Energy Agency
Vienna International Centre, P.O. Box 100
A-1400 Vienna
Austria

e-mail: services@iaeand.iaea.org
fax: (43-1) 26007
telephone: (43-1) 2600-21710
Web: http://www-nds.iaea.org